AD NUMBER
ADC018803
CLASSIFICATION CHANGES
TO: unclassified
FROM: confidential
LIMITATION CHANGES
TO: Approved for public release, distribution unlimited
FROM: Controlling DoD Organization. Naval Electronic Systems Command, Washington, DC.
AUTHORITY
ONR ltr, 31 Jan 2006; ONR ltr, 31 Jan 2006

CONFIDENTIAL

NOSC

NOSC TR 383

(2) LEVEL II

NOSC TR 383

Technical Report 383

BEARING STAKE COHERENCE AND ARRAY SIGNAL GAIN AREA ASSESSMENT REPORT (U)

"NATIONAL SECURITY INFORMATION"

"Unauthorized Disclosure Subject to Criminal Sanctions"

J. A. Neubert

December 1978

Research Report: January 1977 — December 1978

Sponsored by
Naval Electronic Systems Command

Classified by: OPNAVINST S5513.5-03
Review on: 8 October 1994

NAVAL OCEAN SYSTEMS CENTER
SAN DIEGO, CALIFORNIA 92152

CONFIDENTIAL

NAVAL OCEAN SYSTEMS CENTER, SAN DIEGO, CA 92152

AN ACTIVITY OF THE NAVAL MATERIAL COMMAND

RR GAVAZZI, CAPT, USN
Commander

HL BLOOD
Technical Director

ADMINISTRATIVE INFORMATION (U)

(U) The work reported herein was sponsored by the Naval Electronic Systems Command (PME-124). The acoustic survey was conducted from January 1977 through May 1977 and the data processing and analysis was performed from June 1977 through December 1978.

Released by
R.R. Gardner, Head
Environmental Acoustic Division

Under authority of
J.D. Hightower, Head
Environmental Sciences Department

ACKNOWLEDGEMENTS (U)

(U) M.A. Pedersen, Dr. J.D. Northrop, and Dr. A.G. Fabula contributed extensively to the propagation section. P.W. Schey and J.J. Russell performed all of the UNIVAC 1110 processing. Dr. A.C. Fabula, Dr. J.D. Northrop and G.S. Yee reviewed this report and made several valuable suggestions.

CONFIDENTIAL

SECURITY CLASSIFICATION OF THIS PAGE (When Data Entered)

REPORT DOCUMENTATION PAGE

READ INSTRUCTIONS BEFORE COMPLETING FORM

1. REPORT NUMBER: NOSC/TR-383	2. GOVT ACCESSION NO.
3. RECIPIENT'S CATALOG NUMBER	
4. TITLE (and Subtitle): BEARING STAKE COHERENCE AND ARRAY SIGNAL GAIN AREA ASSESSMENT REPORT (U)	5. TYPE OF REPORT & PERIOD COVERED: Research Report - January 1977-December 1978
	6. PERFORMING ORG. REPORT NUMBER
7. AUTHOR(s): J.A. Neubert	8. CONTRACT OR GRANT NUMBER(s)
9. PERFORMING ORGANIZATION NAME AND ADDRESS: Naval Ocean Systems Center, San Diego, CA 92152	10. PROGRAM ELEMENT, PROJECT, TASK AREA & WORK UNIT NUMBERS
11. CONTROLLING OFFICE NAME AND ADDRESS: Naval Electronic Systems Command, Washington, D.C.	12. REPORT DATE: December 1978
	13. NUMBER OF PAGES: 78
14. MONITORING AGENCY NAME & ADDRESS(if different from Controlling Office)	15. SECURITY CLASS. (of this report): CONFIDENTIAL
	15a. DECLASSIFICATION/DOWNGRADING SCHEDULE

16. DISTRIBUTION STATEMENT (of this Report)

Review on: 8 October 1994

17. DISTRIBUTION STATEMENT (of the abstract entered in Block 20, if different from Report)

18. SUPPLEMENTARY NOTES

19. KEY WORDS (Continue on reverse side if necessary and identify by block number)

underwater sound propagation	Indian Ocean
sonar	towed projectors
passive arrays	towed arrays

20. ABSTRACT (Continue on reverse side if necessary and identify by block number)

(C) This report assesses the coherence data taken during BEARING STAKE, a major acoustic survey conducted in the Northwestern Indian Ocean from January through May 1977. The survey was designed to provide (1) acoustic data to determine variability in the acoustic environment, (2) inputs to performance models, and (3) acoustic data for assessing surveillance options in selected areas of the Northwestern Indian Ocean.

(C) During BEARING STAKE measurements were made for determining the array phase coherence and the array signal gain for long, horizontal line arrays receiving multipath signals from long-range, narrowband, low-

DD FORM 1 JAN 73 1473 EDITION OF 1 NOV 65 IS OBSOLETE S/N 0102-LF-014-6601

CONFIDENTIAL

SECURITY CLASSIFICATION OF THIS PAGE (When Data Entered)

20. ABSTRACT (Continued)

frequency towed CW sources in the Northwestern Indian Ocean. A bottom-mounted and two mid-depth towed arrays were used. The phase coherence and the array signal gain results for these arrays are presented and compared.

(C) Since the Northwestern Indian Ocean is usually bottom-limited and the sound-speed profiles are complex in small-scale structure at mid-depths a considerable rangewise variability exists in the phase coherence and the array signal gain for this multipath environment. This variability increases due to the presence of irregular bottom slopes as well as seamounts. This variability is the dominant characteristic of this body of water when the performance of long horizontal acoustic arrays is considered. Hence, a general assessment of signal coherence for the Northwestern Indian Ocean, based on the BEARING STAKE data, is as follows. The coherence will be a manageable problem for the performance of long bottom-mounted and mid-depth towed array systems used for surveillance if sufficient rangewise sampling is employed and the towed arrays are not operated in the depth region of complex sound-speed profile structure.

Classified by: OPNAVINST S5513.5-03
Review on: 8 October 1994

(U) CONTENTS (U)

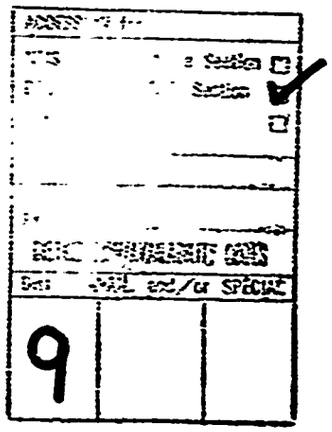

ILLUSTRATIONS (U)

ILLUSTRATIONS (Continued) (U)

(U) TABLES (U)

SUMMARY (U)

PROBLEM (U)

(C) Determine the coherence and the array signal gain during BEARING STAKE for large aperture, horizontal line bottom-mounted and mid-depth towed arrays receiving multipath signals from long-range, narrow-band, low-frequency towed CW sources in the Northwestern Indian Ocean.

APPROACH (U)

(C) During BEARING STAKE measurements were made for determining coherence for a bottom-mounted and two mid-depth towed arrays near five sites in the Northwestern Indian Ocean. These measurement data were digitized and processed on the NOSC UNIVAC 1110 to produce the phase coherence C_p and the array signal gain ASG versus range and frequency for several projector tows surveying much of the Northwestern Indian Ocean. The amplitude fluctuation Σ_A and S/N (the signal plus noise to noise ratio) were also computed. Corrections to the C_p and ASG data for low S/N were not attempted. This report concerns only cases in which the S/N is high enough that the noise correction is negligible.

RESULTS (U)

(C) Since the Northwestern Indian Ocean is usually bottom-limited and the sound speed profiles are complex, a considerable rangewise variability exists in the plots of phase coherence and array signal gain for this multipath environment. This variability increases due to the presence of irregular bottom slopes as well as seamounts for mid-depth towed arrays. This variability is the dominant characteristic of this body of water when the performance of long horizontal acoustic arrays is considered. Thence, a general assessment of signal coherence for the Northwestern Indian Ocean, based on the BEARING STAKE data, is as follows. The coherence will be a manageable problem for the performance of large aperture bottom-mounted and mid-depth towed array systems used for surveillance if sufficient rangewise sampling is employed and the towed arrays are not operated in the depth region of complex sound-speed profile structure. From the detailed area assessment to follow several conclusions can be reached about the performance of large aperture, horizontal acoustic arrays in the Northwestern Indian Ocean.

1. (U) The degree of amplitude fluctuation, as measured by Σ_A, does not change much with frequency and is largely range independent up to about 1000 km, even over irregular sloping bottoms.

2. (U) The phase coherence and the array signal gain decrease severely with increasing frequency, even when the S/N values remain high enough to render noise corrections negligible.

3. (U) The phase coherence and the array signal gain are generally range independent up to about 1000 km except when the projector is passing over an irregular sloping bottom. They decrease and become more variable for a mid-depth towed array, but not for

a bottom-mounted array, when the projector is passing over an irregular sloping bottom. This behavior may reflect the importance of bottom propagated sound paths for a bottom-mounted array.

4. (U) The phase coherence and the array signal gain are widely variable with range due to multipath interference in a bottom-limited environment with a complex sound-speed profile and become more variable in an irregular bottom slope region for a mid-depth towed array but not for a bottom-mounted array. They were less variable at the only site where propagation was not bottom-limited.

5. (C) It appears that for the bottom-limited regions of the Northwestern Indian Ocean, the phase coherence and the array signal gain behavior of bottom-mounted and mid-depth towed (above the depth region of sound-speed profile complexity) arrays are essentially the same except when the projector is passing over an irregular sloping bottom.

6. (U) The sensor spacing configuration for the bottom-mounted array was considerably different from that for the mid-depth towed arrays. To obtain a more accurate comparison of a towed array with the bottom-mounted array, a subset towed array (configured similarly in sensor spacing to the bottom-mounted array) was studied. It was found that the bottom-mounted array performed essentially the same as the subset towed array (except in the irregular bottom slope region). The subset towed array performed essentially the same as the total array for phase coherence and array signal gain.

7. (C) In the Northwestern Indian Ocean the surveillance performance of towed arrays may be significantly dependent upon the array tow depth due to the presence of a mid-depth region of sound-speed profile complexity.

8. (U) When sound was received by a mid-depth towed array from behind a seamount, the phase coherence and the array signal gain were often low due to the reduced S/N values.

RECOMMENDATIONS (U)

1. (U) Changing and incrementing the averaging time intervals would be interesting in conjunction with a study of the detailed acoustic structure behind the sampled values of C_p and ASG used in this report. This would show how the regions of sound-speed profile complexity influence C_p and ASG and would lead to estimates of the optimum averaging time interval as a function of array tow depth.

2. (U) It would be useful to directly investigate the effects on coherence variability of the complex sound-speed profiles by towing an array above and then within this highly structured profile region.

3. (U) It is recommended that more LATA data (Site 5) be processed.

4. (C) The surveillance behavior of bottom-mounted arrays could be better understood by investigating and modeling the possibility of bottom propagation paths in the Northwestern Indian Ocean.

5. (U) It is recommended that in future tests in the Northwestern Indian Ocean, much longer signal periods (say, 25 min for signal and 5 min for noise as a duty cycle) be used at a single low frequency. This would allow a more detailed study of the rangewise structure of C_p and ASG and permit better verification of a sound propagation model of coherence behavior.

(U) NOTATION (U)

ΔT, averaging time interval, sec

A_a, averaging amplitude of Eq. (A-16)

Φ, bearing of source from Eq. (A-3), deg

C_p, phase coherence coefficient of Eq. (A-20)

Σ_A, normalized standard deviation of Eq. (A-15)

C_n, nonhomogeneity coefficient of Eq. (A-17)

C_T, Talpey coefficient of Eq. (A-13)

ASG, array signal gain of Eq. (A-24)

S/N, signal plus noise to noise ratio, dB

R, range from source to array, km

1. (U) INTRODUCTION

(C) In recent years, the Indian Ocean has become an area of increasing strategic and tactical importance to the Navy. Because of the lack of environmental acoustic data from the Indian Ocean of the type required for performance characterization of surveillance systems options, OP-95 tasked NAVELEXSYSCOM PME-124 to conduct environmental acoustic surveys to obtain the data necessary to assess the performance of passive Anti-submarine Warfare (ASW) surveillance systems in the Northwestern Indian Ocean.

(C) Accordingly, PME-124 developed Project BEARING STAKE with these objectives:

a. Conduct environmental and acoustic measurements in five selected areas of the Northwestern Indian Ocean during the period of January through May 1977 with a variety of measurement systems.

b. Collect acoustic data to determine the variability in the acoustic environment and provide inputs to models for systems performance evaluation.

c. Utilize near-surface, mid-depth, and bottom-mounted receivers (such as long horizontal arrays) to determine the following:

- Propagation loss vs frequency and depth
- Omnidirectional noise
- Noise directionality
- Wavefront coherence
- Vertical arrival structure
- Bottom interaction
- Bottom reflectivity

d. Produce an acoustic assessment of the Northwestern Indian Ocean based upon the results obtained.

e. Perform assessment of surveillance systems for the Northwestern Indian Ocean.

(C) The purpose of this report is to present the analysis of the results of the wavefront coherence measurements made during BEARING STAKE in areas near five selected sites in the Northwestern Indian Ocean shown in Fig. 1. From the analysis, a coherence and array signal gain assessment of the areas concerned is presented for a bottom-mounted and two mid-depth towed arrays.

(U) Technical direction of BEARING STAKE was vested in the Naval Oceans Systems Center (NOSC). Participants in BEARING STAKE represented a broad spectrum of organizations. In addition to NOSC, the other Navy organizations involved were the Naval Oceanographic Office (NOO), the Naval Research Laboratory (NRL), the Naval Air Development Center (NADC), and the Naval Ocean Research and Development Activity (NORDA). The Weapons Research Establishment (WRE; now the Weapons Systems Research Laboratory, Defence Research Centre) of the Australian Department of Defence also participated. The industrial and university organizations represented were Western

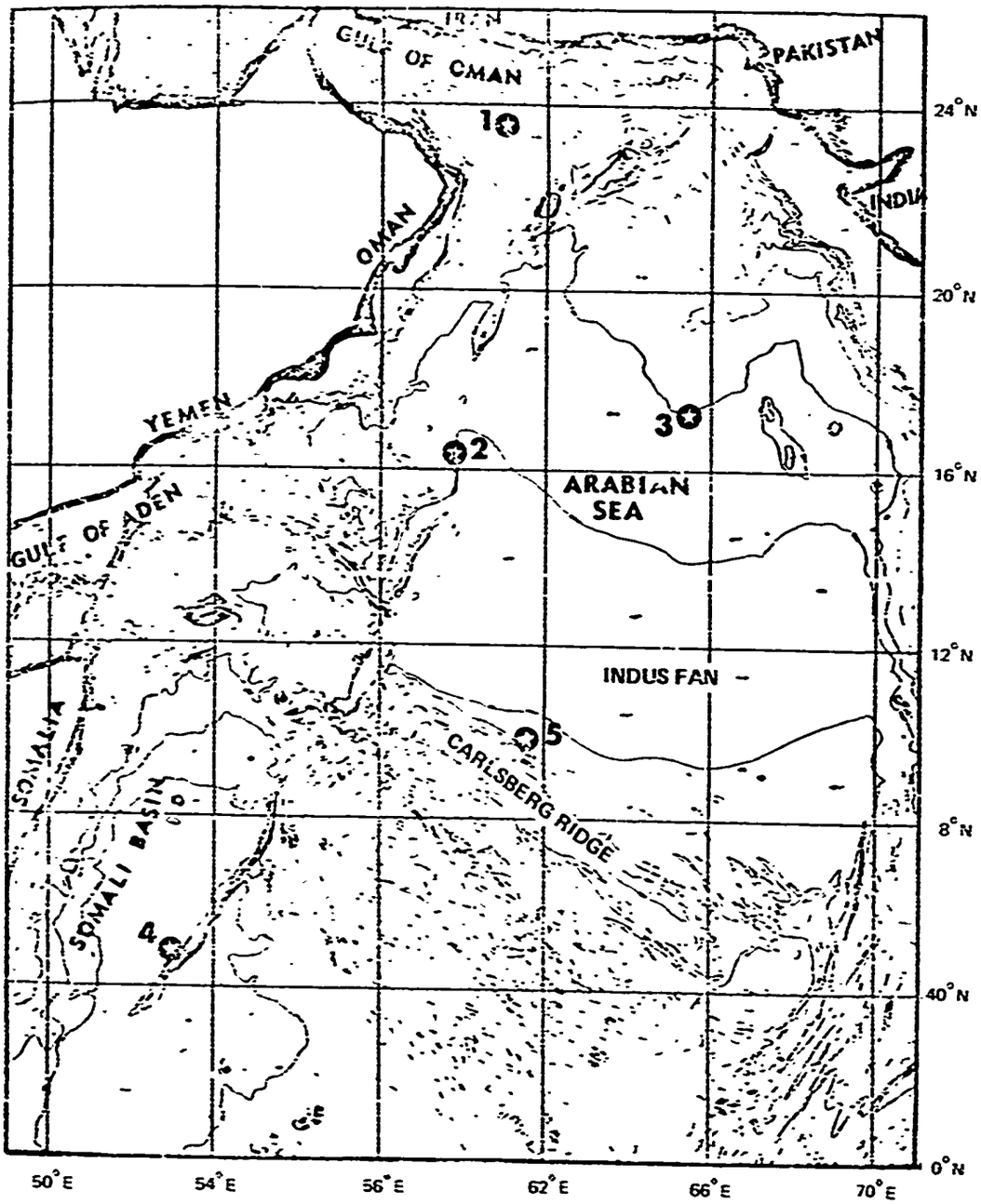

Figure 1. (C) Geographic features of site locations. (U)

Electric Co. (WECo), Sanders, Inc., Woods Hole Oceanographic Institution (WHOI) Applied Research Laboratories, University of Texas at Austin (ARL/UT), TRW, and Planning Systems, Inc. (PSI).

(U) The operational aspects of BEARING STAKE with respect to coherence measurements are described in Section 2. (For a more detailed description of the operational plans and systems involved, see Refs. 1 through 9). In Section 3, the results of the array coherence and array signal gain area assessment are developed. Section 4 presents the conclusions from this study. In the Appendix the methodology for phase coherence and array signal gain and definitions of the terms used in this assessment report are presented.

2. (U) OPERATIONAL ASPECTS

2.1 (U) CHRONOLOGY AND SITES

(C) The BEARING STAKE acoustic measurements, performed near the five sites of Fig. 1, were conducted during the four cruises shown in the following timetable:

Cruise	Dates (1977)	Site Occupied
1	13 Jan–26 Jan	1A
2	30 Jan–25 Feb	3 and 1B
3	5 Feb–30 Mar	4
4	4 Apr– 4 May	5 and 2

Site 1 was occupied twice: hence, the terminology of "Sites 1A" and "1B." Coherence measurements were made for Sites 3, 1B, 4, 5 and 2. Throughout this report the sites will be treated in chronological order as above.

(C) The major geographical features of the Northwestern Indian Ocean and its major shipping lanes were considered in the selection of the locations for Sites 1 through 5 (see Fig. 1). The measurement events conducted for these sites represent a variety of situations that allow assessment of passive surveillance system options against transitting submarines and submarines attempting to interdict shipping.

(C) Site 3 is located in the central portion of the Arabian Sea with a water depth of 3,600 m. Measurements here will be useful in evaluating the surveillance potential close to the Cape of Good Hope-Arabian Sea shipping lanes along the east coast of Africa.

(C) Site 1 is located in the mouth of the Gulf of Oman where the water depth is 3,300 m. This site offers bathymetrically unshielded ranges in a narrow corridor into the Arabian Sea. The data from Site 1 will be useful in evaluating the surveillance potential in the Gulf of Oman and its approaches. Shipping traffic to and from the Persian Gulf passes close to Site 1.

(C) Site 4 is over a slope with depths ranging from 4,000 to 5,000 m. Long-range propagation via refracted paths occurred in the deep waters of the northern Somali Basin (see Ref. 8). This is the only site for which bottom-limited propagation conditions did not prevail during the exercise (see Section 2.4).

(C) Site 5 is located on the northern edge of the Carlsberg Ridge south of the Suez Canal-Orient shipping lanes. The site is situated over the flat top of a low rise (500 m above the sea floor) in 4,500 m of water. The Carlsberg Ridge, on the southern edge of the Arabian Sea, may provide shielding from noise sources to the south of this site for surveillance systems looking into the Arabian Sea.

(C) Site 2 is located on a ridge approximately 370 km (200 nmi) off the coast of the Arabian Peninsula. Data from this site will be useful in evaluating the surveillance potential in the major shipping lanes running along the Arabian Peninsula and into the Arabian sea.

2.2 (U) HORIZONTAL ARRAY SYSTEMS USED FOR COHERENCE DATA COLLECTION

(U) Three coherence measurement systems are discussed in this report. They are:

- Ocean Acoustic Measurement System (OAMS) array from PME-124/NOSC
- Long Acoustic Towed Array (LATA) from WRE, Australia
- Bottom-Mounted Array (BMA) from PME-124/WECo

The OAMS array, the LATA, and the BMA were operated at Sites 3, 1B, 4, 5 and 2.

(U) The ships which participated in BEARING STAKE were the USNS KINGSPORT (T-AG-33), the USNS MYER (T-ARC-G), the USNS MIZAR (T-AGOR-11), the USNS WILKES (T-AGS-33) and the Australian ship HMAS DIAMANTINA (GOR-266). During BEARING STAKE, the KINGSPORT conducted all the long-range projector tows shown in Fig. 2. The MIZAR performed as the OAMS array tow and measurement ship. The DIAMANTINA towed and operated the LATA in coordination with the MIZAR tow runs. The MYER was responsible for all BMA operations. The WILKES performed several oceanographic functions for the BEARING STAKE exercise.

(U) After the conclusion of the BEARING STAKE exercise, the ship navigational logs were used by NORDA to reconstruct the projector tows and the array positions. Therefore, Fig. 2 gives the site overview for BEARING STAKE projector tows, and Figs. 3 through 6 show the details for each site. As can be seen from these figures, BEARING STAKE surveyed much of the Northwestern Indian Ocean.

2.2.1 (U) The Ocean Acoustic Measurement System (OAMS)

(U) The OAMS towed array, manufactured by the Seismic Engineering Co., has 32 directional hydrophone groups spaced over an acoustic aperture of 925.4 m (3036 ft). This array is highly directional due to its tapered design (see Fig. 7 and Ref. 9). This directional behavior arises from two causes: (1) the individual hydrophones in each sensor group are spaced in a cosine pattern, and the groups nearer the aperture ends are longer, and (2) the sensor group centers are spaced in a cosine pattern along the acoustic aperture. (Due to this directional behavior, the CW sources were generally kept within ±15 deg of broadside by the choice of the MIZAR courses.) Vibration isolation modules (VIMs) installed at the head and tail of the acoustic aperture make the total array length of 1535.9 m (5036 ft). See Fig. 8. The maximum design depth ("crush depth") is 305 m (1000 ft). Four depth sensors are distributed along the acoustic aperture.

(U) The OAMS array was operated for Sites 3, 1B and 4 in the vicinity of the BMA, while for Sites 5 and 2 the OAMS array operated more than 400 km for the BMA. See Figs 3 through 5. At each site, the OAMS array was deployed to a cable scope of between 300 to 350 m. During deployment, the speed of the ship was adjusted to keep the array near a nominal tow depth of 198 m (650 ft) and, depending on winds and currents, the speed varied between 2 and 3 knots. The array tilt during most data collection periods was less than ±1 deg. Ship maneuvers at each site consisted of polygon tows, designed to assess the horizontal directionality of the ambient noise field, and straight-line tows, oriented such

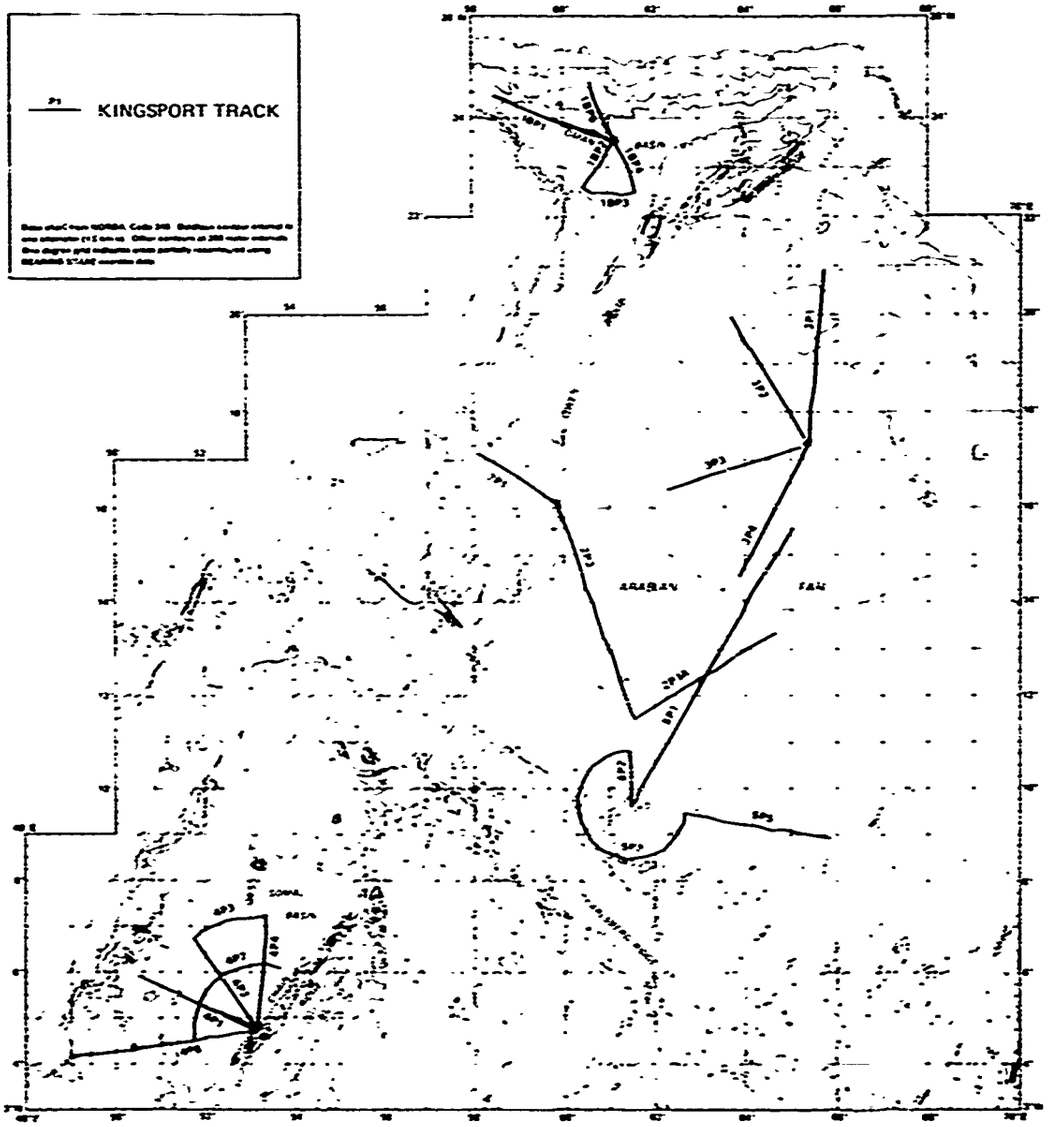

Figure 2. (C) Projector tow overview of the BEARING STAKE exercise. (U)

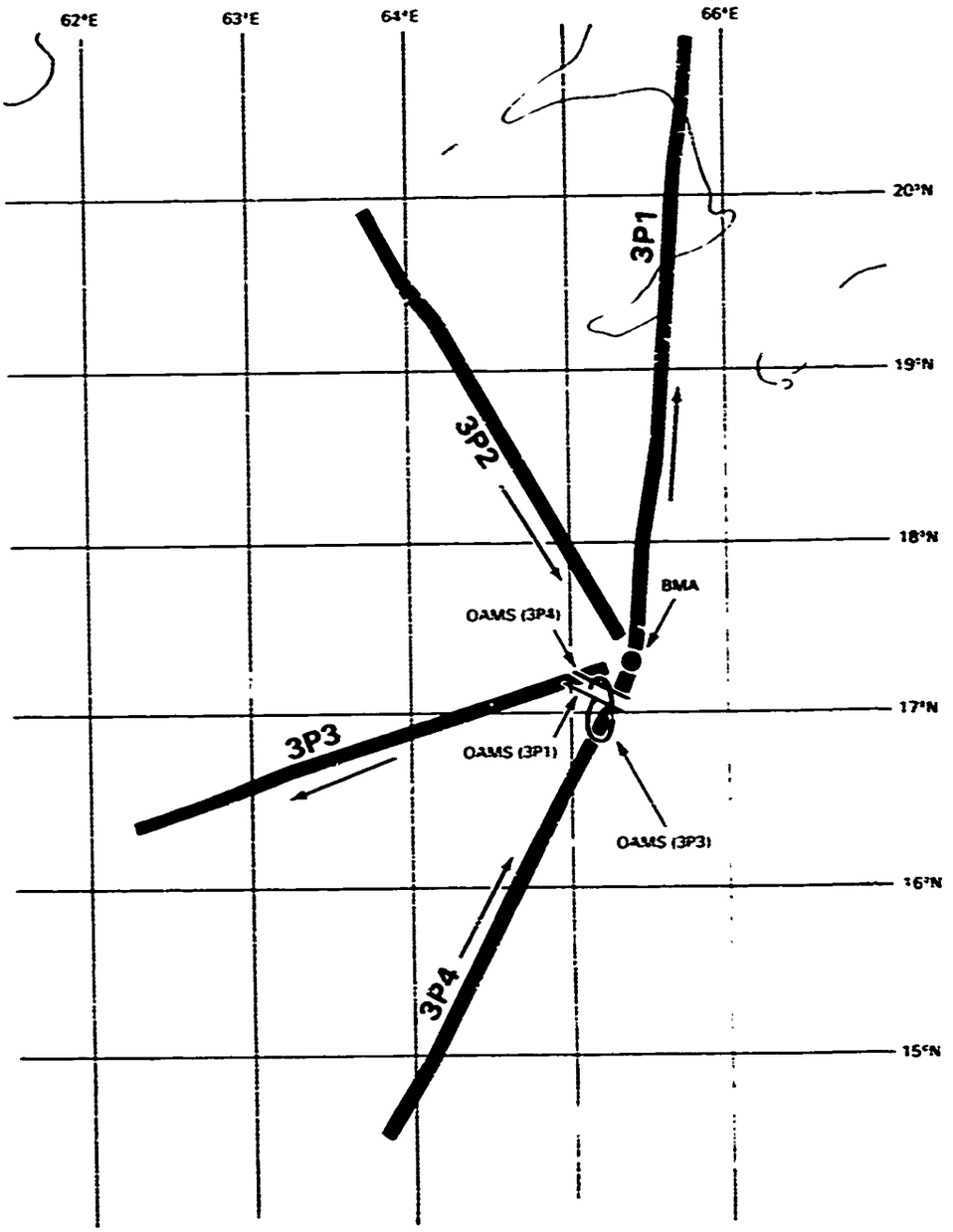

Figure 3. (C) Projector tows for Site 3; locations of BMA and OAMS array. (U)

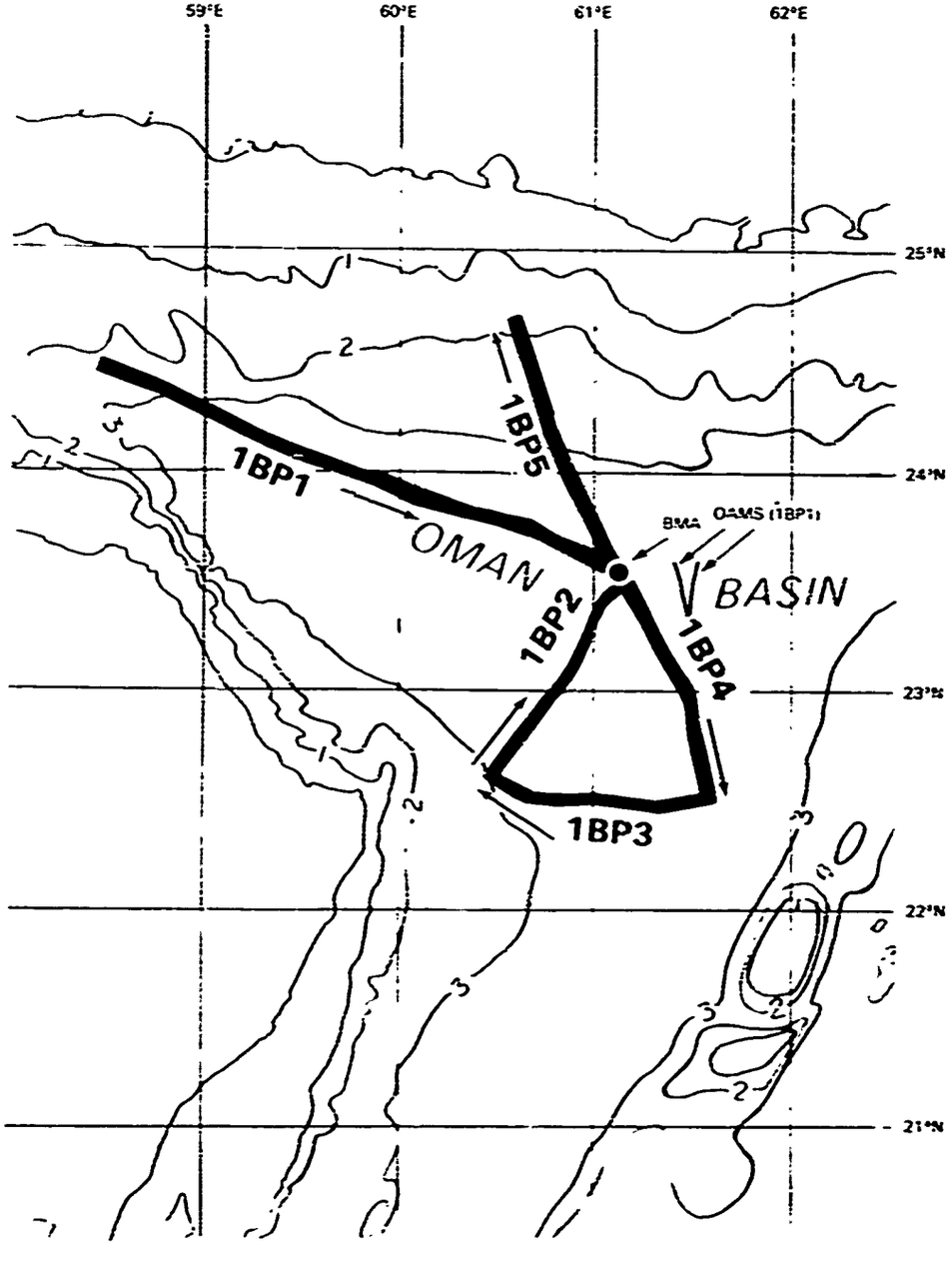

Figure 4. (C) Projector tows for Site 1B; locations of BMA and OAMS array. (U)

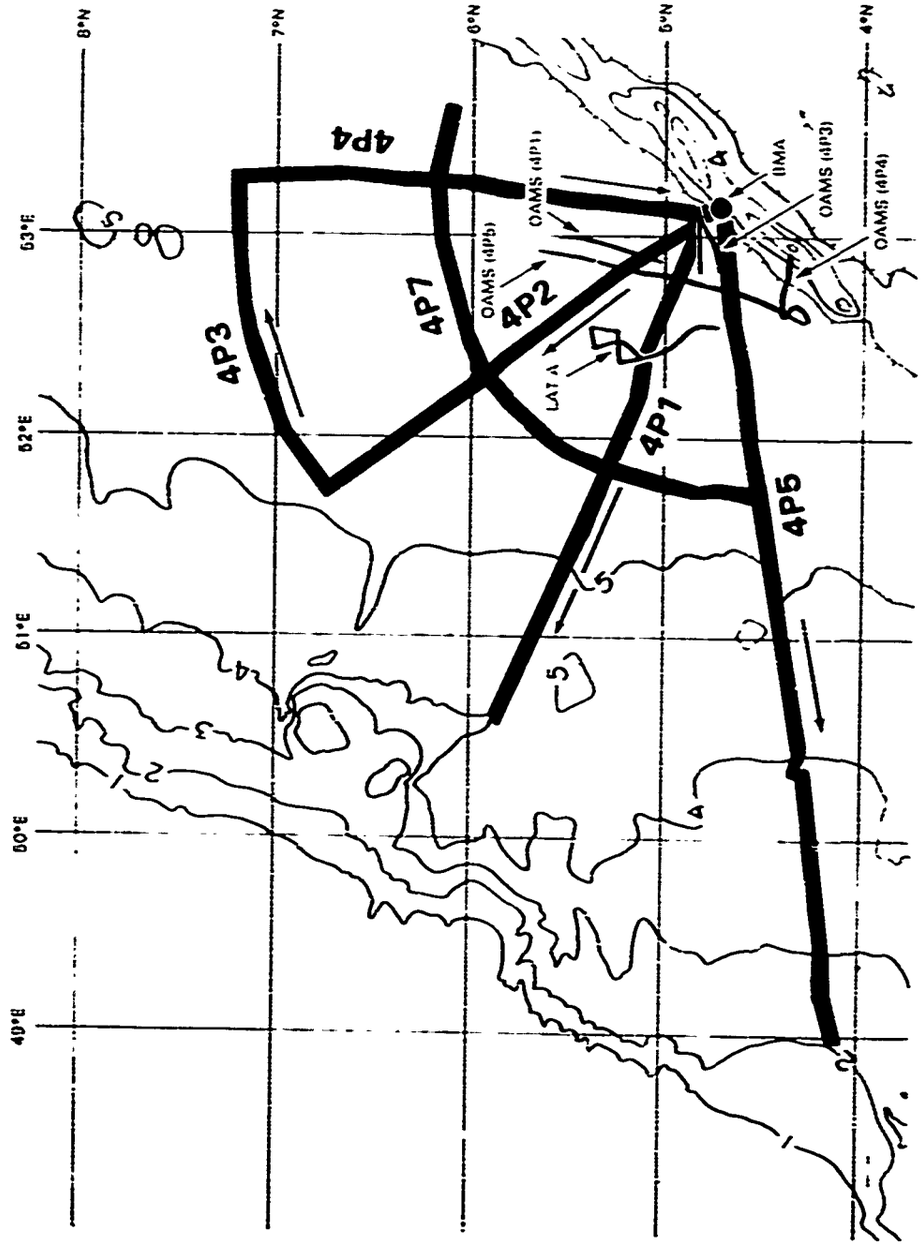

Figure 5. (C) Projector tows for Site 4; locations of LATA and OAMS array. (U)

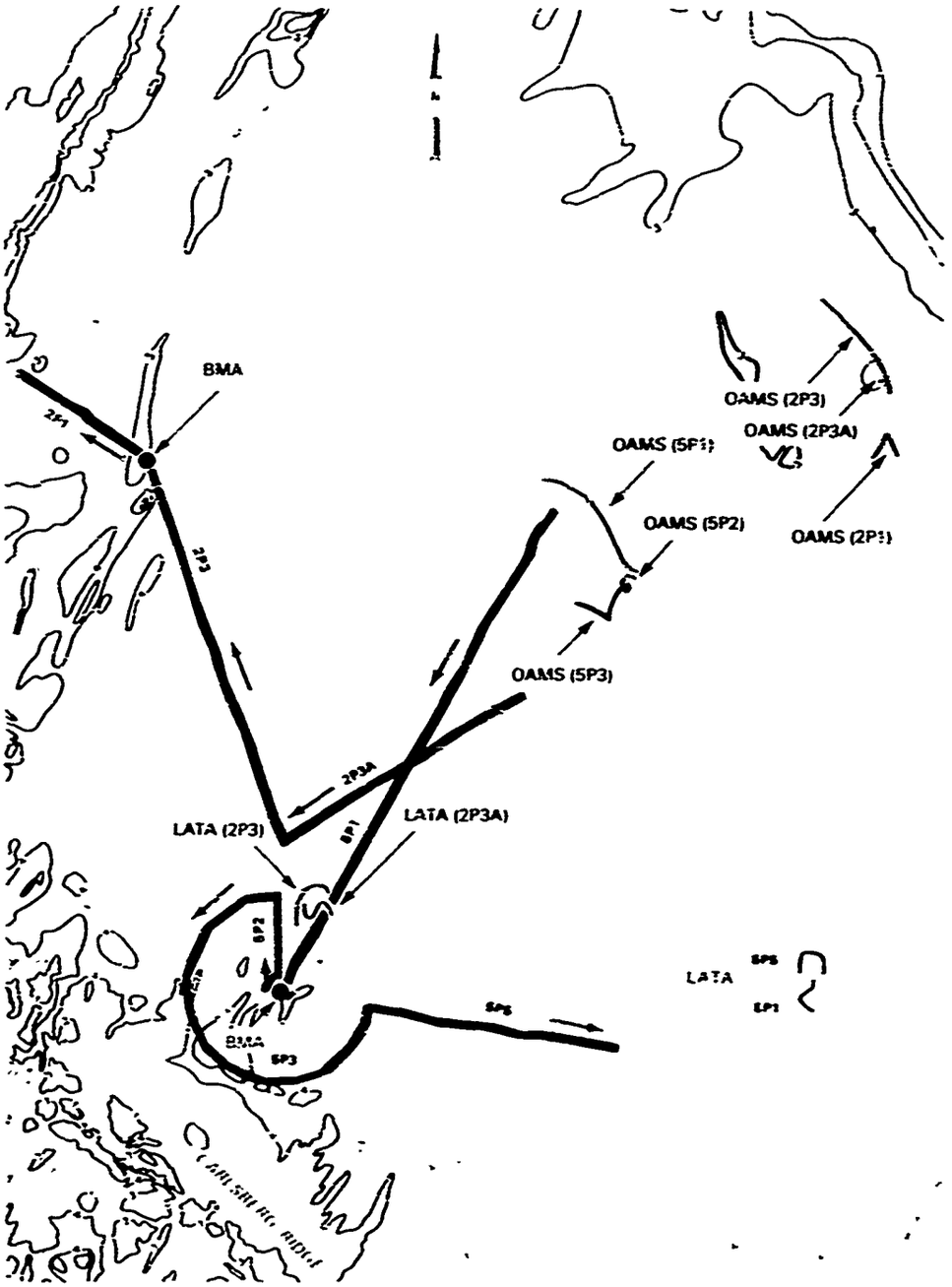

Figure 6. (U) Projector tows for Site 5 and 2; locations of LATA and OAMS array. (U)

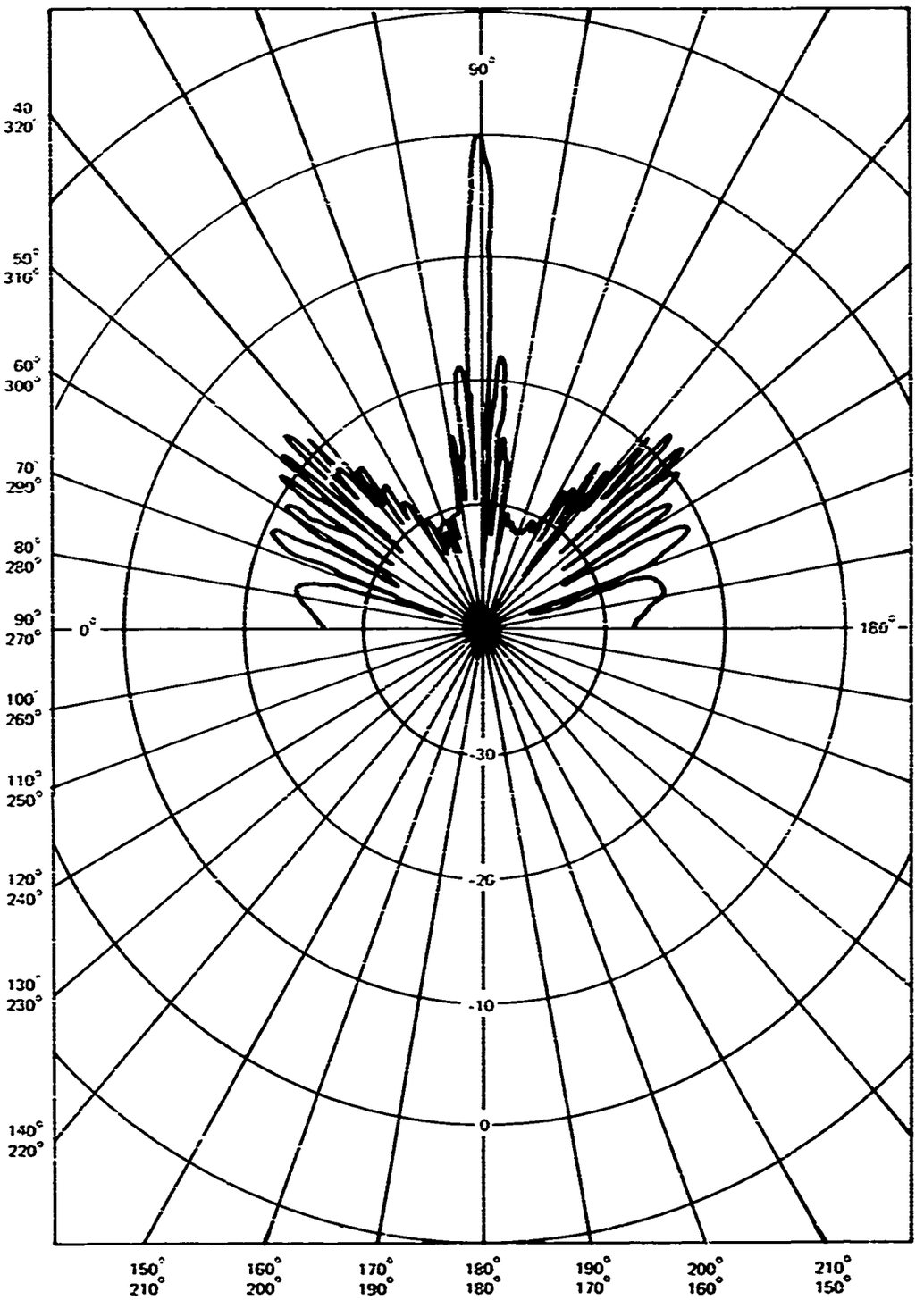

Figure 7. (U) The OAMS array, directional behavior at f = 50 Hz and steering angle = 90°. (U)

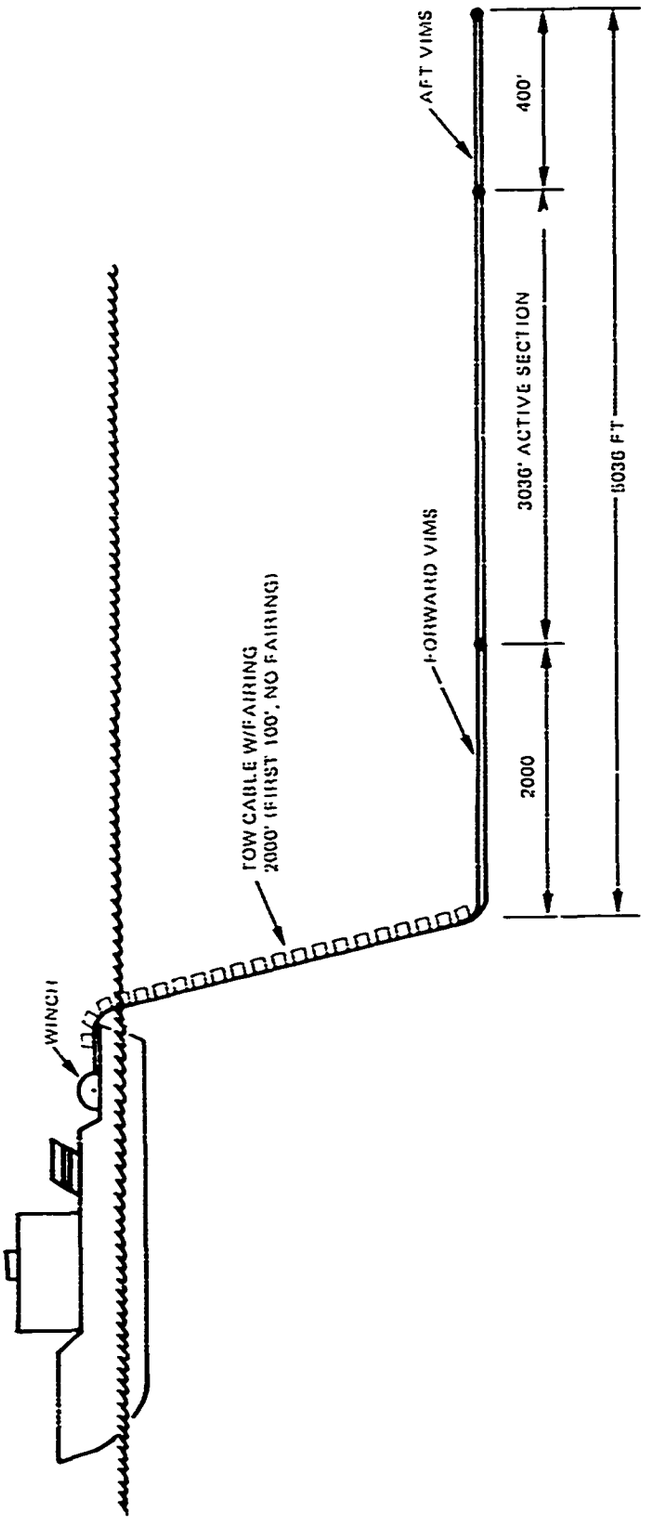

Figure 8. (C) OAMS array and towing configuration. (U)

that acoustic arrivals from the source were generally within ±15 deg of broadside because of the directivity of the OAMS array. Measurements of coherence, propagation loss and beam noise temporal statistics were collected during the straight tows.

(U) The OAMS signal processing system is built around a Hewlett Packard 2100 computer as shown schematically in Fig. 9. As shown in this figure, the individual hydrophone group outputs were amplified by charge coupled amplifiers and then fed through a 32-channel patch panel into the "coherence box" (the quadrature detector) to be put into baseband amplitude and phase quadrature form. The output of the 32-channel quadrature detector was digitized with a Hewlett Packard 2313B 64 channel A/D converter to generate the signal and noise data on digital tapes for later coherence processing (see Appendix). The center frequency of the quadrature detector was adjusted to track the Doppler-shifted received signals. The effective bandwidth of the quadrature detector was 1 Hz.

(U) Monitoring of individual hydrophone groups in real time was accomplished with a Spectral Dynamics Corporation SD309 Real Time Analyzer and associated units. The output could be displayed on a CRT or sampled by the HP2100 computer for further processing. Systems status parameters and depth sensor outputs were logged automatically through the microprocessor general interface unit. Recorded parameters included the time code, depth sensor outputs, the setting of the switches for quadrature detector gain, the HP2100 gain and quadrature detector frequency.

2.2.2 (U) The Long Acoustic Towed Array (LATA)

(C) The LATA, manufactured by the Seismic Engineering Co., has 64 omnidirectional hydrophone groups uniformly spaced 19.05 m apart ($\lambda/2$ at about 40 Hz) over an acoustic aperture of about 1200 m (3936 ft). (The LATA was called the LAMBDA I when used by the U.S. Navy.) VIMs are installed at the head and tail of the acoustic aperture (600 m forward, 300 m aft) for a total length of 2100 m. See Fig. 10. The maximum design depth is 1200 m. Special modules, each containing an array heading sensor and a precision depth sensor, are situated at the head and tail of the acoustic aperture. A cable inclinometer is mounted on the tow cable, above the water at the stern, to provide an indication of the tow speed.

(U) The LATA was operated for Sites 3, 1B and 4 in the vicinity of the BMA, while for Sites 5 and 2 it operated more than 700 km from the BMA. See Figs. 5 and 6. At Site 3 LATA was deployed after the projector operations had ceased, and at Site 1B insufficient LATA coherence data were collected for meaningful processing. Hence, LATA coherence data were processed only for Sites 4, 5 and 2. The LATA array was towed at a nominal depth of 305 m at a speed of 2 to 3 knots. Coherence measurements were made on straight-line tows oriented so that the array would be nearly broadside or nearly endfire to the projector. The array tilt during most data collection periods was less than ±1.5 deg for Sites 4, 5 and 2.

(C) The 64 LATA hydrophone group outputs were collected and processed by the WRE-designed-and-built digital signal processing and display system on board the DIAMANTINA. The group outputs were digitized at a rate of 512 samples per second and multiplexed with outputs from the heading and depth sensors, time, code, ship position,

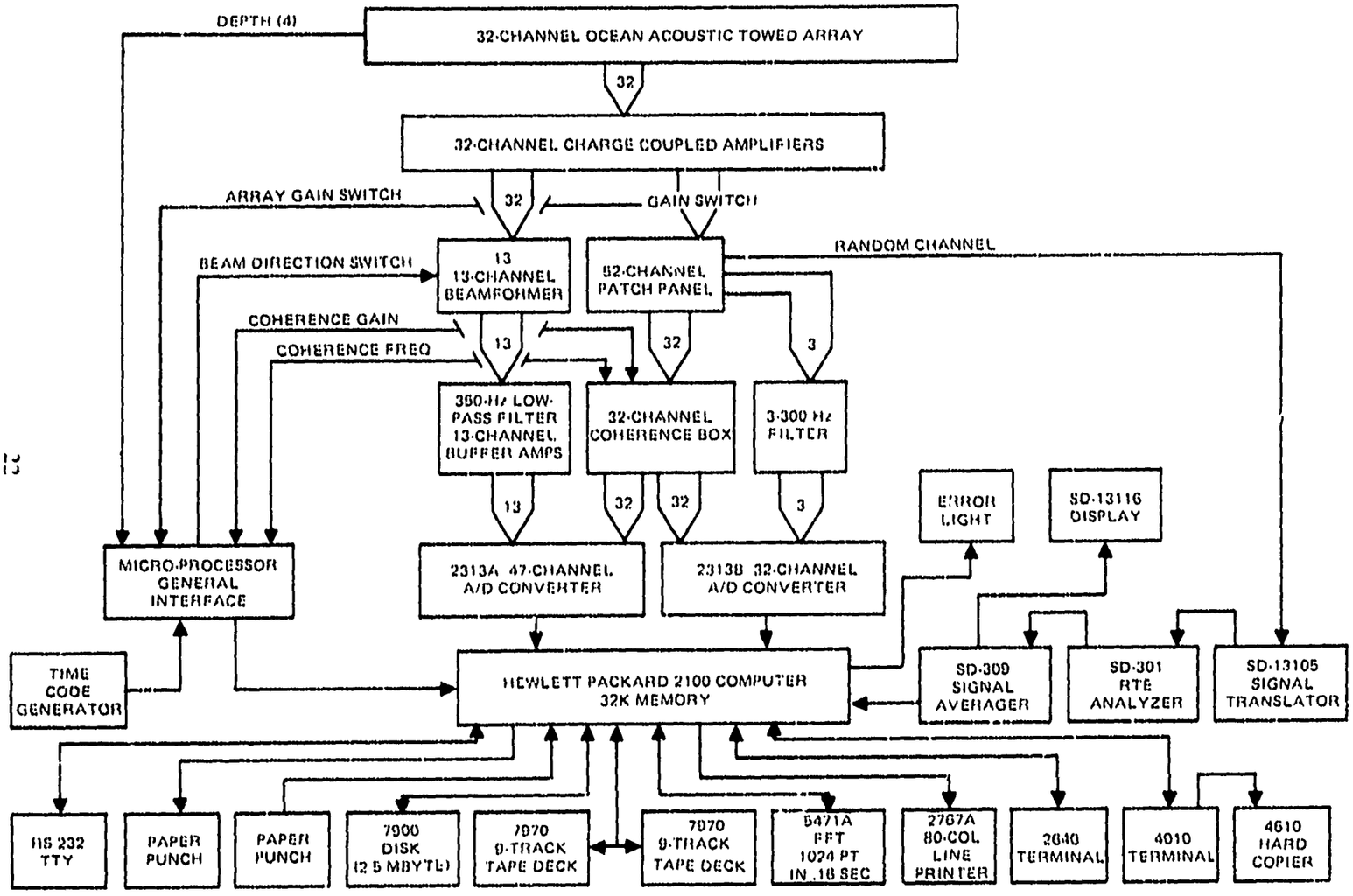

Figure 9. (C) Ocean acoustic measurement system (OAMS), block diagram. (U)

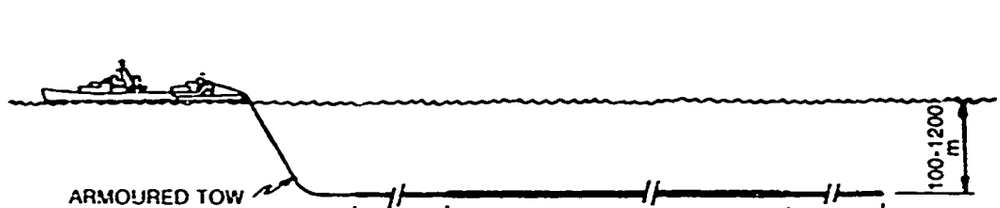

Figure 10. (C) LATA configuration. (U)

course, speed and voice annotation as shown in Fig. 11. The resulting serial bit stream (500 kbps) was recorded on a single track of a SANGAMO digital tape recorder. The bandwidth of the recorded acoustical data was 5 to 226 Hz. The on-board processing and relay system consisted of a demultiplexing unit, a digital filter (with 32 selectable filter bands), and digital "delay-and-sum" beamformer with four shading options with a "deselect" (i.e., zero weighting for any hydrophone group) option, a beam averager, and a ROLM 1602 digital computer for hydrophone group output and beam data processing. This computer was operated in the real-time mode throughout the data-taking periods for coherence measurements. The on-shore LATA processing was conducted at NOSC and is discussed in Ref. 12.

2.2.3 (U) The Bottom-Mounted Array (BMA)

(U) The BMA consisted of eight unequally spaced omnidirectional hydrophones and was installed at all five BEARING STAKE sites. WECo was responsible for installing the BMA at each site from the MYER and for collecting analog tape data from the BMA. Figure 12 illustrates the physical configuration of the BMA installed at Site 1A. Figure 13 shows the BMA hydrophone configuration at Site 1B, and Fig. 14 shows the configurations at Sites 3, 4, 5 and 2. Although the the BMA and the OAMS array were co-located at Sites 3, 1B and 4 (see Figs 3 through 5), the BMA was configured as a horizontal line array only at Sites 3 and 1B (see Figs. 13 and 14). Hence, comparison between the BMA and the OAMS data was confined to Sites 3 and 1B.

(U) To ensure the compatibility of the BMA data with the OAMS data, the BMA analog tapes were played back into the OAMS instrumentation (i.e., through the quadrature detector, the A/D converter and the HP2100 computer system) *in situ* and afterwards at NOSC. This put the BMA coherence data on digital magnetic tape in quadrature format for further processing and analysis (see Section 2 and Ref. 11). Thus, the BMA coherence data analysis is especially well coordinated with the OAMS array data analysis and allows a detailed comparison of their respective results (see Section 3).

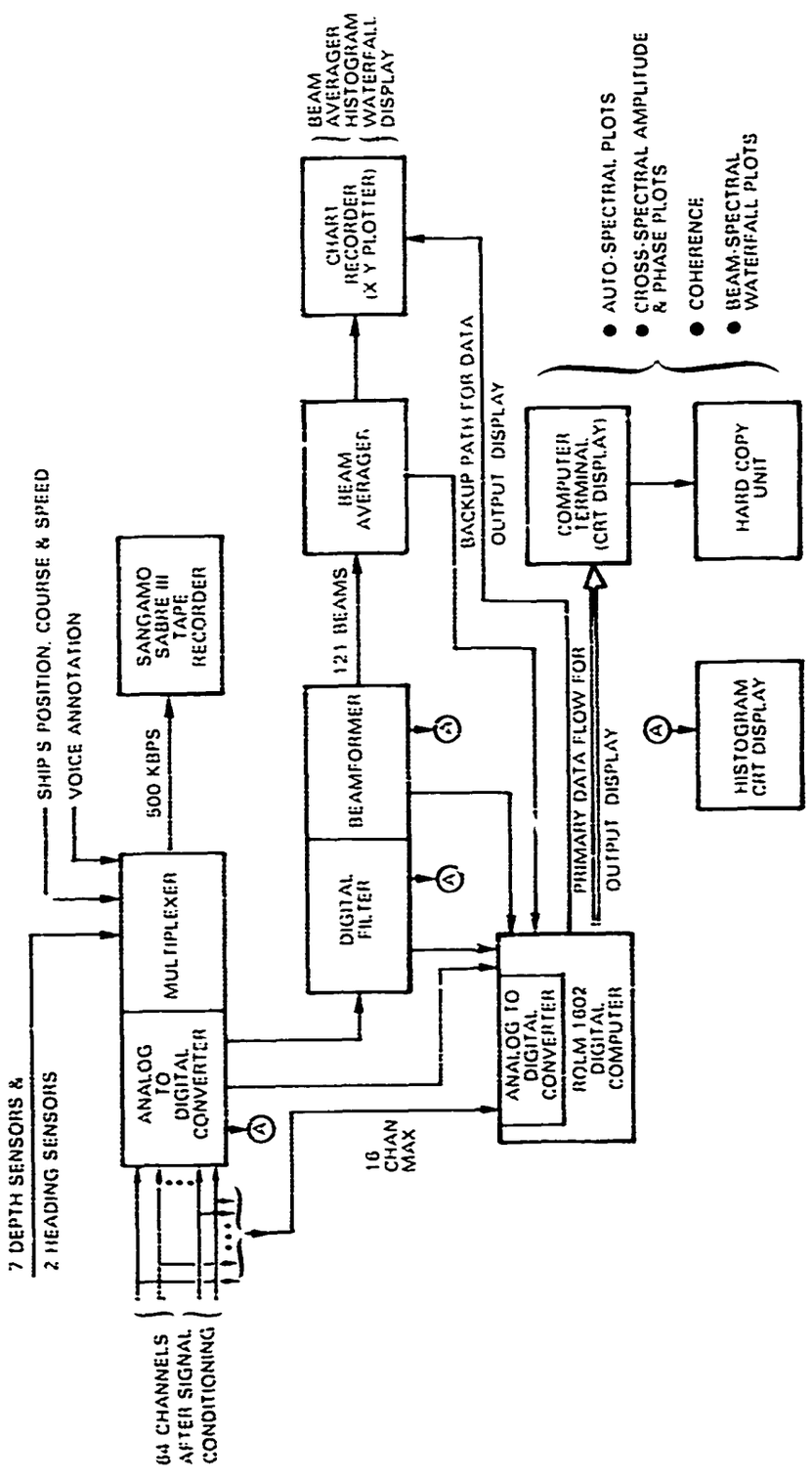

Figure 11. (C) Block diagram of LATA signal processing and display system. (U)

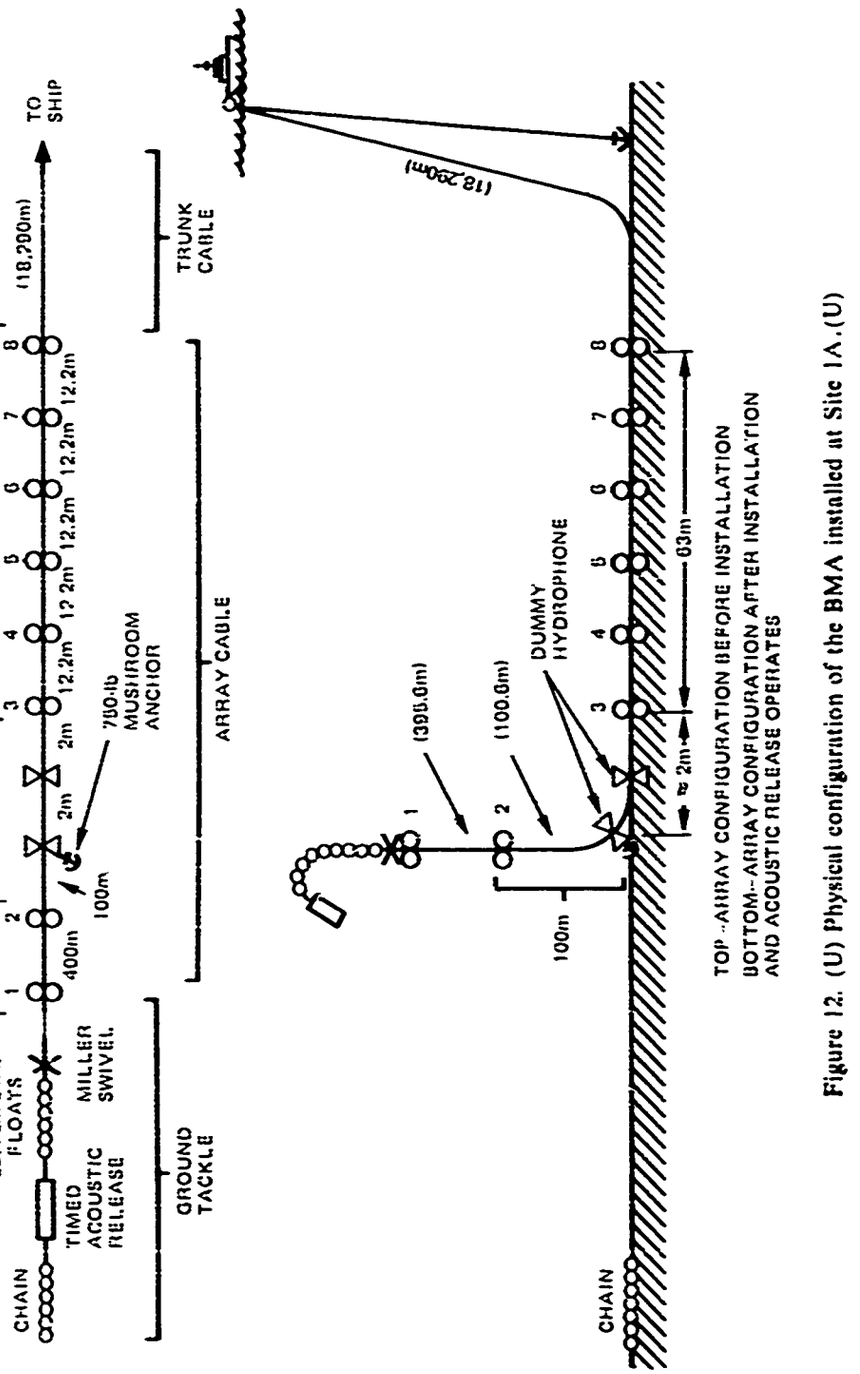

Figure 12. (U) Physical configuration of the BMA installed at Site 1A.(U)

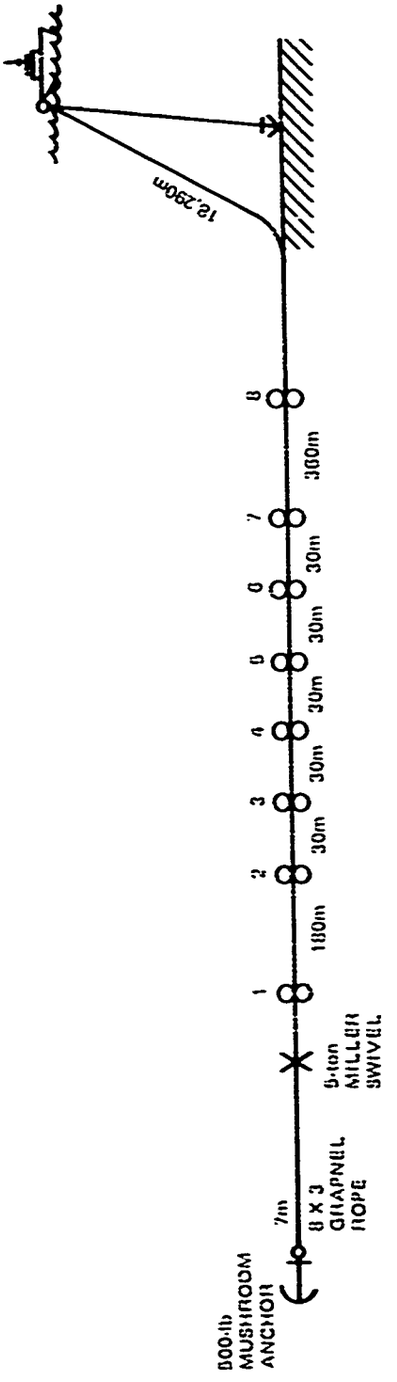

Figure 13. (U) BMA configuration at Site 1B.(U)

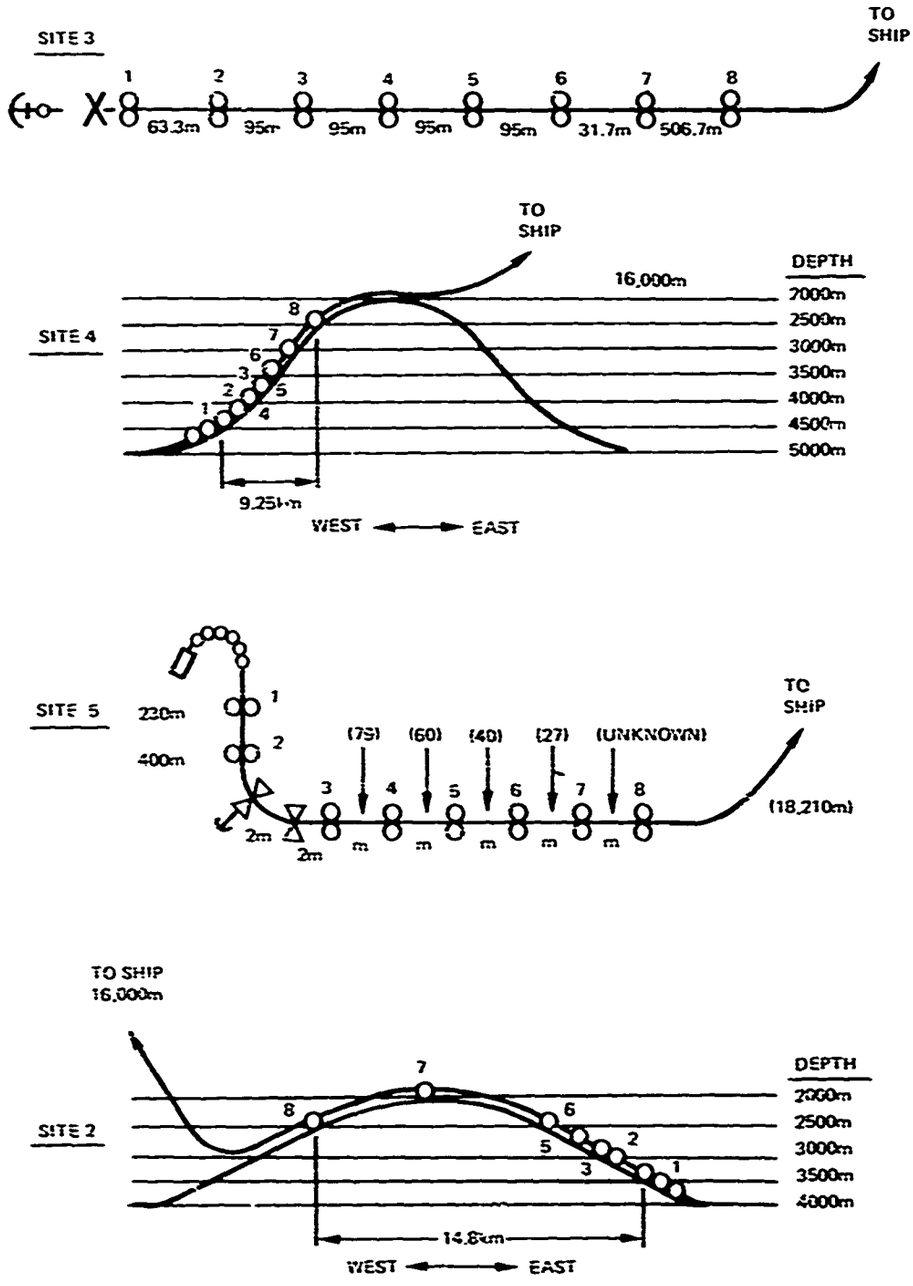

Figure 14. (U) BMA configuration at Site 3, Site 4, and Site 2. (U)

2.3 (U) ACOUSTIC SOURCES

(U) Both narrowband (CW) projector and broadband (explosive) sources were used during BEARING STAKE. Only the narrowband projectors will be discussed here because the coherence data are based on these CW sources.

(C) Two projectors were used: (1) a Minneapolis Honeywell HZ-295 transducer (140 and 290 Hz) and (2) a MK-6 projector driven at 22, 25, 36, 39 and 42 Hz. Source levels ranged from 176 dB/μPa to 195 dB/μPa as shown in Table 1.

Table 1. (C) The CW Projector Source Levels for BEARING STAKE. (U)

Frequency	Site	Source Level (dB/μPa)
22	all	188
25	all	190
36	all	192
39	all	193.5
42	all	195
140	1A	184
140	1B	183
140	2	181.5
140	3	182
140	4 except 4P7	186.5
140	4P7	180.5
140	5	181.5
290	all except 4P7	182
290	4P7	176

(the terminology 4P7 refers to projector tow P7 at Site 4, etc.)

(U) All projector tows were made from the KINGSPORT along the tracks shown in Figs. 2 through 6. The duty cycle for all projectors was 10 min on and 5 min off.* At Site 1A tows were made at a nominal speed of 12 knots. For Sites 3, 1B, 4 and 5, the MK-6 tow speed was reduced to 8 knots. At Site 2, a modified towing fairing installed on the MK-6 allowed tow speeds to be increased to 11 knots without source malfunctions.

(C) Minor problems arose in using the MK-6 projectors. The MK-6 was unable to stabilize at 42 Hz, as per specifications, at a tow speed above 8 knots and at a depth of 91 m. This problem was resolved by operating the MK-6 at 36 Hz at 8 knots and at a depth between 77.7 m (255 ft) and 83.8 m (275 ft). For the Hz-294 transducer the tow depth was 30 m.

*Actually the projector frequency was shifted by 3 or 5 Hz instead of being turned off.

2.4 (U) SOUND PROPAGATION CONDITIONS DURING BEARING STAKE

(U) Sound propagation conditions during BEARING STAKE are now discussed briefly in regard to their importance for this coherence study. Sound propagation near the five BEARING STAKE sites was very good. This good propagation occurred despite the "bottom-limited" conditions whereby the surface sound speed exceeds the bottom sound speed. This is seen in Fig. 15, where sound-speed profiles representative of the site areas and of the times of the exercises are shown. Of course, the source and receiver depths are also important since these really determine whether the significant ray paths interact with the bottom in a nominally bottom-limited situation. If the sound speed at the depth of the source (or receiver) is less than the bottom sound speed, then there is a "depth excess," so that there are ray paths from the source (or receiver) that do not contact the bottom. Their importance will depend on the amount of depth excess and how close such rays come to the receiver (or source). Thus, using Fig. 15, Table 2 is constructed to show the depth excesses from the source and receiver depths. Note that for the 91-m source, there was a depth excess only for Site 4. For the 200-m-deep OAMS array there was a depth excess for Sites 4, 5 and 2. Only for the 300-m-deep LATA was there a depth excess for all five sites. Since the longest acoustic wavelength relevant to this work (for 22 Hz) is 68 m, even the smallest depth excess (110 m) in Table 2 is significant.

Table 2. (U) Depth Excesses for Source and Receiver Depths for the Representative Sound-Speed Profile for Each Site. (U)

	Site				
Depth (m)	3	1B	4	5	2
91		–	490		–
200			1600	720	222
300	330	110	2200	1700	610

(U) Sites 1B and 4 are the extreme cases in Fig. 15; Figs. 16 and 17 give the ray trace plots for typical radial projector runs away from these two sites. Twenty-five rays at 1-deg intervals in the deflection elevation range of −12 to +12 deg are traced away from a 200-m-deep receiver for both figures. Figure 16 for projector tow 1BP1 (i.e., projecter tow P1 at Site 1B) shows that all those rays reflect from the bottom, while Fig. 17 for projector tow 4P1 shows that only the −12 and +12 deg rays contact the bottom. Note also that there are strong convergence zones observed for Site 4. Here the fifth zone is about 350 km, which gives an average zone spacing of about 58 km. Thus, with respect to this coherence area assessment work, it is noteworthy that the degree of bottom interaction did vary from site to site region, with the least near Site 4 and the most near Site 1B.

(U) Site 2 presents a special problem for the OAMS array since it received sound propagation from behind a seamount. See Fig. 6. Figure 18 gives a ray trace plot for a typical vertical plane over the seamount and away from the OAMS array. Although Fig. 18 shows the seamount interacting with most of the paths that reach the OAMS array, the predicted effect on transmission loss depends completely on the bottom-reflection loss (BRL) model assumed. If the propagation loss is calculated (via the RAYWAVE computer model program of Ref. 14) with the seamount replaced by a flat bottom, curve (a) of

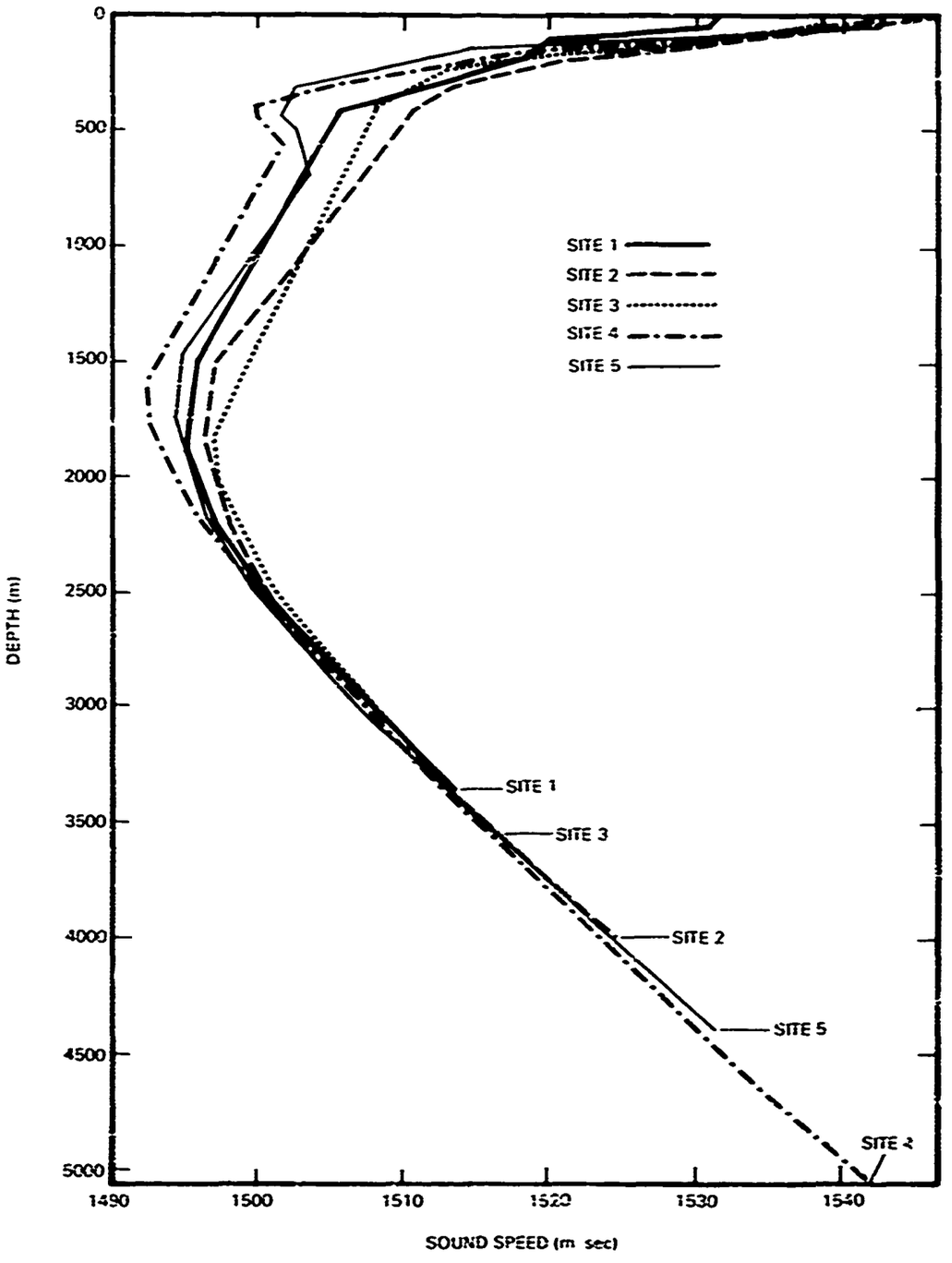

Figure 15. (U) Representative sound-speed profile for BEARING STAKE. (U)

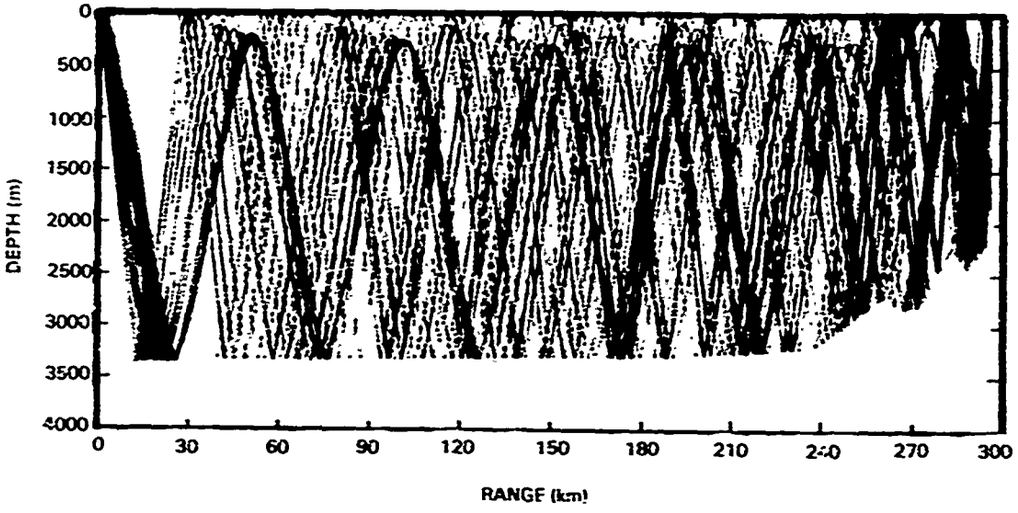

Figure 16. (U) Ray trace for projector tow 1BP1 track. (U)

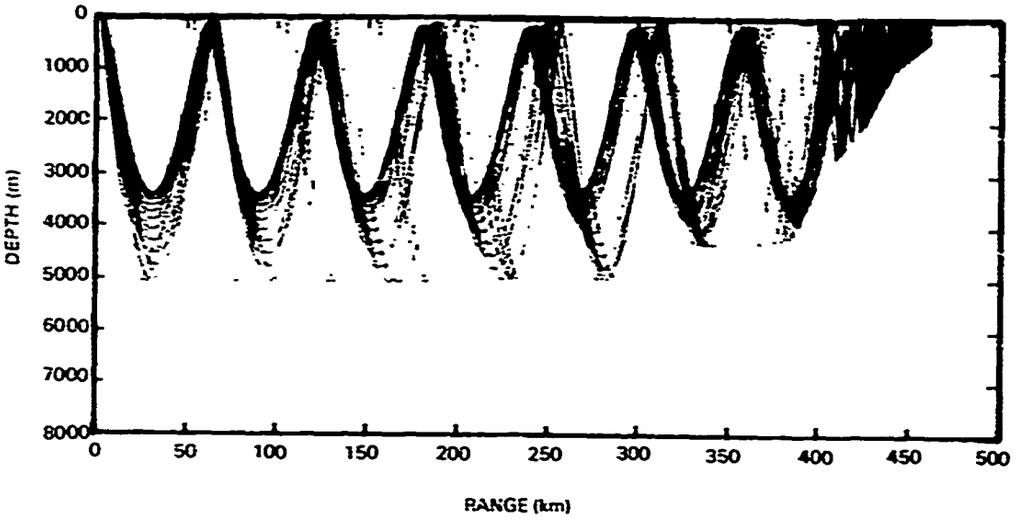

Figure 17. (U) Ray trace for projector tow 4P1 track. (U)

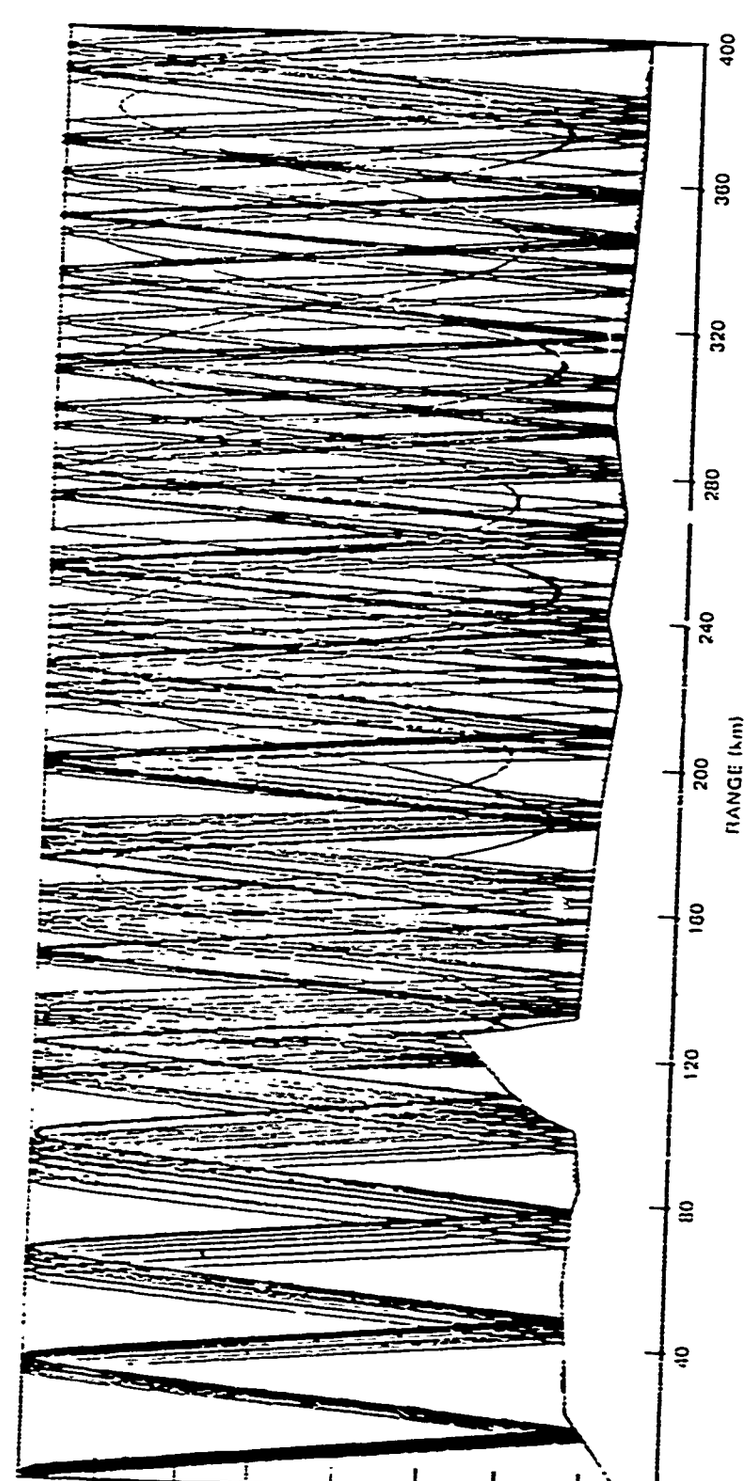

Figure 18. (U) Ray trace plot with seamount present. (U)

Fig. 19 results. The other three plots in Fig. 19 are for the seamount retained with various possible models of BRL versus grazing angle for rays contacting the sides of the seamount. The three cases of BRL behavior are as follows:

Curve	Seamount BRL Model
(b)	Same as for Site 3 (from Ref. 15)
(c)	Estimate for seamount slopes
(d)	Infinite loss for all grazing angles

Comparing curve (a) with the others shows that only for curve (d) is there some appreciable propagation loss at longer ranges due to the seamount. In Section 3.7.1 a comparison of the OAMS array received levels for projector tow 2P3A (with seamount interference) and for projector tow 5P1 (without seamount interference) shows that curve (d) agrees best with the observations.

(U) The preceding discussion of propagation conditions was based upon simplified, representative sound-speed profiles, such as those shown in Fig. 15. Thus, the smaller scale structure of the sound-speed profiles were neglected. This neglect may not be reasonable in considering certain aspects of array performance as the following discussion indicates.

(U) A mid-depth interval of sound-speed profile complexity is a characteristic feature of the western Indian Ocean (see Ref. 16). The BEARING STAKE sound speed profile measurements show that this complexity, marked by closely spaced relative maxima and minima with significant sound speed differences, was most pronounced in the Site 4 area. This was as expected, since the Red Sea is the source of the highly saline water that is the major cause of the sound-speed profile complexity. Figure 20 shows four sets of profiles collected along various Site 4 track events. Profiles for Sites 3, 1B, 5 and 2 also showed some similar complexity (see Figs. 21, 22, 23 and 24, respectively) and, for all five sites, the complexity began at roughly 250 m. Thus, the OAMS array operated above this mid-depth interval of complexity while the LATA operated in it; the BMA was always well below that depth interval. Since the propagation paths to all three arrays must pass through this mid-depth interval, some of the effects of the profile complexity should be the same for all three. However, it seems significant that the LATA coherence and array gain results (discussed in Section 3) display noticeably greater scatter than those for the OAMS array and the BMA. Since that scatter was clearly associated with multipath interference effects that were also more noticeable on LATA than on the other two arrays (see Ref. 12), it seems likely that the particular operating depth of the LATA is the explanation (particularly since the differences in array construction, discussed in Sections 2.2.2 through 2.2.4, did not account for this difference in the performances of the LATA and the OAMS array; see also the discussion of the "subset OAMS array" in Sections 3.3.3 and 3.4.3). This indication suggests that the Northwestern Indian Ocean is an area where the surveillance performance of towed arrays may be significantly dependent on the array tow depth.

(U) We now consider the effect that multipath propagation has on array beamforming. The study of Ref 17 shows that the presence of rapid increases in propagation loss (fades) as the range is varied is accompanied by a pronounced nonlinearity of phase, i.e., the

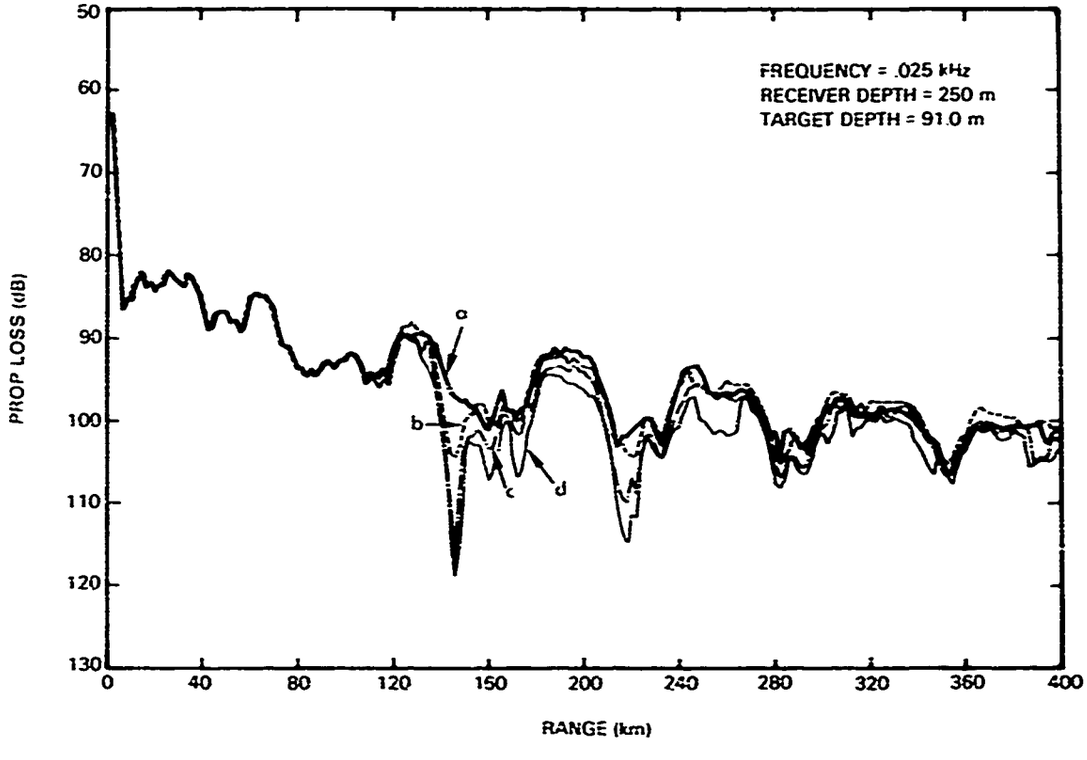

Figure 19. (U) Propagation loss for various seamount models. (U)

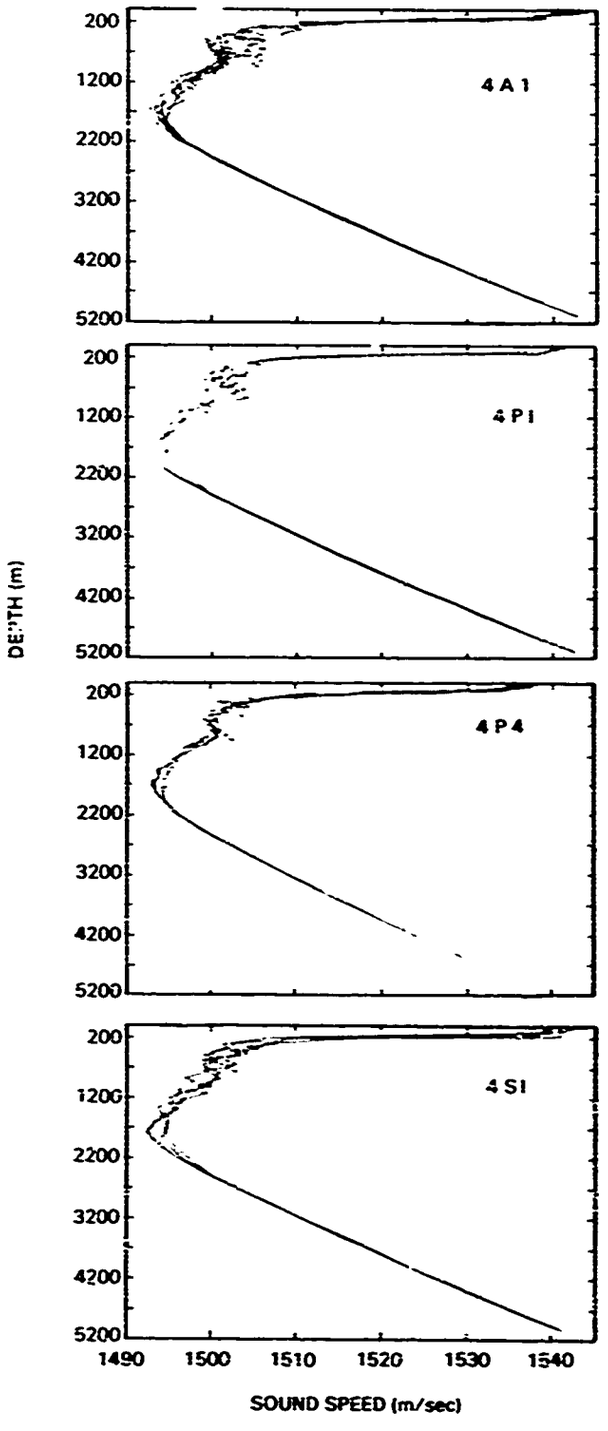

Figure 20. (U) Detailed sound-speed profiles near Site 4. (U)

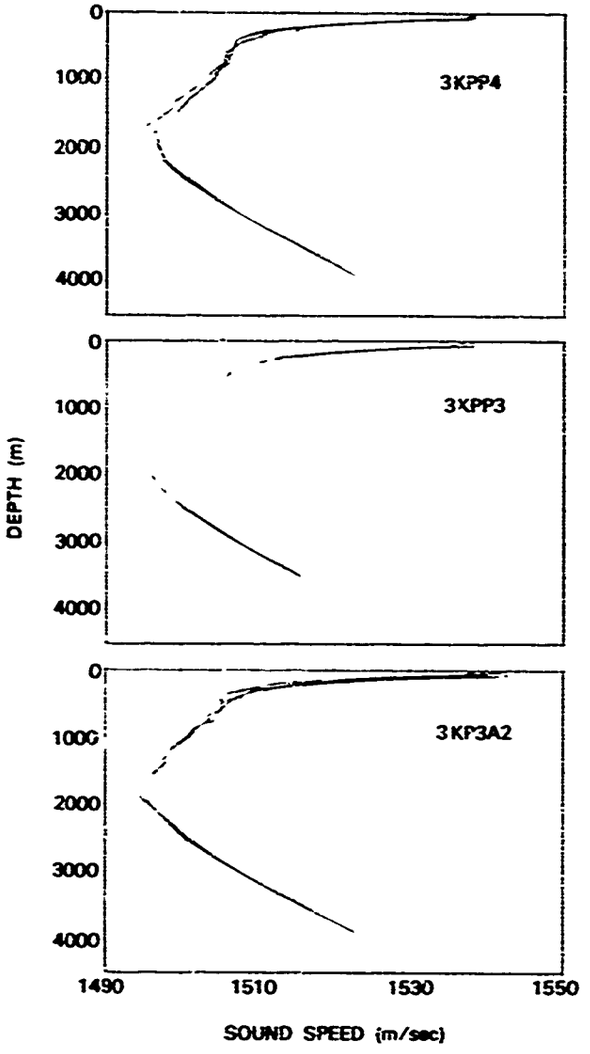

Figure 21. (U) Detailed sound-speed profiles near Site 3. (U)

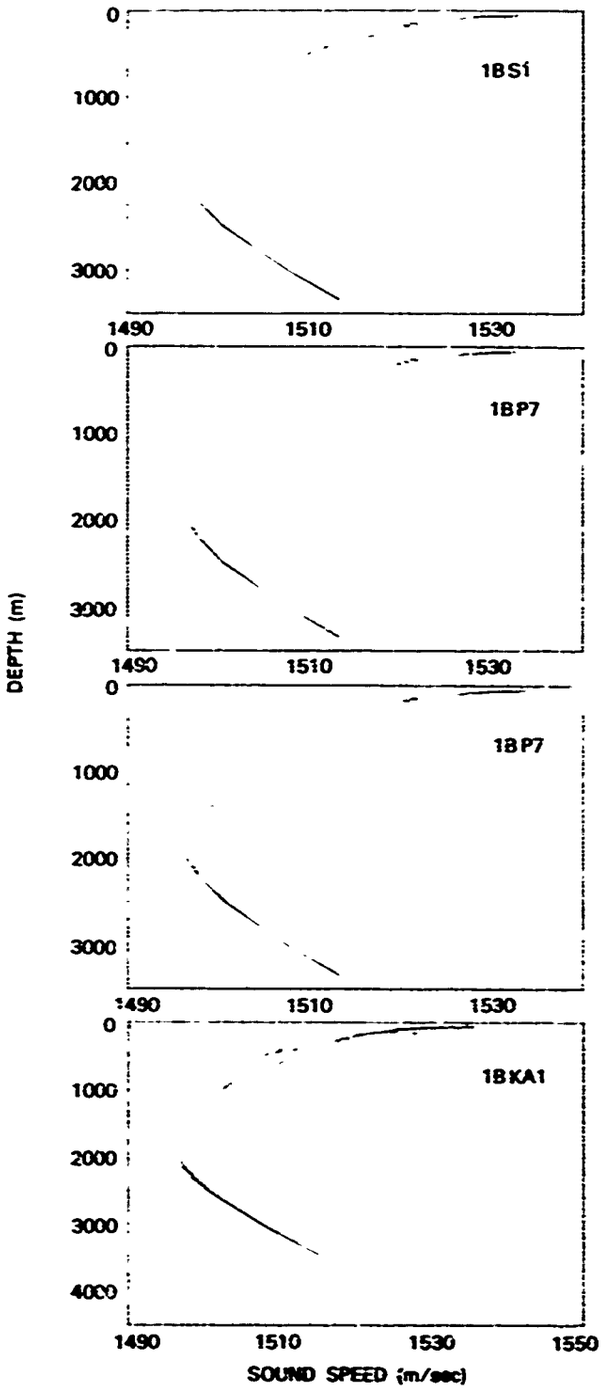

Figure 22. (U) Detailed sound-speed profiles near Site 1B. (U)

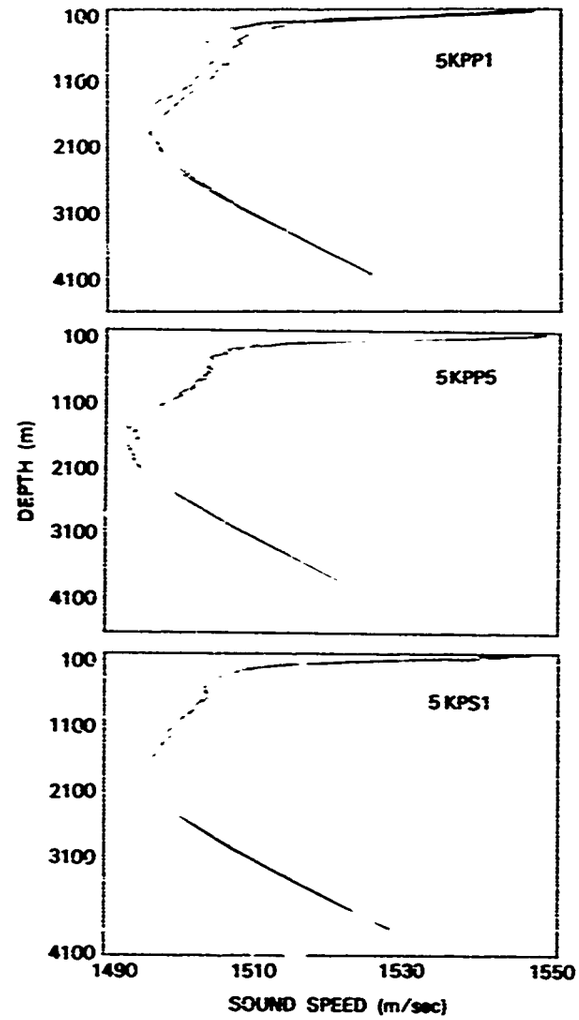

Figure 23. (U) Detailed sound-speed profiles near Site 5. (U)

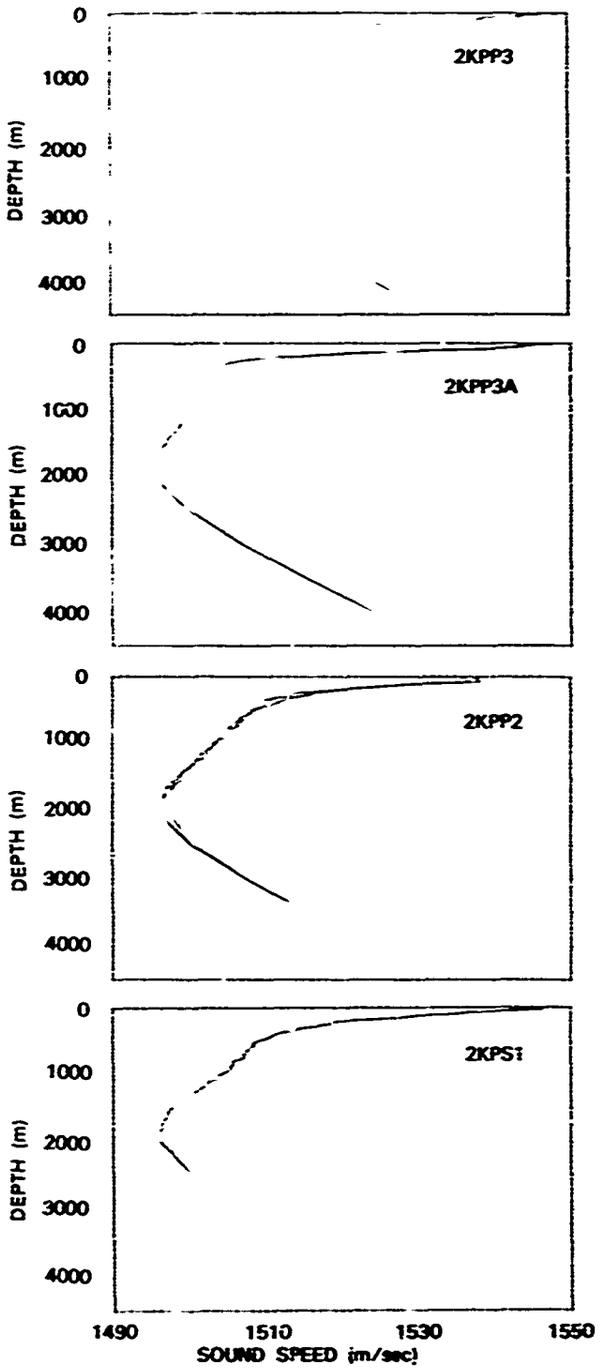

Figure 24. (U) Detailed sound-speed profiles near Site 2. (U)

phase relationships between receivers is no longer a linear function of the spatial displacement between receivers. Examples from Ref. 17 show that rapid increases of 23, 18, and 14 dB were accompanied by a departure from linear phase of 140, 115, and 100 deg, respectively, for receivers on opposite sides of the fade. Reference 17 points out that the effect of nonlinear phase is a decrease of several dB in array signal gain as well as possible bearing errors.

(U) The fades result from multipath interference. Since the bottom losses for most BEARING STAKE sites are very small at low frequencies we may anticipate a large number of fades due to multipaths. In order to examine this effect, a normal mode model of coherent propagation loss was developed for Site 1B based on a typical sound-speed profile and on a detailed sub-bottom structure.

(C) Figure 25 presents the normal model propagation loss at 25 Hz as a function of range over the range interval from 175 to 225 km. The receiver depth is fixed at 3348.9 m and corresponds to the bottom-mounted ACODAC at Site 1B. The dots are the experimental measurements of the ACODAC. The propagation is indeed characterized by large numbers of fades.

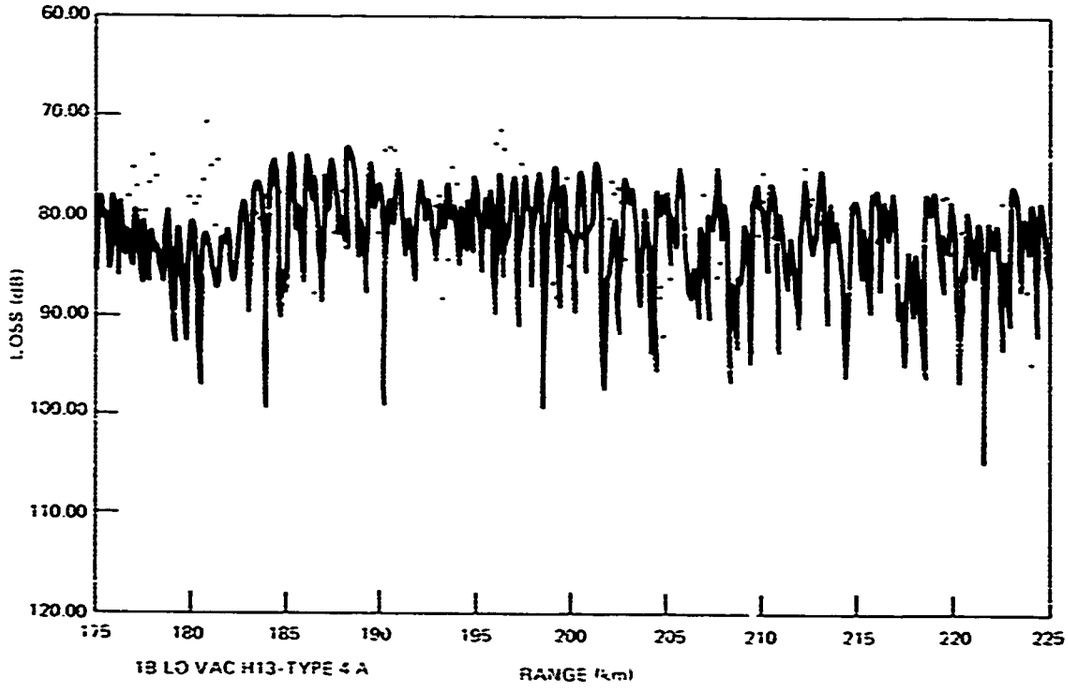

Figure 25 (C) Theoretical and experimental propagation loss at 25 Hz for a receiver on the ocean bottom (C)

(C) The number of fades was counted over various range intervals and expressed as the average distance between fades. For example, in Fig. 25 the average distance between fades exceeding 5 dB os 0.9 km. For fades exceeding 10 dB the average distance is 2 km. Computation made over the same range interval at 50 Hz yielded corresponding values of 0.6 and 1.3 km, respectively. Computation for other range intervals showed a strong range dependence. For example, in the range interval from 25 to 75 km one could, on the average, expect a 10-dB fade every 1.4 km at 25 Hz and every 0.8 km at 50 Hz. The corresponding values at 463 to 550 km are 3.6 and 2.2 km. This range dependence results because the number of multipaths is reduced by bottom loss. Reference 18 discusses similar computations made under convergence zone conditions in the Pacific and Atlantic for this latter interval of 463 to 550 km. Values obtained for 10-dB fades at 25 and 50 Hz were from 10.3 to 20.5 km and from 6.9 to 30.8 km, respectively. It then appears that 10-dB fades in propagation loss for the Indian Ocean occur at least three times as often as they do for convergence zone propagation in the Atlantic or Pacific Oceans. We may then anticipate more problems with array beamforming in the Indian Ocean than in the Atlantic or Pacific Oceans.

(U) The study just described involved looking at the variation with range for a fixed receiver depth. This variation would be applicable to a horizontal array in an endfire configuration. However, the LATA and the OAMS array were operated in a near-broadside configuration.

(U) The nominal depth of the front end of the OAMS array was 200 m, with an upward tilt of about 1 deg. The corresponding values for the LATA were 300 m and 1.5 deg. Since the OAMS array is 925 m long, the nominal depth of the tail end was about 189 m. The corresponding values for LATA were 1200 and 269 m. Thus, even in a broadside configuration, the arrays are subject to a variation in propagation loss from element to element due to the fact that the elements are at different depths.

(C) The nominal range of interest for an examination of array performance was given as 200 km. Figure 26 is a propagation loss contour plot generated by the normal mode model for Site 1B at a frequency of 25 Hz. Contours are presented at 5-dB intervals from 85 to 95 dB. The receiver depth interval covered is from 180 to 345 m and the range interval is from 195 to 205 km. This plot covers the depth intervals of interest for the two arrays. The propagation loss plot of Fig. 26 exhibits a "patchiness" which is characteristic of a large number of bottom bounce multipaths. Figure 26 presents a good overview of the situation, but does not provide the detail necessary to assess the amount of variation in propagation loss across each array.

(U) This variation was assessed by a special normal mode computer run adapted to determine the variation in propagation loss over some given depth interval for a fixed range. The given depth intervals were from 187 to 200 m in 2-m steps and from 270 to 300 m in 3-m steps. These intervals correspond to nominal array tilts of 1.1 deg for the OAMS array and 1.4 deg for the LATA. The normal mode program was run from 195 to 205 km in range increments of 50 m. This results in 201 range samples.

(C) Figure 27 presents propagation loss as determined by the normal mode program at a frequency of 50 Hz. Propagation loss is shown as a function of receiver depth over the interval of 270 to 360 m at fixed ranges of 196.0, 196.2, and 196.4 km. The variation

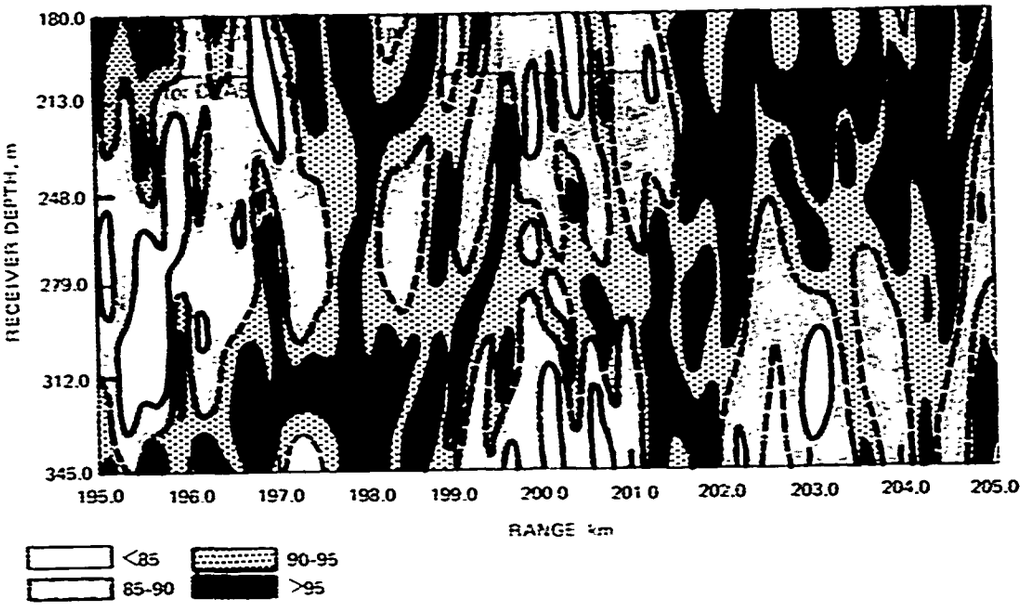

Figure 26 (U) Propagation loss contour plot for 25 Hz using 79 modes, 5-dB contours from 85 to 95 dB, source at 102 m (U)

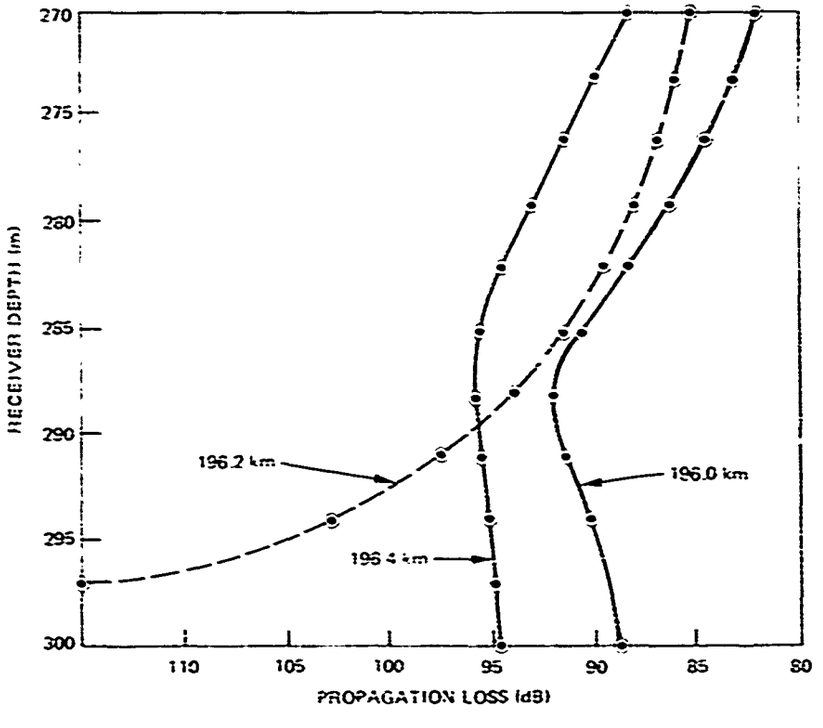

Figure 27 (C) Propagation loss at 50 Hz vs receiver depth at fixed ranges of 196.0, 196.2, and 196.4 km (C)

across this depth interval is 8.4, 29.8, and 7.0 dB, respectively, for the three fixed ranges. This example was chosen to depict a very deep fade. Since computations are made in range increments of 50 m, there are three additional range cuts available between 196.0 and 196.2 km and also between 196.2 and 196.4 km. These data have also been plotted but are not presented here. These additional data show a smooth transition between the cuts shown in Fig. 27. On the basis of the data sample and on other samples, it has been established that the range and depth sampling considered here is adequate to determine the variability across the interval.

(C) All of the data for the special normal mode computer runs were summarized in terms of the percentage of range samples for which the propagation loss variation over the depth interval (for the fixed-range sample) exceeded 5 dB and then 10 dB. The results for several different configurations and for frequencies of 25 and 50 Hz are summarized in Table 3. For example, at 25 Hz, 8 percent of 201 range samples (i.e., 16 samples) had a 10-dB or greater variation over the depth interval from 187 to 200 m.

Table 3. (C) Percentage of Range Cuts in the Range Interval from 195 to 205 km for which the Depth Variation in Propagation Loss over the given Depth Interval exceeds 5 dB and 10 dB. (U)

ROW	FREQ. (Hz)	DEPTH INTERVAL (m)	DEPTH STEP (m)	5 dB	10 dB
1	25	187-200	2 m	25	8
2	25	270-300	3 m	45	16
3	25	170-200	3 m	41	15
4	50	187-200	2 m	46	17
5	50	270-300	3 m	66	31
6	50	170-200	3 m	68	31

(C) Rows 1 and 4 pertain to the OAMS array configuration and rows 2 and 5 to the LATA configuration. The first important feature to note is that the percentage values for the LATA are larger than for the OAMS array at both frequencies. This is in agreement with the experimental measurements of coherence, which were generally better for the OAMS array than for the LATA. The question now arises as to whether this is a result of the OAMS array and the LATA being at different depths. This was examined by making calculations for the interval from 170 to 200 m. Thus, the results of rows 3 and 6 represent the case where the LATA is placed at 200 m rather than 300 m. Note that the results of row 2 are close to those of row 3 and the results of row 5 are close to those of row 6. Thus, the important feature for this model is not the difference in the nominal depth of LATA. The significant feature is that the longer length and larger tilt angle of the LATA result in a larger depth interval and an increased chance of large variation in propagation loss along the array. In other words, comparing rows 2 and 3 and rows 5 and 6 of Table 3 shows that, for this model, which does not consider a region of mid-depth sound-speed profile complexity, there is no depth dependence for the variation of propagation loss.

It attributes increased variation to an increased depth interval for the LATA. However, a subset LATA (configured in sensor spacing similarity to the OAMS array — see Ref. 12) showed that the depth interval (not including tilt differences) did not account for the increased LATA C_p and ASG variation. Thus, the depth-dependent sound-speed profile complexity remains the most plausible cause of the increased C_p and ASG variation for the LATA, and using a sound-speed profile that does have a mid-depth region of complexity should resolve this question.

(C) The second important feature of Table 3 is that the percentages increase with frequency. Indeed the values in the "10 dB" column for 50 Hz are almost exactly twice as large as the corresponding 25-Hz values. Thus, the percentages scale directly as the frequency in this case. Since the percentage cannot exceed 100 percent, the dependence on frequency cannot continue to be linear but must saturate. The values in the "5 dB" column begin to show the effect of saturation. The ratios of rows 4 to 1, 5 to 2, and 6 to 3 are, respectively, 1.8, 1.5, and 1.7 rather than a 2.0 ratio of frequencies. There were no LATA or OAMS array measurements at 50 Hz. However, the coherence measurements were very poor at frequencies of 140 and 290 Hz (see Ref. 10). The calculations of Table 3 strongly suggest that variation across the array is a principal cause of the loss of coherence. The present study was limited to a frequency of 50 Hz because of storage limitations in the normal mode computer program. Computations at 140 Hz could be made but would be relatively expensive, require considerable effort and are beyond the scope of the present study.

(C) The adequacy of the range sampling in generating Table 3 was tested at 25 Hz by calculating percentages of range samples taken at 100-m range increments. These percentages were essentially the same as those already described for 50-m range increments. It appears then that 100-m increments were adequate for 25 Hz and, since the sampling rate should be proportional to frequency, 50-m increments should be adequate for 50 Hz. The adequacy of the sampling rate was also determined by the investigation of Fig. 27 as previously discussed.

(U) There is a further question about the normal mode results which is not answered by Table 3. What is the distribution of range intervals for the categories of Table 3, i.e. do the percentages of Table 3 result from many small isolated intervals or from several hugh contiguous intervals? As the initial step in addressing this question, two pieces of data from row 5 of Table 3 were investigated in detail, i.e., the distribution of range intervals where the variation was under 5 dB and over 10 dB.

(U) Figure 28 presents the percentage of range samples as a function of run length. For example, for 8.5 percent of 201 range samples (i.e., 17 samples) the variation was over 10 dB for a single 50-m interval. The longest range interval for which the variation was over 10 dB was 300 m and this occurred only once. However, the variation was less than 5 dB over three intervals which were 250 m long.

(U) Consider now the case where the variation was under 5 dB. The longest range interval for which the variation was less than 5 dB was 350 m and this occurred twice. Intervals of 150, 200, and 250 m occurred only once, once, and twice, respectively.

(U) An analysis, similar to that of Fig. 28, was made for all the configurations in Table 3. The first three columns of Table 4 are the same as those of Table 3. The next

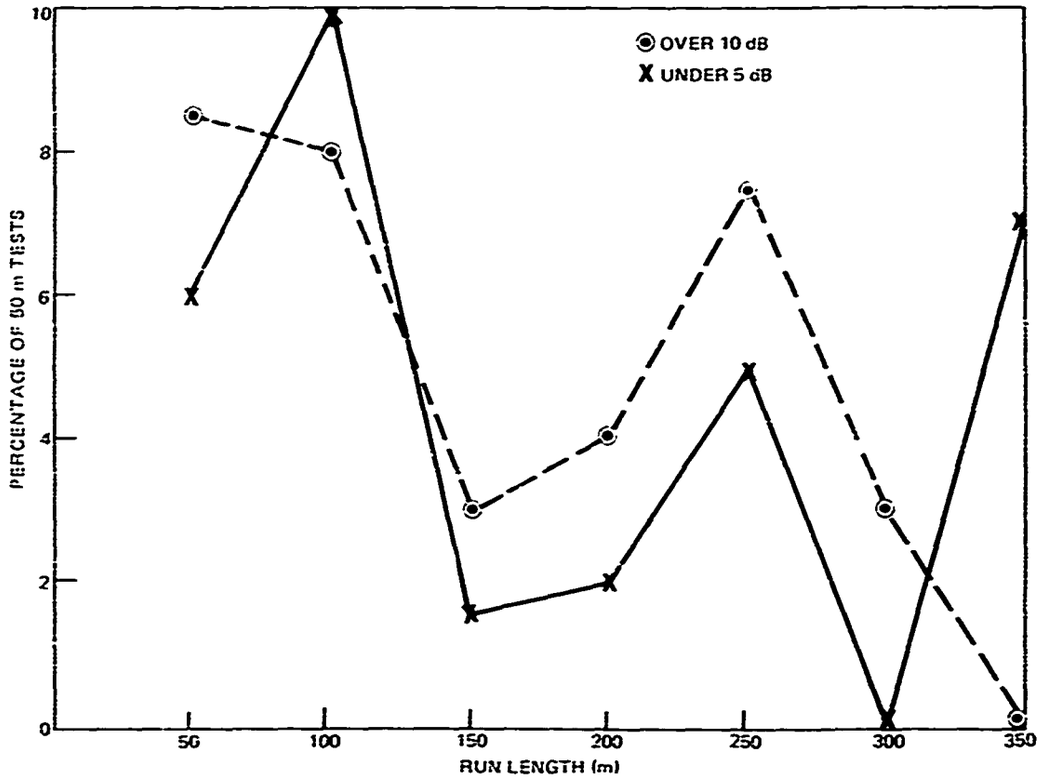

Figure 28. (C) Percentage of 50-m range cuts vs run length over which the depth variation in propagation loss at 50 Hz exceeds 10 dB or is less than 5 dB. (C)

Table 4. (C) Length of three longest Range Intervals for which the Depth Variation in Propagation Loss is less than 5 dB or greater than 10 dB. (U)

			VARIATION LESS THAN 5 dB			VARIATION GREATER THAN 10 dB		
ROW	FREQ	DEPTH INTERVAL (m)	LONGEST (m)	2ND (m)	3RD (m)	LONGEST (m)	2ND (m)	3RD (m)
1	25	187-200	1600	700	650	150	150	100
2	25	270-300	900	650	550	250	150	150
3	25	170-200	1550	500	500	400	300	250
4	50	187-200	600	500	500	200	200	150
5	50	270-300	300	150	150	350	350	250
6	50	170-200	350	350	300	500	400	300

three columns of Table 4 present the length of the three longest runs in the data where the variation in propagation loss over the depth interval was less than 5 dB. The last three columns of Table 4 are the corresponding values for instances in which the variation is greater than 10 dB.

(C) Note that the run lengths for less than 5 dB are greater at 25 Hz than their 50-Hz counterparts. This is not unexpected because it is already known that the fades occur much more often at 50 Hz. These fades break up the less than 5-dB regions, resulting in shorter run lengths. In contrast, the run lengths for greater than 10 dB are longer at 50 Hz than for their 25-Hz counterparts. This result is somewhat surprising and may depend on the particular level (i.e., 10 dB) chosen for analysis.

(U) In any case Table 4 and Fig. 28 indicate that the propagation is quite patchy. The process is not statistical in the sense that it is random. The process is variable, with a structure that is not clear-cut so that it may be described in some statistical sense.

(U) Note that in 10 out of 12 cases, the entries of row 3 and row 6 are longer than those of row 2 or row 5, respectively. This suggests that the patch sizes are longer for a depth of 200 m than for a depth 300 m. Thus, array performance might be more sporadic at the deeper depth. This may account in part for the difference between the OAMS array and the LATA performance.

(U) The application of Table 4 to towed arrays depends on range rate and integration time. The range rate at Site 1B was 8 knots, or 247 m minute. The integration time for both the OAMS array and the LATA was 4 min. Thus, the range changed by 988 m over the integration time. A determination of the exact manner in which fades affect array coherence is beyond the scope of this investigation. However, whenever a fade appears across the array during the integration time, a nonlinear component of phase will be included in the processing procedure and the coherence will be degraded to some extent.

(U) Consider now that the patch size over which no significant fades occur is x and that the integration time corresponds to a range interval y. The probability that y lies completely within x is the following:

$$0 \text{ for } x \leqslant y \quad . \tag{1a}$$

$$\frac{x - y}{y} \text{ for } y \leqslant x \leqslant 2y \quad . \tag{1b}$$

and

$$1 \text{ for } x \geqslant 2y \quad . \tag{1c}$$

(C) As an example of the application of this analysis, assume that no significant degradation occurs if the variation in propagation loss is less than 5 dB. Thus, x takes on the values of columns 4 to 6 of Table 4 while y is 988 m, corresponding to a 4-min integration time and 8-knot range rate. The only values of x for which the probability is not zero are the two longest run entires in Table 4 at 25 Hz. The probability of these entries for the OAMS array is 0.62, while the probability for the LATA at 200 m depth is 0.57. Based on this assumption, performance would be poor even at 25 Hz because there is only one run interval over the range from 195 to 205 km where a detection could be made.

There are no such intervals at 50 Hz. This analysis is hypothetical. However, it provides a reasonable explanation of measured observations, i.e., array coherence is sporadic with range, array coherence is better for the OAMS array than for the LATA, and array coherence is very poor at higher frequencies.

(C) We anticipate that the general conditions investigated here theoretically for Site 1B would also hold for Sites 1A, 2, 3, and 5. Site 4, however, is not bottom-limited but has a small depth excess. Convergence zones are prominent in propagation data at 290 Hz but appear indistinct at 25 Hz. There are two aspects of Site 4 which would tend to increase the patch size of good propagation and, hence, array coherence. The first aspect is the presence of convergence zones. The second is a greater bottom loss in the Somali Basin (Site 4) than in the Gulf of Oman or in the Indus Fan (remaining sites). This greater loss would reduce the number of multipaths and, hence, increase the patch size.

(U) This analysis of array coherence in terms of the variation of propagation loss across the array has been largely speculative. However, present plans call for a detailed theoretical study in FY 80 of array processing in the BEARING STAKE environment. A normal mode model would be developed for Sites 3, 4, and 5 as discussed here for Site 1B. The acoustic field as generated by the mode model would be used as inputs to the array processing, beamforming, and coherence algorithms. The theoretical outputs of these algorithms will be compared with those measured during the experiment. This analysis should also determine if there is a significant difference in the results of the OAMS array algorithms compared to the LATA algorithms. The question of optimum or improved algorithms for the BEARING STAKE environment should also be addressed.

3. (U) AREA ASSESSMENT OF COHERENCE AND ARRAY SIGNAL GAIN

3.1 (U) INTRODUCTION

(C) For BEARING STAKE, phase coherence processing was done at six frequencies (22, 25, 42, 36, 140 and 290 Hz) and at five sites (Site 3, 1B, 4, 5 and 2) for the OAMS array data, and the results are reported in Ref. 10. Phase coherence processing was done at 25 and 36 Hz and at Sites 3 and 1B for the BMA, and the results are reported in Ref. 11. Phase coherence processing was done at 22 and 25 Hz and at Sites 4, 5 and 2 for the LATA, and the results are reported in Ref 12. Array signal gain processing was done only at 25 Hz for the OAMS array, the BMA, and the LATA, and the results are reported in Ref. 13. The purpose of this section is to take this material from Refs. 10 through 13 and perform an area assessment of phase coherence and array signal gain for these five sites in the Northwestern Indian Ocean.

(U) The information for this phase coherence and array signal gain area assessment report is taken from Refs. 10 through 13 and is treated below in chronological order (i.e., Sites 3, 1B, 4, 5 and 2). The tables and figures from these references are prefixed by I, II, III and IV for Refs. 10, 11, 12 and 13, respectively. For example, Table 5 from Ref. 12 is denoted as Table III-5.

(U) The phase coherence and array signal gain data for all three arrays can be compared directly by using the timing of the data samples and the known positions versus

time of the arrays and of the projector tow ship. When the arrays are not co-located (Sites 5 and 2) the possibly different propagation conditions along the different propagation paths from the projector to the receivers should be kept in mind. Even when two arrays are co-located, their different depths have to be considered with regard to possible differences of major propagation paths to each receiver (see Section 2.4).

3.2 (U) EFFECT OF SOUND PROPAGATION ON AMPLITUDE FLUCTUATION

(U) Before beginning the site-by-site area assessment for BEARING STAKE, it is convenient to appraise the effect of multipath sound propagation on amplitude fluctuation over all the selected sites in the Northwestern Indian Ocean. In Section 2.4 the nature of sound propagation during the BEARING STAKE exercise was discussed on a site-by-site basis. It was shown that the degree of bottom interactions (as indicated by how many of the important rays contact the bottom and at what angles) was highest for Site 1B and lowest for Site 4.

(U) The tables in Ref. 10 give C_p [see Eq. (A-20)], Σ_A [see Eq. (A-15)], and S/N (the signal plus noise to noise ratio) for the OAMS array; these quantities for the BMA and the LATA are found in the tables of Refs. 11 and 12, respectively. These tables show that generally the degree of amplitude fluctuation, as measured by Σ_A, is largely range independent and does not increase much with frequency at each site and for each array. This behavior is shown in Table 5 on a site-by-site basis for each array (the OAMS array data covers all five sites while the BMA data applies only to Sites 3 and 1B, and the LATA data apply only to Sites 4, 5 and 2) and for signal plus noise and for noise.

Table 5. (U) The Degree of Amplitude Fluctuation, Σ_A. (U)

	OAMS		BMA(3,1B)/LATA(3,5,2)	
	Signal plus Noise	Noise	Signal plus Noise	Noise
Site 3	0.3-0.5	0.5-0.6	0.3-0.5	0.5-0.55
Site 1B	0.3-0.5	0.5-0.6	0.25-0.5	0.5-0.55
Site 4 (before "crush event")	0.2-0.4	0.5-0.6	0.2-0.5	0.5-0.55
Site 4 (after "crush event")	0.3-0.6	0.6	0.2-0.5	0.5-0.55
Site 5	0.3-0.5	0.55	0.2-0.5	0.5-0.5
Site 2	0.4-0.55	0.55	0.2-0.5	0.55

(U) The S/N levels for the OAMS array were high and comparable for Sites 3, 1B, 4 and 5 and significantly lower for Site 2, where the seamount was present (see Section 2.4). Still Table 5 shows that the values of Σ_A are comparable for all these sites. However, a closer scrutiny of Table 5 does reveal some agreement with three phenomena that occurred during BEARING STAKE. Note that Site 4 is divided into two parts in the table: before

and after the "crush event." The "crush event" occurred at 0400Z on 16 March 1977, when the OAMS approached its nominal crush depth (305 m). See Ref. 10 for more details. Note that OAMS signal plus noise amplitude fluctuations were less at Site 4 before the "crush event" than after it, suggesting that the individual hydrophones are producing more self-noise after having been damaged by the "crush event." (This interpretation is supported by noting that the OAMS noise amplitude fluctuation was also increased after the "crush event.") This is the first phenomenon that is discernible in Table 5. The second is seen by noting that the OAMS signal plus noise amplitude fluctuations are less at the first part of the Site 4 test than at any previous site. This occurs because the propagation conditions were less disturbed by bottom interaction at Site 4 than at the other sites, which were bottom-limited (e.g., compare Figs. 16 and 17). The third phenomenon relates to the OAMS array being towed behind the seamount during the Site 2 exercise (as discussed in Section 2.4). Note in Fig. 6 that projector tows for Sites 5 and 2 overlap in the Indus Fan. Therefore, it appears that the main difference between projector tows 5P1 and 2P3A is the presence of the seamount between the 2P3A projector tow track and the OAMS array. As observed from the tables in Ref. 10, the S/N values are lower for Site 2 than Site 5 by about 5 dB. Table 5 agrees with this by showing higher OAMS signal plus noise amplitude fluctuation at Site 2 than at Site 5.

(U) Here are some further observations from Table 5. With respect to BMA and OAMS signal plus noise amplitude fluctuation behavior, Sites 3 and 1B are essentially the same. Note that at both Sites 3 and 1B that the BMA and OAMS signal plus noise amplitude fluctuation behavior is essentially the same. The LATA (in contrast to the OAMS) fails to detect less signal plus noise amplitude fluctuation at Site 4 (which has little bottom interaction) than at Site 5 (which is bottom-limited). In fact, the LATA sensed similar signal plus noise amplitude fluctuation at Sites 4, 5 and 2. This appears to be due to the more complex sound-speed profile that occurs at the LATA tow depth; see Section 2.4. Note that Sites 3 and 1B for the BMA and Sites 4, 5 and 2 for the LATA are essentially the same with respect to signal plus noise amplitude fluctuation. Finally note that the noise amplitude fluctuation as measured with all three arrays is quite similar at all five sites.

3.3 (U) DISCUSSION OF SITE 3

3.3.1 (U) OAMS Array Phase Coherence and Array Signal Gain

(C) The OAMS phase coherence data analysis for Site 3 is summarized in Tables I-1 through I-9 and in Figures I-2 through I-28 (Ref. 10) for 25, 42, 140 and 290 Hz. The OAMS array signal gain data analysis for Site 3 is summarized in Tables IV-1 through IV-3 and Figures IV-2 through IV-7 (Ref. 13) for 25 and 42 Hz. The tables give ΔT (the averaging time interval) $20 \log_{10} A_a$, the source bearing $\bar{\Phi}$ [see Eq. (A-3)], C_p, Σ_A, C_T [see Eq. (A-13)], ASG [for weighted and unweighted beamformers; see Eq. (A-24)], S/N (the signal plus noise to noise ratio in dB), and the range R. Based upon these results some observations can be made about the phase coherence (as measured by C_p) and the array signal gain (as measured by ASG) at Site 3 for the OAMS array.

(C) The OAMS array phase coherence and array signal gain data were taken on three linear projector tows across the center of the Indus Fan; see projector tows 3P1 (i.e., projector tow P1 for Site 3), 3P3 and 3P4 in Fig. 3. The relevant figures and tables of Ref. 10 show that the phase coherence decreases severely as the frequency increases from 25 to 290 Hz, while the S/N values remain comparable and high. This S/N behavior is explained as follows. Although the projector source level was less at higher frequencies and although the propagation loss increases with frequency due to higher bottom reflection losses, the ambient noise level also was less at higher frequencies, and this kept the S/N values high. While there is a decrease in phase coherence with increasing frequency (while S/N remains high), which is relevant to array performance for these higher frequencies (i.e., 140 and 290 Hz), the real significance of this trend must be considered in terms of array length divided by the wavelength. This is important because it has been observed that coherence can decrease as the aperture length (in units of wavelength) increases. Therefore, the best way to compare arrays at different frequencies is in terms of phase coherence for constant aperture length in units of wavelength. This latter procedure is suggested for more detailed studies of phase coherence versus frequency.

(C) Figures I-2 through I-10 (Ref. 10) and Figures IV-2 through IV-7 (Ref. 13) show that the phase coherence and the array signal gain, respectively, are generally range independent up to about 310 km. As an example see Figs. 29 and 30, which correspond to projector tow 3P4 at 25 Hz. (For examples of 140- and 290-Hz results, see Figs. 31 and 32, respectively.) Note the wide variability of C_p and ASG with range due to multipath interference in this bottom-limited environment with its complex sound-speed profile structure (see Section 2.4). Reference 12 discusses the varying structure of the signal field along the array that causes the high variability of C_p and ASG. The scatter of values that appear in Figs. 29, 30, etc. is due to undersampling of rangewise continuous functions. Figures IV-2 and IV-3, IV-4 and IV-5, and IV-6 and IV-7 show that the values of ASG are somewhat better for the Hamming-weighted OAMS array than for the unweighted array. This is, of course, not surprising in a multipath environment since the weighting decreases the contribution to ASG of sensor group pairs at greater separations, i.e., reducing the effective array aperture.

3.3.2 (U) BMA Phase Coherence and Array Signal Gain

(C) The BMA phase coherence data analysis for Site 3 is summarized in Tables II-1 and II-2 and in Figures II-5 and II-6 (Ref. 11) for 25 and 36 Hz. The BMA array signal gain data analysis for Site 3 is summarized in Tables IV-14 and IV-15 and in Figures IV-28 and IV-29 (Ref. 13) for 25 and 36 Hz. The BMA phase coherence and array signal gain data were taken on two straight projector tows across the center of the Indus Fan; see projector tows 3P2 and 3P4 in Fig. 3. Figures II-15 and II-16 and Figures IV-30 and IV-31 show that the phase coherence and the array signal gain, respectively, are generally range independent up to 300 km. As an example, see Figs. 33 and 34, which correspond to projector tow 3P4 at 25 Hz. Note the wide variability of C_p and ASG with range that was observed in Section 3.3.1.

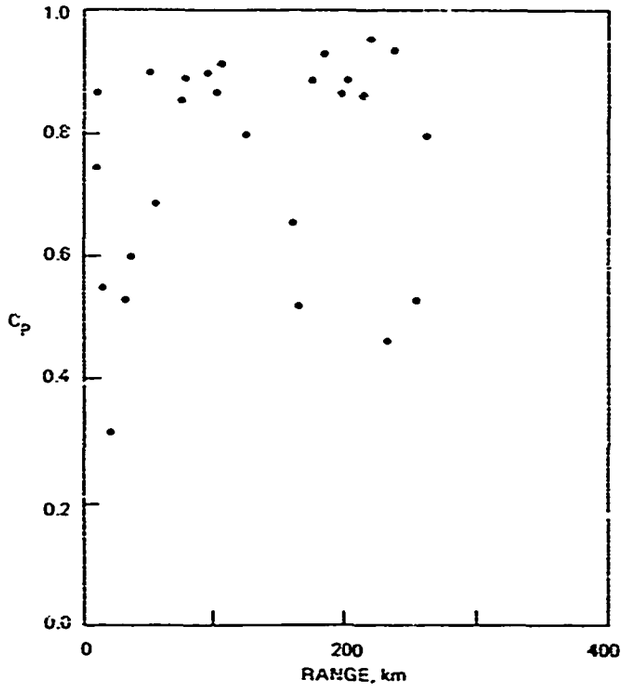

Figure 29. (C) Phase coherence as a function of range; OAMS array; Site 3; track 3P4; 25 Hz; 10-11 February 1977. (C)

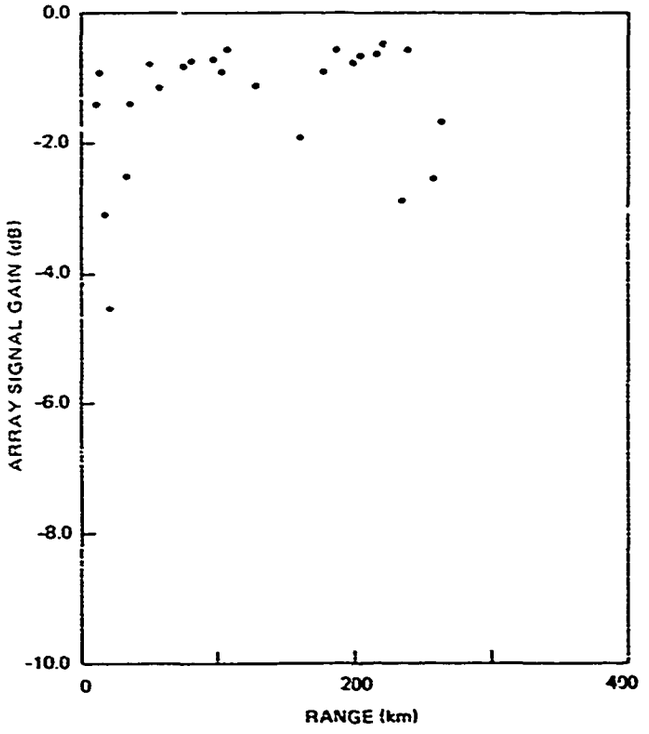

Figure 30. (C) Array signal gain vs range, calculations with unity weights. OAMS array; Site 3, track 3P4; 10-11 February 1977; 25 Hz. (C)

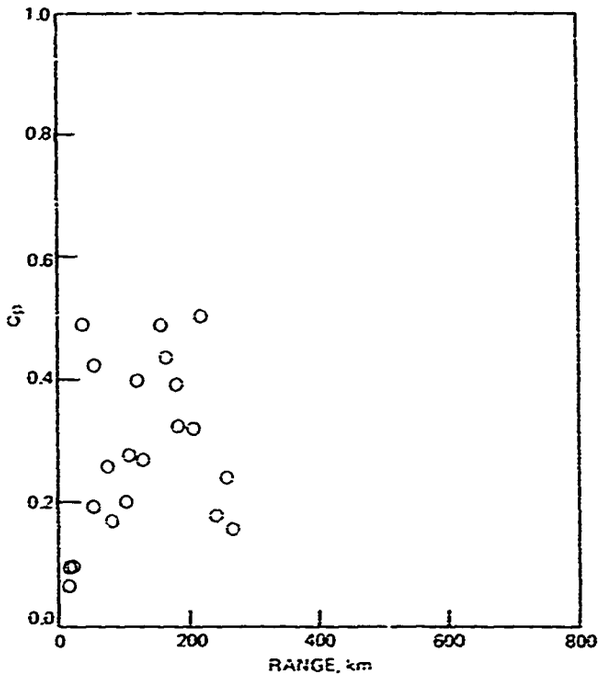

Figure 31. (C) Phase coherence as a function of range: OAMS array: Site 3: track 3P4: 140 Hz: 10-11 February 1977. (C)

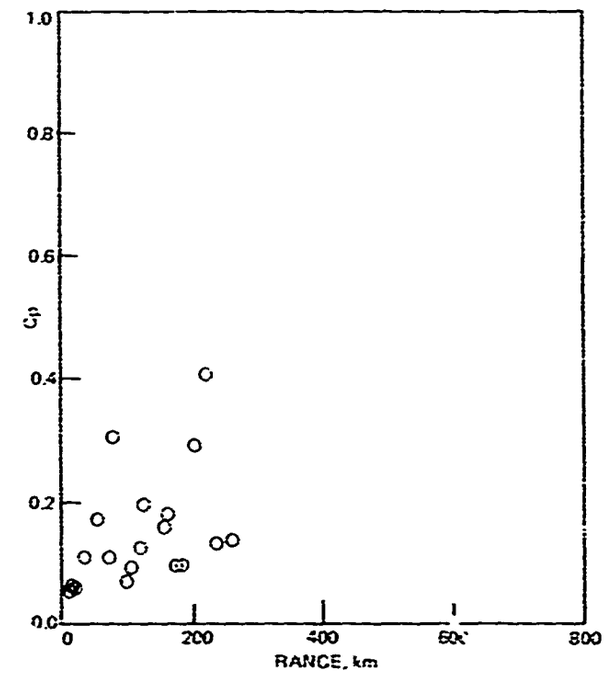

Figure 32. (C) Phase coherence as a function of range: OAMS array: Site 3: track 3P4: 290 Hz: 10-11 February 1977. (C)

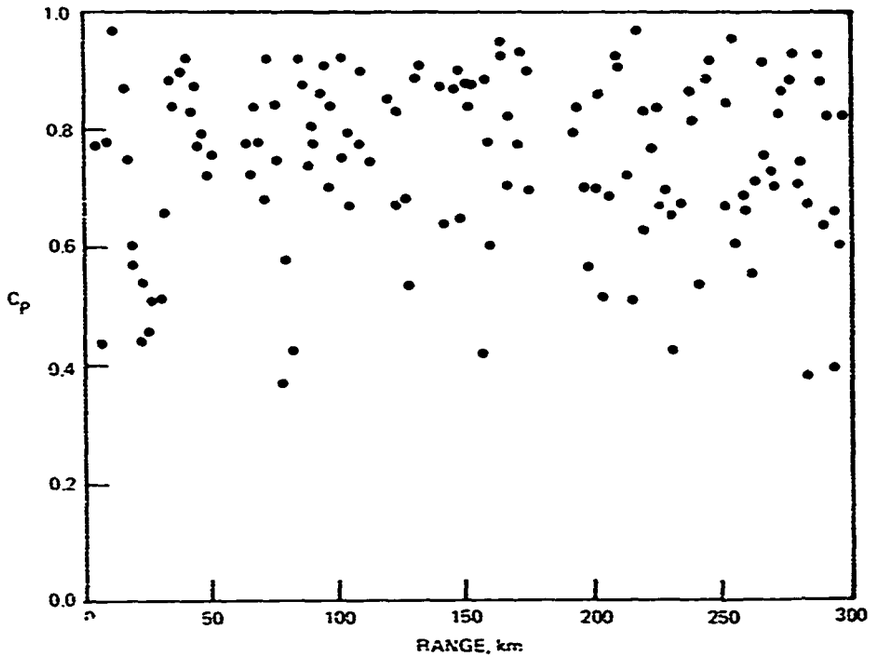

Fig 3. (C) Phase coherence as a function of range. BMA; Site 3, track 3P4; 10-11 Feb ary 1977; 25 Hz. (C)

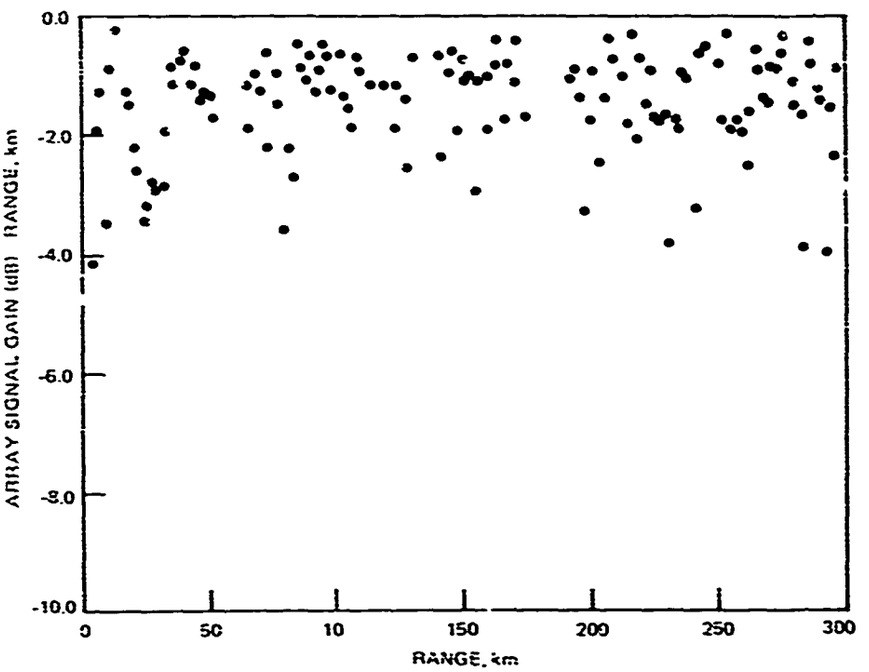

Figure 34. (C) Array signal gain vs range, calculations with unity weights. BMA, Site 3; track 3P4; 10-11 February 1977; 25 Hz. (C)

3.3.3 (U) Comparison of the BMA and the OAMS Array

(C) Figures 29, 30, 33, and 34 give the relative phase coherence behavior and the relative array signal gain behavior on projector tow 3P4 of the OAMS array (with the source bearing near 90 deg) i.e., near broadside and the BMA (with the source bearing near 16 deg) as a function of range at 25 Hz. As can be seen from these figures, the performances of the bottom-mounted and the mid-depth towed arrays are comparable. Therefore, it appears that for this bottom-limited region of the Northwestern Indian Ocean, the phase coherence and the array signal gain performances are essentially the same for bottom-mounted and mid-depth towed arrays. As was shown in Ref. 11, the sensor spacing for the BMA at Site 3 was considerably different from that for the OAMS array. To obtain a more nearly accurate comparison of the towed array with the BMA, a subset OAMS array (configured similarly in sensor spacing to the BMA at Site 3) was studied. References 11 and 13 show that this subset towed array performed essentially the same as the bottom-mounted array with regard to phase coherence and array signal gain behavior. Incidentally, Figures IV-6, IV-7 and IV-35 show that the unweighted total and subset OAMS arrays are similar in ASG range-wise performance, while the weighted OAMS array slightly outperforms both these cases.

3.4 (U) DISCUSSION OF SITE 1B

3.4.1 (U) OAMS Array Phase Coherence and Array Signal Gain

(C) The OAMS array phase coherence data analysis for Site 1B is summarized in Tables I-10 through I-12 and in Figures I-29 through I-31 (Ref. 10) for 25, 140 and 290 Hz. The OAMS array signal gain data analysis for Site 1B is summarized in Table IV-4 and in Figures IV-8 and IV-9 (Ref. 13) for 25 Hz. The OAMS array phase coherence and array signal gain data were taken on one linear projector tow over the Oman Basin; see projector tow 1BP1 in Fig. 4. The relevant figures and tables of Ref. 10 show that the phase coherence decreases severely as the frequency increases from 25 to 290 Hz while the S/N values remain comparable and high. This is similar to the behavior for Site 3 and the explanation given in Section 3.3.1 applies here also. Figures 35 and 36 show that the phase coherence and the array signal gain is generally range independent up to about 200 km, where they decrease somewhat with range out to about 300 km. This decrease in phase coherence and array signal gain corresponds to the source being towed over an irregular sloping bottom as shown in Fig. 4. There is no significant decrease in S/N values during the tow over the sloping irregular bottom, so the decrease in phase coherence and array signal gain appears to be caused by the irregularity of the bottom contour. Note the wide variability in C_p and ASG with range due to multipath interference is increased by the irregular bottom slope region. Comparing Figures IV-8 and IV-9 shows that the values of ASG are somewhat better for the weighted OAMS array than for the unweighted array. This was also observed in Section 3.3.1.

3.4.2 (U) BMA Phase Coherence and Array Signal Gain

(C) The BMA phase coherence data analysis for Site 1B is summarized in Tables II-3 through II-7 and in Figures II-21 through II-35 (Ref. 11) for 25, 36, and 42 Hz. The

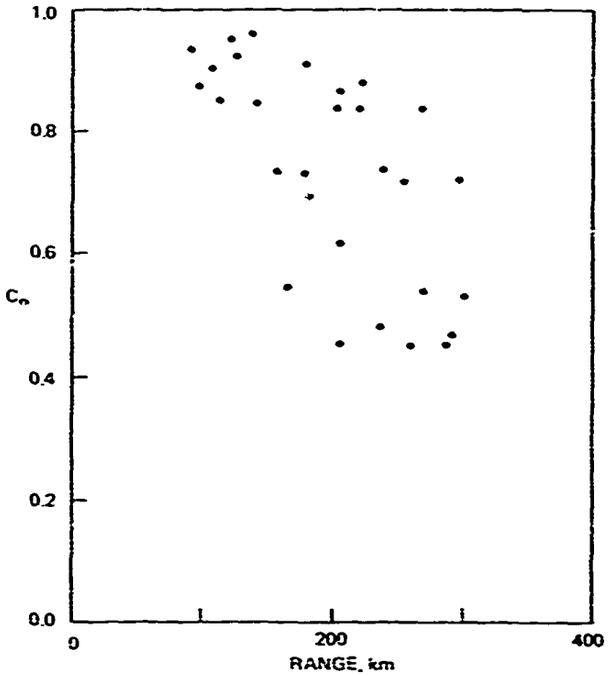

Figure 35. (C) Phase coherence as a function of range: OAMS array: Site 1B; track 1BP1; 25 Hz; 19-20 February 1977. (C)

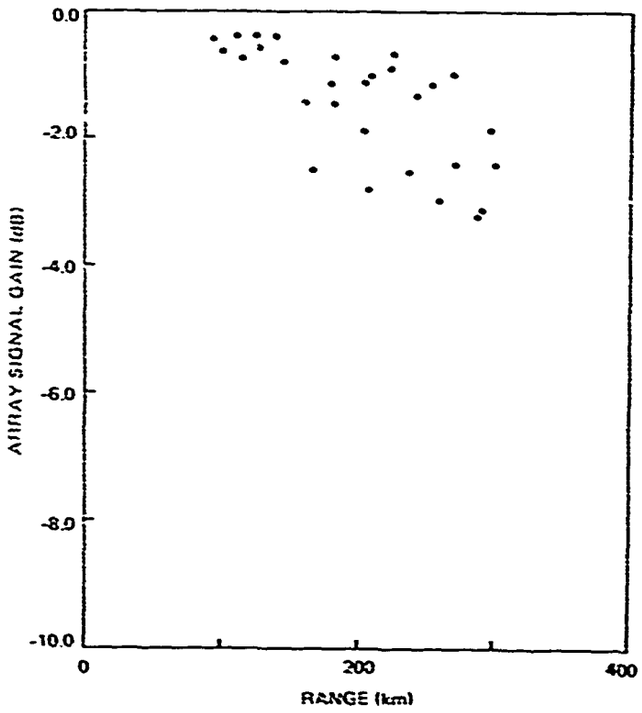

Figure 36. (C) Array signal gain vs range, calculations with unity weights. OAMS array: Site 1B; track 1BP1; 19-20 February; 25 Hz. (C)

BMA array signal gain data analysis for Site 1B is summarized in Tables IV-16 through IV-20 and in Figures IV-30 through IV-34 (Ref. 13) for 25, 36, and 42 Hz. The BMA phase coherence and array signal gain data were taken on five projector tows over the Oman Basin: see projector tows 1BP1, 1BP4, 1BP3, 1BP2 and 1BP5. Only the results for projector tow 1BP1 are of interest here since the results for the other tows agree with the behavior for tow 1BP1 discussed. Figures 37 and 38 show that the phase coherence and the array signal gain are generally range independent up to about 300 km, and the irregular bottom slope has no apparent effect on ASG beyond 200 km. Note the wide variability of C_p and ASG with range due to multipath interference is not increased by the irregular bottom slope region.

3.4.3 (U) Comparison of the BMA and the OAMS Array

(C) Figures 35 through 38 give the relative phase coherence behavior and the relative array signal gain behavior on projector tow 1BP1 for the OAMS array (with the source bearing generally between 75 and 100 deg) and the BMA (with the source bearing near 160 deg) as a function of range at 25 Hz. As can be seen from these figures, for the bottom-mounted array the phase coherence and the array signal gain showed no rangewise increase in variability and no rangewise change due to the irregular bottom slope (possibly due to the presence of bottom paths). On the other hand, for the mid-depth towed array, the phase coherence and the array signal gain decreased and became more variable as the projector was towed over the irregular sloping bottom. Observe that the phase coherence behavior and the array signal gain behavior of the bottom-mounted and the mid-depth towed arrays were comparable before the irregular bottom sloping ranges (this is in agreement with the results for projector tow 3P4 in Section 3.3.3). Therefore, it appears that for this bottom-limited region (near Site 1B) of the Northwestern Indian Ocean the phase coherence and the array signal gain performances are essentially the same for bottom-mounted and mid-depth towed (above 250 m; see Section 2.4) arrays except for the irregular bottom slope region. Figures 29, 30, and 33 through 38 show that the phase coherence behavior and the array signal gain behavior at Site 3 and at Site 1B (until the irregular bottom slope region) are comparable for the BMA and the OAMS array. Therefore, it appears that there is no significant difference in phase coherence and array signal gain behavior between these two sites. This is especially true due to the wide rangewise variability of C_p and ASG caused by the multipath interference in these bottom-limited regions with their complex sound-speed profiles. As was shown in Ref. 11, the sensor spacing for the BMA at Site 1B was considerably different from that for the OAMS array. To obtain a more nearly accurate comparison of the towed array with the BMA, a subset OAMS array (configured similarly in sensor spacing to the BMA at Site 1B) was studied. References 10 and 11 show that this subset towed array performed essentially the same as the bottom-mounted array with regard to phase coherence and array signal gain behavior except that the BMA behavior was much less disturbed by the irregular sloping bottom. This latter phenomenon may indicate that the BMA was receiving a significant amount of sound propagation through bottom paths. Incidentally, Figures IV-8, IV-9 and IV-36 show that the unweighted and the subset OAMS arrays are similar in ASG rangewise behavior, while the weighted OAMS array slightly outperforms both these cases.

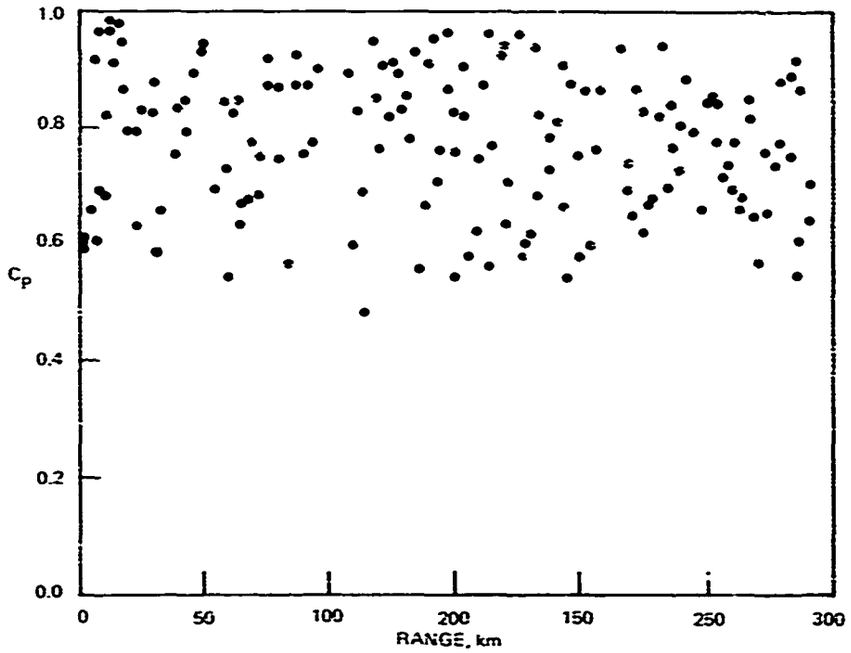

Figure 37. (C) Phase coherence as a function of range. BMA; Site 1B; track 1BP1; 19-20 February 1977; 25 Hz. (C)

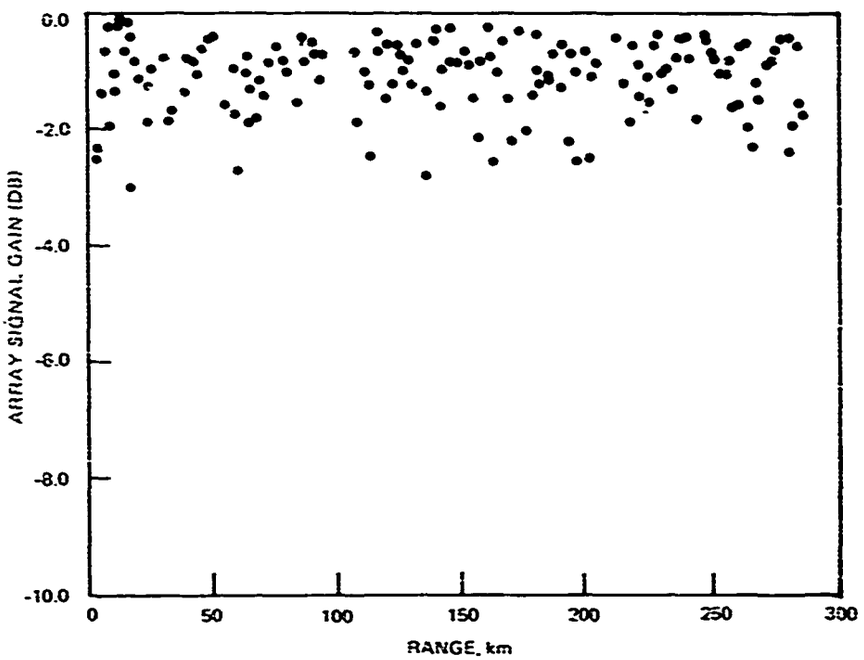

Figure 38. (C) Array signal gain vs range, calculations with unity weights. BMA; Site 1B, track 1BP1; 19-20 February 1977; 25 Hz. (C)

3.5 (U) DISCUSSION OF SITE 4

3.5.1 (U) OAMS Array Phase Coherence and Array Signal Gain

(C) The OAMS phase coherence data analysis for Site 4 is summarized in Tables I-13 through I-20 and in Figures I-38 through I-41 (Ref. 10) for 25, 36 and 140 Hz. The OAMS array signal gain data analysis for Site 4 is summarized in Tables IV-5 through IV-7 and in Figs. IV-10 through IV-15 (Ref. 13) for 25 and 36 Hz. The OAMS array phase coherence and array signal gain data were taken on three projector tows in the Somali Basin: see projector tows 4P1, 4P3 and 4P5 in Fig. 5. The relevant figures and tables of Ref. 10 show that the phase coherence decreases severely as the frequency increases from 25 to 140 Hz, while the S/N values remain comparable and high. This is similar to the behavior for Sites 3 and 1B and the explanation is given in Section 3.3.1. Figures 39 and 40 show that the phase coherence and the array signal gain are generally range independent up to about 150 km on projector tow 4P1 at 25 Hz. Note the wide variability of C_p and ASG with range due to multipath interference. Comparing Figs. 29, 30, 39, and 40 shows that the phase coherence and the array signal gain is less variable on projector tow 4P1 than on projector tow 3P4. This behavior reflects the fact that the Site 3 is bottom-limited while Site 4 is not (see Section 2.4). Figures 41 and 42 show that the phase coherence and the array signal gain are apparently range independent on projector tow 4P5 at 36 Hz up to about 250 km. This decrease in space coherence and array signal gain corresponds to the source being towed over an irregular sloping bottom as shown in Fig. 5. Because there is no significant decrease in S/N values during the tow over the irregular sloping bottom, the decrease in phase coherence and array signal gain appears to be caused by the irregularity of the bottom slope region. This behavior also occurred on 1BP1 and is discussed in Section 3.3.1. Figures I-39 and IV-13 show the C_p and ASG values, respectively, for the arc tow 4P3 at 25 Hz. Here the low values occur at low S/N values and there appears to be no bearing dependence in C_p and ASG. Figures IV-10 and IV-11, IV-12 and IV-13, and IV-14 and IV-15 show that the values of ASG are somewhat better for the weighted OAMS array than for the unweighted arrays. This was also observed in Sections 3.3.1 and 3.4.1. Unfortunately much interesting OAMS coherence data was lost on 17 and 18 March 19?? because the source frequency went to 39 Hz rather than the planned frequency of 36 Hz. (The quadrature detector had not been built to handle 39 Hz.)

3.5.2 (U) LATA Phase Coherence and Array Signal Gain

(C) The LATA phase coherence data analysis for Site 4 is summarized in Tables III-2 through III-4 and in Figs. III-17, III-21, and III-25 (Ref. 12) for 25 Hz. The LATA array signal gain data analysis for Site 4 is summarized in Tables IV-2 through IV-4 and in Figs IV-17, IV-21, and IV-25 (Ref. 13) for 25 Hz. The LATA array signal gain data analysis for Site 4 was taken on three projector tows in the Somali Basin: see projector tows 4P1, 4P2 and 4P3 in Fig. 5. Only the results for projector tow 4P1 will be considered here since the results for projector tows 4P2 and 4P3 are essentially the same. Figures 43 and 44 show that both the phase coherence and the array signal gain are generally range independent up to about 200 km, but both vary greatly due to multipath interference and the sound-speed profile small-scale structure discussed in Section 2.4.

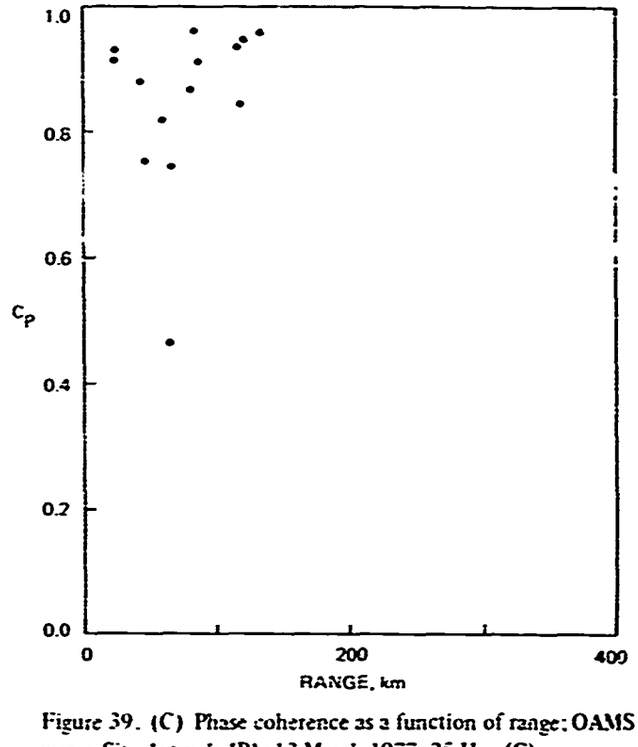

Figure 39. (C) Phase coherence as a function of range; OAMS array; Site 4; track 4P1; 13 March 1977; 25 Hz. (C)

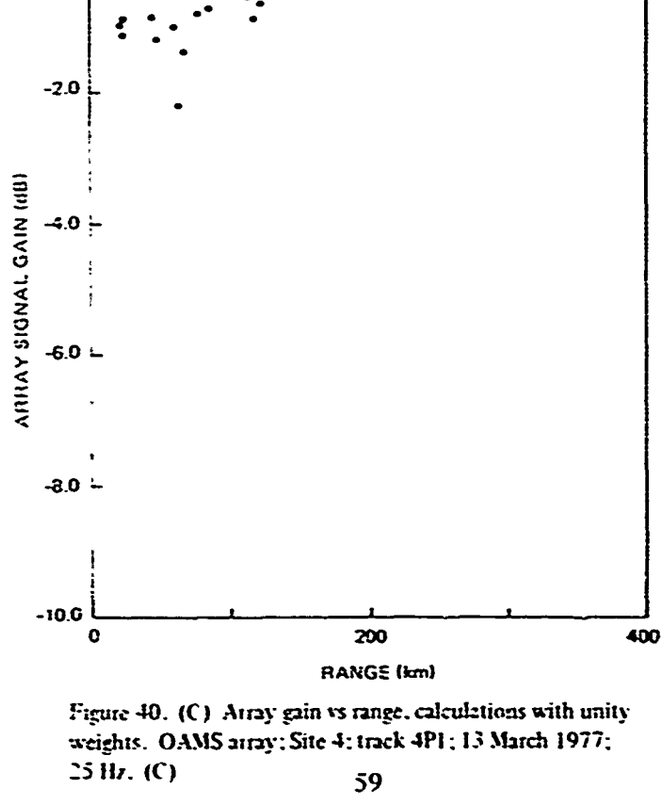

Figure 40. (C) Array gain vs range, calculations with unity weights. OAMS array; Site 4; track 4P1; 13 March 1977; 25 Hz. (C)

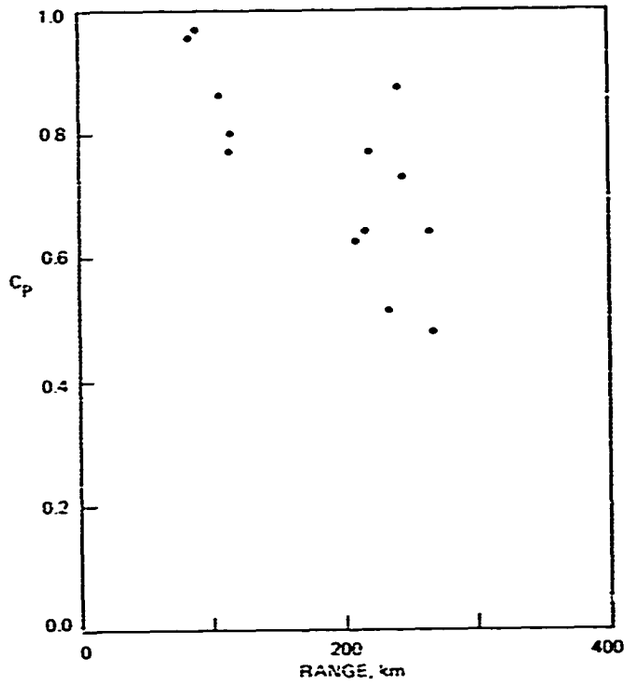

Figure 41. (C) Phase coherence as a function of range. OAMS array. Site 4, track 4P5, 18-19 March 1977; 36 Hz. (C)

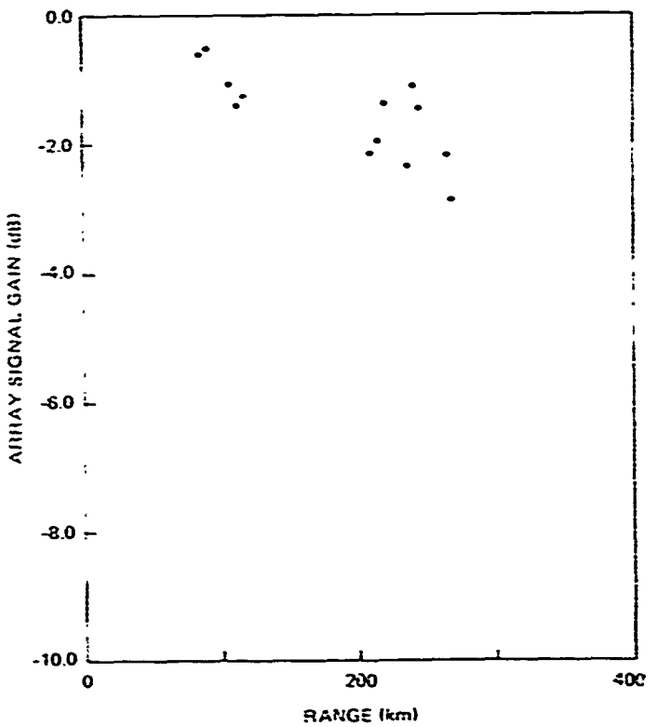

Figure 42. (C) Array signal gain vs range, calculations with unity weights. OAMS array; Site 4, track 4P5; 18-19 March 1977; 36 Hz. (C)

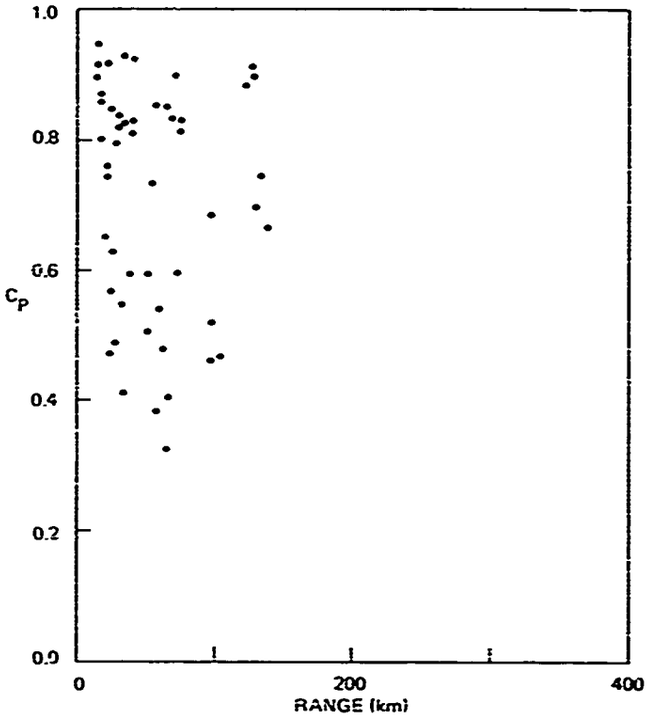

Figure 43. (C) Phase coherence vs range: LATA array; Site 4; track 4P1; 13-14 March 1977; 25 Hz. (C)

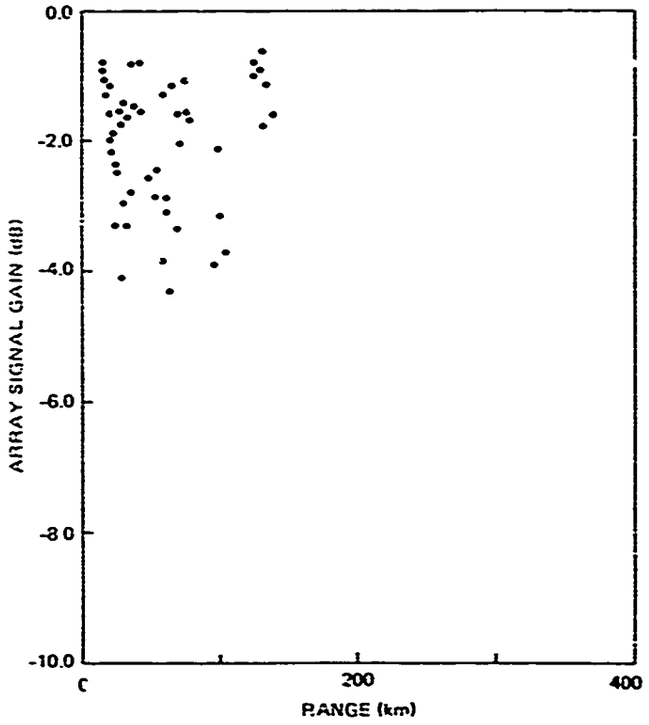

Figure 44. (C) Array signal gain vs range calculations with unity weights. LATA array; Site 4; track 4P1; 13-14 March 1977; 25 Hz. (C)

3.5.3 (U) Comparison of the LATA and the OAMS Array

(C) Figures 39, 40, 43 and 44 give the relative phase coherence behavior and the relative array signal gain behavior on the projector tow 4P1 of the OAMS array (with the source bearing near 90 deg) and of the LATA (with source bearing varying from 30 to 180 deg) as a function of range at 25 Hz. As can be seen from these figures, the OAMS phase coherence and array signal gain was higher and far less variable than for the LATA. As discussed in Section 2.4, this difference in behavior is attributed to the OAMS array operating at 200 m, which is above the complex sound-speed profile structure that occurs below about 250 m, and the LATA operating at 300 m, which is definitely in the more complex profile structure.

(U) The different aperture lengths and hydrophone group spacing of LATA with respect to those for the OAMS array have to be considered in this comparison. By using a LATA subset array that matched the OAMS array geometry fairly well (see Ref. 12), it is shown that the rangewise variability in the subset LATA data was only slightly reduced from that for the total LATA.

3.6 (U) DISCUSSION OF SITE 5

3.6.1 (U) OAMS Array Phase Coherence and Array Signal Gain

(C) The OAMS array phase coherence data analysis for Site 5 is summarized in Tables I-21 through I-25 and in Figures I-48 through I-52 (Ref. 10) for 25, 36, 140 and 290 Hz. The OAMS array signal gain data analysis for Site 5 is summarized in Tables IV-8 through IV-10 and in Figures IV-16 through IV-21 (Ref. 13) for 25 and 36 Hz. The OAMS array phase coherence and array signal gain data were taken on three projector tows over the Indus Fan and the Carlsberg Ridge; see projector tows 5P1, 5P3 and 5P5 in Fig. 6. Only the results for projector tow 5P1 will be considered here since the S/N values on the other projector tows were generally low. The relevant figures and tables of Ref. 10 show that the phase coherence decreases severely as the frequency increases from 25 to 140 Hz, while the S/N values remain comparable and high. This is similar to the behavior for Sites 3, 1B and 4, and the explanation is given in Section 3.3.1. Figures 45 and 46 show that the phase coherence and the array signal gain are generally range independent up to about 750 km. Note again the wide variability in C_p and ASG with range due to multipath interference. Comparing Figs. 39, 40, 45, and 46 shows that the phase coherence and the array signal gain are less variable on projector tow 4P1 than on projector tow 5P1. This behavior reflects the fact that the data for the bottom-limited Site 5 is more variable than the data for Site 4, which is not bottom-limited (see Section 2.4). Figures IV-16 and IV-17 show that the values of ASG are somewhat better for the weighted OAMS array than for the unweighted array.

3.6.2 (U) LATA Phase Coherence and Array Signal Gain

(C) The LATA phase coherence data analysis for Site 5 is summarized in Table III-5 and in Figure III-29 (Ref. 12) for 25 Hz. The LATA array signal gain data analysis for Site 5 is summarized in Table IV-26 and in Fig. IV-40 (Ref. 13) for 25 Hz. Nothing will be said about the LATA results at Site 5 since not much LATA data was processed for Site 5 due to time constraints placed on the project.

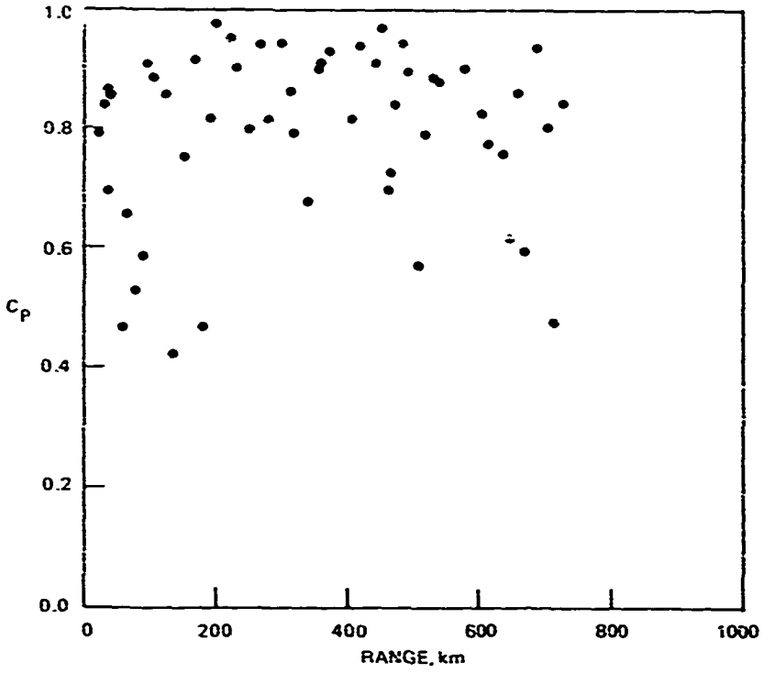

Figure 45. (C) Phase coherence as a function of range; OAMS array; Site 5; track 5P1, 12-14 April 1977; 25 Hz. (C)

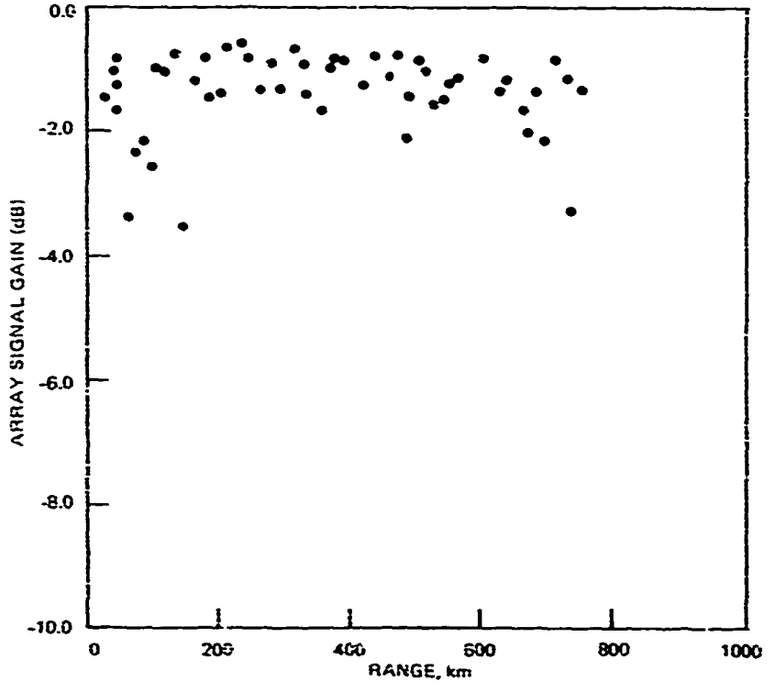

Figure 46. (C) Array signal gain vs range, calculations with unity weights. OAMS array; Site 5; track 5P1; 12-14 April 1977. (C)

3.7 (U) DISCUSSION OF SITE 2

3.7.1 (U) OAMS Array Phase Coherence and Array Signal Gain

(C) The OAMS array phase coherence data analysis for Site 2 is summarized in Tables I-26 through I-31 and in Figures I-63 through I-68 (Ref. 10) for 25 and 140 Hz. The OAMS array signal gain data analysis for Site 2 is summarized in Tables IV-11 through IV-13 and in Figures IV-22 through IV-27 (Ref. 13) for 25 Hz. The OAMS array phase coherence and array signal gain data were taken on three projector tows over the Indus Fan; see projector tows 2P2, 2P3A and 2P3 in Fig. 6. Unfortunately all the OAMS array tows for Site 2 were conducted, as shown in Fig. 6, behind an elongated seamount in the eastern Indus Fan. Figure 18 shows the effect of the seamount on some ray traces for a typical Site 2 case, and Section 2.4 discusses the consequences of the presence of a seamount near Site 2. Figures 47 and 48 show that the phase coherence and the array signal gain were generally range independent up to about 1000 km but were somewhat reduced and much more variable on projector tow 2P3A (seamount) than the comparable case of projector tow 5P1 (no seamount) shown in Figs. 45 and 46. Tables I-21 and I-28A show that the S/N values were about an average of 5 dB higher and less variable at similar ranges for projector tow 5P1 than for projector tow 2P3A. In short, given conditions which are otherwise identical (i.e., same range and source strength), the seamount produces perturbations in the measurements of phase coherence and array signal gain that would otherwise not have appeared. This situation seems to account for the reduced S/N values for Site 2.

3.7.2 (U) LATA Phase Coherence and Array Signal Gain

(C) The LATA phase coherence data analysis for Site 2 is summarized in Table III-6 and III-7 and in Figures III-33 and III-34 (Ref. 12) for 25 Hz. The LATA array signal gain analysis for Site 2 is summarized in Tables IV-27 and IV-28 and in Figures IV-41 and IV-42 (Ref. 13) for 25 Hz. The LATA phase coherence and array signal gain analysis data were taken on two projector tows over the Indus Fan; see projector tows 2P3A and 2P3 in Fig. 6. The results for these two tows are very similar. Figures 49 and 50 show that both the phase coherence and the array signal gain are generally range independent up to about 550 km, but both vary greatly due to multipath interference and the small-scale sound-speed profile structure discussed in Section 2.4. The source bearing varied from 10 to 150 deg. Due to the influence of the seamount on the OAMS data, a useful comparison of the LATA and the OAMS array results at Site 2 cannot be made.

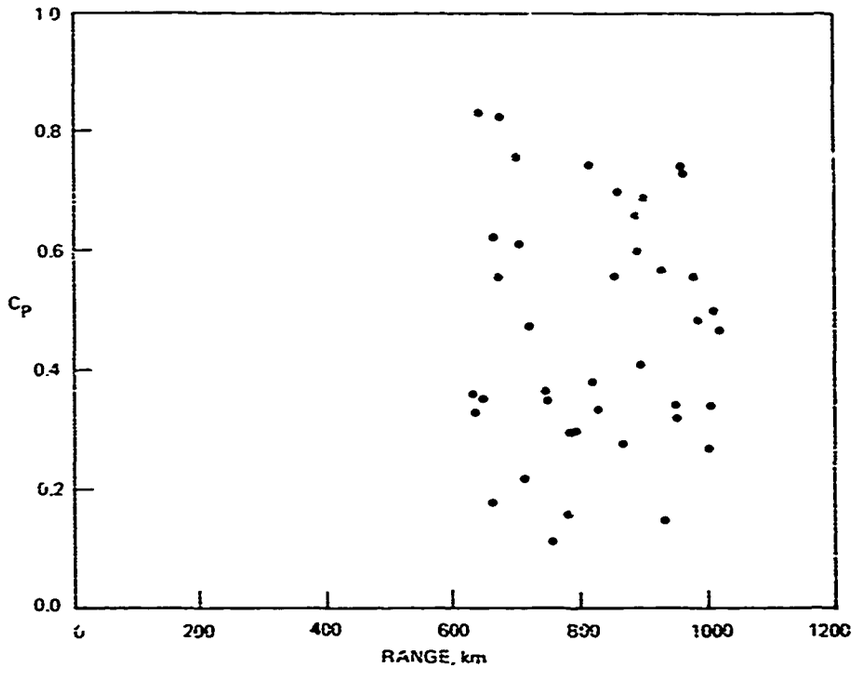

Figure 47. (C) Phase coherence as a function of range. OAMS array: Site 2, track 2P3; 27-28 April 1977; 25 Hz. (C)

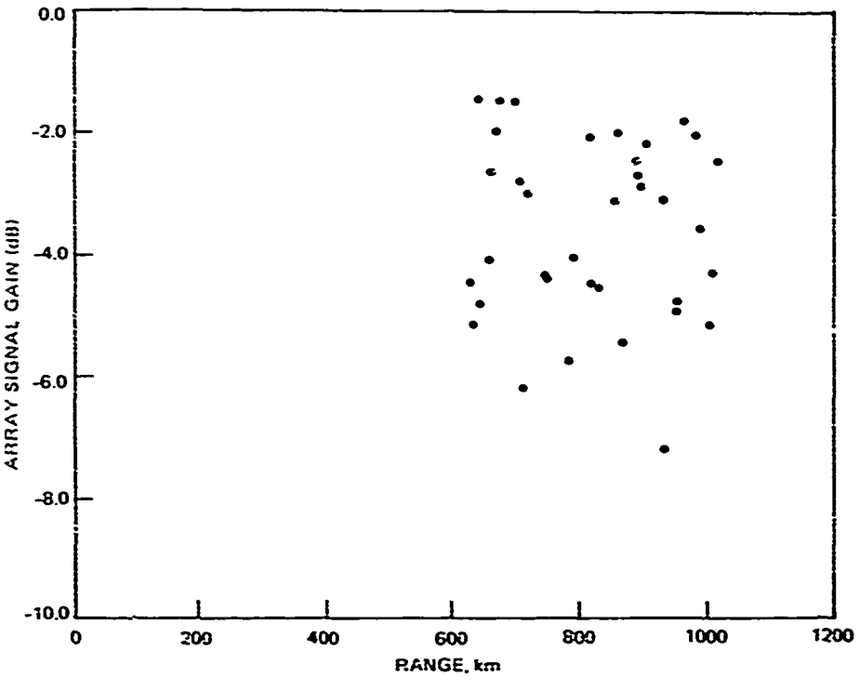

Figure 48. (C) Array signal gain vs range, calculations with unity weights. OAMS array: Site 2; track 2P3A; 27-28 April; 25 Hz. (C)

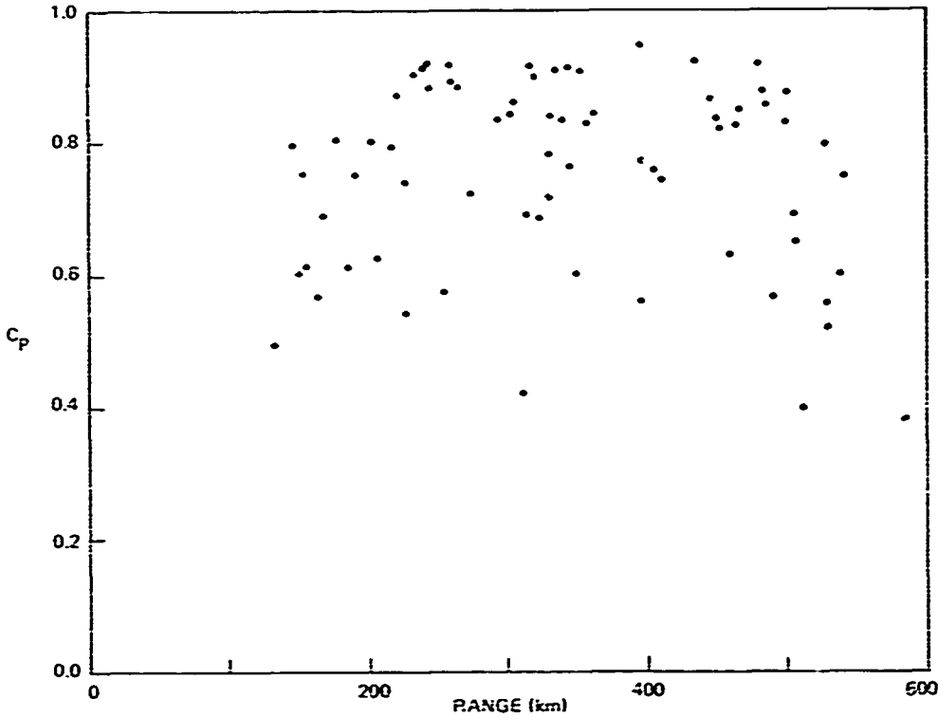

Figure 49. (C) Phase coherence vs range: LATA array, Site 2, track 2P3; 28-29 April 1977; 25 Hz. (C)

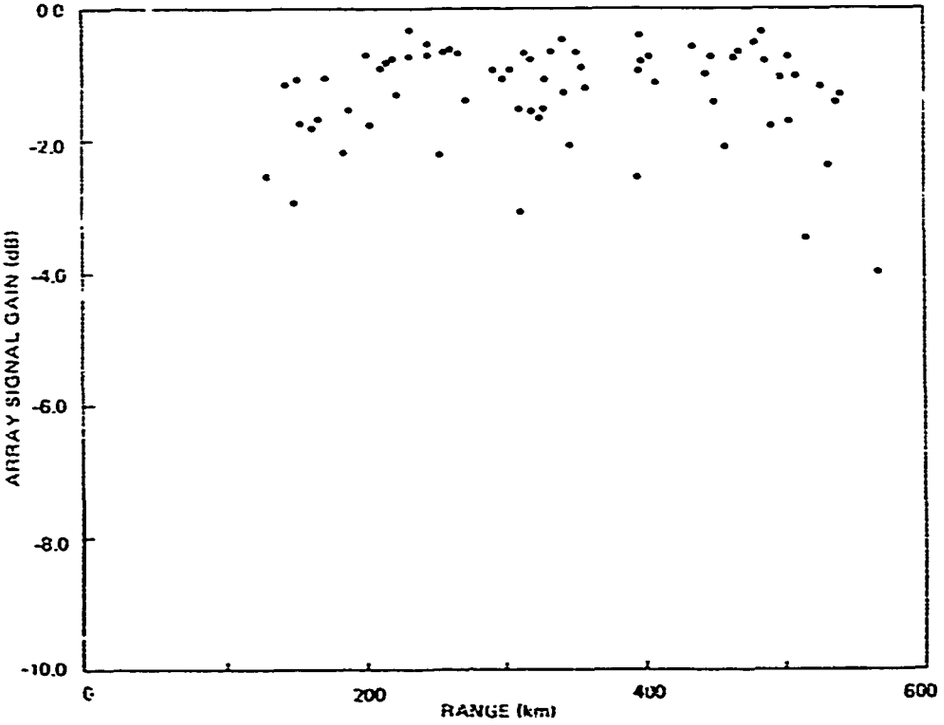

Figure 50. (C) Array signal gain vs range, calculations with unity weights. LATA array: Site 2, track 2P3, 28-29 April 1977; 25 Hz. (C)

5. (U) CONCLUSIONS

(C) Since the Northwestern Indian Ocean is usually bottom-limited and the sound-speed profiles are complex, a considerable rangewise variability exists in the plots of phase coherence and array signal gain for this multipath environment. This variability increases due to the presence of irregular bottom slopes as well as seamounts. This variability is the dominant characteristic of this body of water when the performance of long horizontal acoustic arrays is considered. Thence, a general assessment of signal coherence for the Northwestern Indian Ocean, based on the BEARING STAKE data, is as follows. The coherence will be a manageable problem for the performance of long bottom-mounted and mid-depth towed array systems used for surveillance if sufficient rangewise sampling is employed and the towed arrays are not operated in the depth region of complex sound-speed profile structure.

(C) From the detailed area assessment in Section 3 several conclusions can be reached about the performance of long horizontal acoustic arrays in the Northwestern Indian Ocean.

1. (U) The degree of amplitude fluctuations, as measured by Σ_A, does not change much with frequency and is largely range independent up to about 1000 km even over irregular sloping bottoms.

2. (C) The phase coherence decreases severely with increasing frequency, even when the S/N values remain high enough that noise correlations are negligible. This behavior is discussed in detail in Section 3.3.1. Because the phase coherence decreases severely with increasing frequency, the array signal gain should also decrease markedly with frequency increases: see Appendix.

3. (U) The phase coherence and the array signal gain are generally range independent up to about 1000 km except when the projector is passing over an irregular sloping bottom. They decrease and become more variable for a mid-depth towed array, but not for a bottom-mounted array, when the projector is passing over an irregular sloping bottom. This behavior may reflect the importance of bottom-propagated sound paths for a bottom-mounted array.

4. (U) The phase coherence and the array signal gain are widely variable with range due to multipath interference and become more variable in an irregular bottom slope region for a mid-depth towed array, but not for a bottom-mounted array. They were less variable at the only site (Site 4), where propagation was not bottom-limited.

5. (C) The relative phase coherence behavior and the relative array signal gain behavior of a mid-depth towed array and of a bottom-mounted array were compared on projector tows 3P4 (in Section 3.3.3) and 1BP1 (in Section 3.4.3) at 25 Hz. The performances of the bottom-mounted array (at about 20 deg off endfire) and the mid-depth towed array (near broadside) were comparable and neither array showed a rangewise deduction in phase coherence and in array signal gain (except in the irregular bottom slope region on projector tow 1BP1). Therefore, it appears that for the bottom-limited regions of the Northwestern Indian Ocean the phase coherence and the array signal gain behavior of the bottom-mounted and mid-depth (above about 250 m) towed arrays are essentially the same. See Section 2.4 for a discussion of arrays towed below 250 m.

6. (U) It was observed that the sensor spacing configuration for the BMA at Sites 3 and 1B were considerably different from the OAMS array sensor group spacing. To obtain a more accurate comparison of the towed array with the BMA, subset OAMS arrays (configured similarly in sensor spacing to the BMA at Sites 3 and 1B) were studied. It was found that the bottom-mounted arrays performed essentially the same as the subset towed arrays and that again no array showed any rangewise reduction in phase coherence and array signal gain (except in the irregular bottom slope region on projector tow 1BP1). The subset OAMS arrays performed essentially the same as the total OAMS array for phase coherence and array signal gain.

7. (U) There is no significant difference in phase coherence or in array signal gain behavior between the bottom-limited regions near Sites 3 and 1B, while the Site 4 region (which is not bottom-limited) evinced less variable behavior.

8. (C) In the Northwestern Indian Ocean, the surveillance performance of towed arrays may be significantly dependent on the array tow depths because of the presence of a mid-depth region of sound-speed profile complexity (see Section 2.4).

9. (U) When sound was received by the OAMS array from a source towed behind a seamount for Site 2, the S/N was often too low to allow estimation of phase coherence and array signal gain.

(U) REFERENCES (U)

1. Naval Undersea Center. OOS-2105-76. "Acoustic Survey Program: Planning Document (U)." 15 June 1976 (SECRET).

2. WECo. TS 196-76, Contract N00039-76-C-0216. "Technical Specifications for Project BEARING STAKE Acoustic Survey (U)." 18 November 1976 (SECRET).

3. Naval Undersea Center. OOS-4061-76. "Supplements to Technical Specifications for Project BEARING STAKE (U)." 17 December 1976 (SECRET).

4. Naval Ocean Systems Center. OOS-1005-77. "BEARING STAKE Data Analysis Plan (U)." May 1977 (SECRET).

5. A.G. Fabula and D. G. Strahle. "Preliminary Report on HMAS DIAMANTINA Participation in BEARING STAKE (U)." NOSC TN 235, September 1977 (SECRET).

6. Naval Ocean Systems Center. "BEARING STAKE Exercise: Preliminary Results (U)." NOSC TR 169, 31 October 1977 (CONFIDENTIAL).

7. A.G. Fabula. "A Mobile-Mobile CMAP Experiment (U)." NOSC TR 294, August 1978 (CONFIDENTIAL).

8. J.D. Northrop, et al., "Environmental Acoustic Predictions for the Northwestern Indian Ocean (U)." NOSC TN 104, May 1977 (CONFIDENTIAL).

9. Seismic Engineering Co. "Proposal for the Ocean Acoustic Measuring System," 9 April 1975.

10. J.A. Neubert, "BEARING STAKE Coherence Data Analysis: Part I. The OAMS Array (U)," NOSC TN 380, 6 February 1978 (CONFIDENTIAL).

11. J.A. Neubert, "BEARING STAKE Coherence Data Analysis: Bottom-Mounted Array (U)," NOSC TN 452, 31 May 1978 (CONFIDENTIAL).

12. A.G. Fabula and J.A. Neubert, "BEARING STAKE Data Analysis: LATA (U)," NOSC TN 589, November 1978 (CONFIDENTIAL).

13. J.A. Neubert, "BEARING STAKE Array Signal Gain Data Analysis (U)," NOSC TN 624, December 1978 (CONFIDENTIAL).

14. W.H. Watson and R.W. McGirr, "Raywave II: A Propagation Loss Model for the Analysis of Complex Ocean Environments," NUC TN 1516, 1975.

15. Personal communication from Dr. Aubrey Anderson of NORDA.

16. J.G. Colborn, "Sound-Speed Distribution in the Western Indian Ocean (U)," NUC TP 502, February 2976 (CONFIDENTIAL).

17. D.F. Gordon and E. R. Lloyd, "Acoustic Propagation Effects in Beamforming of Long Arrays (U)," *JUA* 29, January 1979 (CONFIDENTIAL).

18. D.F. Gordon, "Multipath interference Nulls in Long-Range, Low-Frequency, Acoustic Propagation by Normal Modes," (to be submitted to *JASA*).

19. T.E. Talpey, "Array Response in the Presence of Simultaneous Amplitude and Phase Fluctuations (U)," Office of Naval Research, ONR-ACR-170, *Proceedings of the 28th Navy Symposium on Underwater Acoustics*, Vol. 1, pp. 291–303, November 17–18, 1970 (CONFIDENTIAL).

APPENDIX:
METHODOLOGY OF COHERENCE AND ARRAY SIGNAL GAIN (U)

A.1 (U) INTRODUCTION

(C) Coherence measurements were conducted during BEARING STAKE because signal plus noise coherence gives a quantitative measure of array performance under a variety of oceanographic conditions when the S/N is sufficiently high. This permits the evaluation and direct comparison of passive surveillance systems under varying test conditions. In particular, in comparing the fixed horizontal bottom-mounted array with the towed horizontal mid-depth arrays in the Northwestern Indian Ocean environment, the coherence along each array yields performance as a function of frequency and of range from the towed source as it travels over a varying ocean bottom. The array with the largest coherence (normalized to have a maximum of unity) will give the better signal input to the beamformer at the given frequency. A plane wave (i.e., a unidirectional received signal), homogeneous in amplitude along a straight horizontal array, is assumed in the design of conventional beamformers. Therefore, the coherence along the array can be used as a measure of beamformer performance degradation due to nonplanar, nonhomogeneous signals and/or array deformation. The phase coherence and array signal gain measure the degradation in beam directivity as a function of range and frequency while the amplitude nonhomogeneity relates to the degradation in the expected sidelobe suppression. Thus, the measurement of phase coherence and array signal gain gives the relative merits of arrays. Since the array with the largest coherence (when the aperture size is comparable and the frequency is the same) provides the best mean signal plus noise input to a conventional beamformer, it represents the best detection performance capabilities under the prevailing conditions. Likewise, the largest array signal gain yields the best output for a conventional beamformer.

(U) This report is concerned with the study of phase coherence and array signal gain for long, horizontal line arrays receiving multipath signals from long-range, narrowband, low-frequency towed CW projectors in the generally bottom-limited Northwestern Indian Ocean. Narrowband analysis techniques permit the understanding and quantification of fundamental signal data that significantly effect realizable system performance. Therefore, they provide a valuable method for evaluating and comparing passive surevillance array systems. The phase coherence permits relating the array signal data to the reduction in the actual array performance from that expected for an ideal array in an ideal (vertically variable only) medium. Considering array signal gain directly relates actual performance to that expected for a conventional linear beamformer under ideal conditions.

A.2 (U) PHASE COHERENCE

(U) The narrowband, multipath signal plus noise arriving at the j^{th} sensor group along the long horizontal array at time t can be described by the relation $A_j \cos(\phi_j - \omega t)$, where A_j is the amplitude, ϕ_j is the received phase, and ω is the angular frequency. (The quantities A_j, ϕ_j and ω are all real.) It is assumed, when using the above signal plus noise form, that the slowly varying functions A_j and ϕ_j can be considered constant for time

periods less than $20\pi\ \omega$. The classical definition for the coherence of two complex waveforms F_1 and F_2 is

$$\left(\gamma_{12}^{c}\right)^2 \equiv \frac{\langle F_1 F_2^{*}\rangle^2}{\langle F_1 F_1^{*}\rangle \langle F_2 F_2^{*}\rangle} \leq 1 \quad . \tag{A-1}$$

where the operator $\langle \cdot \rangle$ represents the time average (generally over about 4 min for BEARING STAKE data) and the asterisk denotes the complex conjugate. For convenience in narrowband sonar array analysis, the classical coherence approach is modified as follows. the composite (due to multipath arrivals) instantaneous, narrowband response of the j^{th} sensor group can be represented (after basebanding by a quadrature detector) by

$$F_j = A_j e^{i[\phi_j - t(\omega - \omega_0)t]} \quad . \tag{A-2}$$

where ω_0 is the angular frequency at the center of the frequency bin. To determine the bearing Φ of the source of interest the appropriate peak $B(\Phi)$ of the phase-only linear beamformer output,

$$B(\Phi) \equiv \frac{1}{J^2} \sum_{j=1}^{J} \sum_{\ell=1}^{J} \langle \cos[(\phi_j - \phi_\ell) - k_0(d_j - d_\ell)\cos\Phi] \rangle \leq 1 \tag{A-3}$$

is found, where k_0 is the wavenumber, J is the total number of sensor groups in the array, and d_j is the distance from the center of the first sensor group to the center of the j^{th} sensor group ($d_1=0$). Φ is chosen to be zero for a forward endfire arrival. Then the "steered phase"

$$\theta_j \equiv \phi_j - k_0 d_j \cos\Phi \tag{A-4}$$

is computed. (Note that $\phi_j = \phi_\ell$ for all $j \neq \ell$ with $j,\ell \in [1,J]$ when a plane wave is received by a linear, horizontal array.) The signal plus noise, steered toward Φ, is obtained as

$$f_j \equiv A_j e^{i[\theta_j - t(\omega - \omega_0)]} = F_j e^{-ik_0 d_j \cos\Phi t} \tag{A-5}$$

It is assumed that the instantaneous amplitude can be written as

$$A_j = \langle A_j \rangle + \delta A_j \quad . \tag{A-6}$$

where δA_j is the amplitude fluctuation and $\langle A_j \rangle = \langle A_\ell \rangle$ for $j \neq \ell$ represents the amplitude variation nonhomogeneity. The term "fluctuation" denotes the rapid time-wise changes that can be averaged out, leaving the slowly changing mean structure that is referred to as the "variation" of the physical parameter of interest.

(U) It is interesting to consider briefly the multipath decomposition of f_j. For M multipaths to sensor group j

$$A_j e^{i\phi_j} \equiv \sum_{m=1}^{M} a_{mj} e^{i\psi_{mj}} \quad . \tag{A-7}$$

where $\psi_{mj} \equiv k_o d_j \cos \Phi_m$, is a linear superposition so a linear beamformer treats each contributing path independentiy. Then

$$f_j = A_j e^{i[\theta_j - (\omega-\omega_o)t]} \equiv e^{-i(\omega-\omega_o)t} \sum_{m=1}^{M} a_{mj} e^{i\varphi_{mj}} \quad . \tag{A-8}$$

where $\varphi_{mj} \equiv k_o d_j(\cos \Phi_m - \cos \bar{\Phi})$. Define the beamformer output (before averaging and with weights W_j) as

$$\left| \sum_{j=1}^{J} W_j f_j \right|^2$$

$$= \sum_{j=1}^{J} \sum_{\ell=1}^{J} W_j W_\ell f_j f_\ell^*$$

$$= \sum_{j=1}^{J} \sum_{\ell=1}^{J} W_j W_\ell A_j A_\ell \cos(\theta_j - \theta_\ell)$$

$$= \sum_{m=1}^{M} \sum_{n=1}^{M} \sum_{j=1}^{J} \sum_{\ell=1}^{J} W_j a_{mj} W_\ell a_{n\ell} \cos(\phi_{mj} - \phi_{n\ell})$$

$$= \sum_{m=1}^{M} \sum_{j=1}^{J} \sum_{\ell=1}^{J} W_j a_{mj} W_\ell a_{m\ell} \cos(\phi_{mj} - \varphi_{m\ell})$$

$$+ 2 \sum_{m=1}^{M-1} \sum_{n=m+1}^{M} \sum_{j=1}^{J} \sum_{\ell=1}^{J} W_j a_{mj} W_\ell a_{n\ell} \cos(\phi_{mj} - \phi_{n\ell}) \quad . \tag{A-9}$$

where the operator $|\cdot|^2$ represents the complex product and where the first term in Eq. (A-9) represents the same path contributions and gives a linear superposition of the formed beams. The second term in Eq. (A-9) represents the cross-path contributions, and unless the presence of many paths causes this term to average to zero, it will represent a distortion of the sidelobe structure (which becomes apparent when Φ is varied from $\bar{\Phi}$ through all its values).

(U) The classical coherence $(\gamma^c_{j\ell})^2$ between sensor groups j and ℓ could be synopsized by the coherence coefficient

$$C_c \equiv \frac{1}{J^2} \sum_{j=1}^{J} \sum_{\ell=1}^{J} (\gamma^c_{j\ell})^2 \quad . \tag{A-10}$$

However, $(\gamma^c_{j\ell})^2$ mixes the amplitude A_j and phase ϕ_j of the j^{th} sensor group signal plus noise F_j in a manner which is difficult to interpret in terms of the causes of the array performance degradation. Therefore, the phase and amplitude are separated by a quadrature detector and θ_j is found via Eq. (A-4) and B(Φ). Then the array coherence between the j^{th} and ℓ^{th} sensor groups is defined as

$$\gamma_{j\ell} \equiv \text{Re} \left\{ \frac{\langle f_j f^*_\ell \rangle}{\langle f_j \rangle \langle f_\ell \rangle} \right\} \tag{A-11}$$

$$= \frac{\langle A_j A_\ell \cos(\theta_j - \theta_\ell) \rangle}{\langle A_j \rangle \langle A_\ell \rangle} \tag{A-11a}$$

$$= \frac{\langle A_j A_\ell \rangle}{\langle A_j \rangle \langle A_\ell \rangle} \langle \cos(\theta_j - \theta_\ell) \rangle \tag{A-11b}$$

under the Talpey decorrelation assumption (see Ref. 17)

$$\langle A_j A_\ell \cos(\theta_j - \theta_\ell) \rangle = \langle A_j A_\ell \rangle \langle \cos(\theta_j - \theta_\ell) \rangle . \tag{A-12}$$

where $\langle A_j A_\ell \rangle$ is an element of the amplitude correlation matrix and $\langle \cos(\theta_j - \theta_\ell) \rangle$ is an element of the phase coherence matrix. Defining $\text{Re} \langle A_j A_\ell e^{i(\theta_j - \theta_\ell)} \rangle$ as the array coherence would have allowed the scatter of $\langle A_j A_\ell \rangle$ (due to $\langle A_j \rangle = \langle A_\ell \rangle$) to confuse the good quality of the coherence that is usually present. The Talpey decorrelation assumption that was applied in Eq. (A-11b) is not meant to imply that A_j and θ_j are statistically independent, but only that the quantities $A_j A_\ell$ and $\cos(\theta_j - \theta_\ell)$ are at most weakly correlated, so that Eq. (A-12) is just a good approximation. The Talpey decorrelation assumption was tested synoptically by the Talpey coefficient

$$C_T \equiv \frac{2}{J(J-1)} \sum_{j=1}^{J-1} \sum_{\ell=j+1}^{J} \frac{\langle A_j A_\ell \cos(\theta_j - \theta_\ell) \rangle}{\langle A_j A_\ell \rangle \langle \cos(\theta_j - \theta_\ell) \rangle} \tag{A-13}$$

and found to be generally justified (i.e., C_T is usually near unity) as shown in the tables in Refs. 10 through 13. However, for reservations on the application of C_T in the Northwestern Indian Ocean, see Ref. 12.

(U) The output E of a standard processor (i.e., the beamformed, squared and time-averaged output) can be written in the useful form (with the Talpey decorrelation assumption):

$$E = \sum_{j=1}^{J} \langle A_j^2 \rangle + 2 \sum_{j=1}^{J-1} \sum_{\ell=j+1}^{J} \langle A_j A_\ell \rangle \langle \cos(\theta_j - \theta_\ell) \rangle \quad . \tag{A-14}$$

The amplitude correlation matrix $[\langle A_j A_\ell \rangle]$ is related to the composite amplitude nonhomogenity. The phase coherence matrix $[\langle \cos(\theta_j - \theta_\ell) \rangle]$ evinces the relative array distortion due to wavefront corrugation (i.e., nonplanar arrivals) and/or array deformation. The amplitude nonhomogeneity that results, through multipath addition, from a linear superposition of array signal plus noise cannot be decomposed through amplitude correlation techniques and, therefore, these techniques cannot be used to study their effects on the outputs of linear beamformers; they can only treat their effects on the outputs of arrays. (This applies to phase coherence but not to array signal gain; see below.) The components of the linear superposition of array signal plus noise are simply acted on individually by the beamformer as shown in Eq. (A-9). Therefore, neither the amplitude correlation matrix $[\langle A_j A_\ell \rangle]$, nor the normalized amplitude correlation matrix $[\langle A_j A_\ell \rangle / \langle A_j \rangle \langle A_\ell \rangle]$, nor the phase coherence matrix $[\langle \cos(\theta_j - \theta_\ell) \rangle]$ can predict the results at the output of a linear beamformer from their behavior at the output of the array sensor groups alone. Thus, the array signal gain will be considered later since it gives the results at the beamformer output.

(U) To facilitate treatment of the large coherence data base for BEARING STAKE, five synoptic measures of performance (in addition to C_T) have been devised. The degree of amplitude fluctuation due to correlated amplitude fluctuations can be synopsized by the normalized standard deviation Σ_A, which is defined as

$$\Sigma_A \equiv \sigma_{A_J} / A_a \geq 0 \quad . \tag{A-15}$$

where

$$\sigma_A^2 \equiv \frac{1}{J} \sum_{j=1}^{J} \langle (A_j - \langle A_j \rangle)^2 \rangle \tag{A-15a}$$

$$= \frac{1}{J} \sum_{j=1}^{J} \langle (\delta A_j)^2 \rangle \tag{A-15b}$$

[when Eq. (A-6) is assumed] and

$$A_a \equiv \frac{1}{J} \sum_{j=1}^{J} \langle A_j \rangle \quad . \tag{A-16}$$

Normalizing by $\bar{A}_a$ avoids changes in the propagation conditions from biasing the measure Σ_A. The smaller Σ_A is, the smaller the amount of amplitude fluctuation present. The degree of array nonhomogeneity (but not the degree of its sidelobe distorting influence) can be synopsized by the nonhomogeneity coefficient C_n which is defined as

$$C_n \equiv \frac{\sum_{j=1}^{J} \left| \langle A_j \rangle - \bar{A}_a \right|}{J\bar{A}_a} \geq 0 \qquad \text{(A-17)}$$

and equals zero for a homogeneous sound field.

(U) It is useful to synopsize an upper bound for the array coherence $\gamma_{j\ell}$ by means of Eq. (A-11b). First form for any $i \in [1,J]$.

$$\frac{1}{J}\sum_{j=1}^{J} \frac{\langle A_i A_j \rangle}{\langle A_i \rangle \langle A_j \rangle} = 1 + \frac{1}{J}\sum_{j=1}^{J} \frac{\langle \delta A_i \delta A_j \rangle}{\langle A_i \rangle \langle A_j \rangle}$$

$$\approx 1 + \frac{\frac{1}{J}\sum_{j=1}^{J} \langle \delta A_i \delta A_j \rangle}{\bar{A}_a^2}$$

$$\leq 1 + \frac{\frac{1}{J}\sum_{j=1}^{J} \langle (\delta A_j)^2 \rangle}{\bar{A}_a^2} = 1 + \frac{\bar{\sigma}_A^2}{\bar{A}_a^2}$$

$$= 1 + \bar{\Sigma}_A^2 \equiv C_\Sigma \qquad \text{(A-18)}$$

via Eqs. (A-6), (A-16), (A-15b) and (A-15) as well as

$$\sum_{j=1}^{J} \langle \delta A_i \delta A_j \rangle < \sum_{j=1}^{J} \langle (\delta A_j)^2 \rangle \quad . \qquad \text{(A-19)}$$

Thus, C_Σ synopsizes the normalized amplitude matrix $[\langle A_i A_j \rangle / \langle A_i \rangle \langle A_j \rangle]$ of the array coherence matrix $[\gamma_{ij}]$. Next define the phase coherence coefficient C_p as

$$C_p \equiv \frac{1}{J^2}\sum_{j=1}^{J}\sum_{\ell=1}^{J} \langle \cos(\theta_j - \theta_\ell) \rangle \leq 1 \qquad \text{(A-20)}$$

$$= B(\bar{\Phi}) \tag{A-20a}$$

via Eqs. (A-3) and (A-4). Thus, C_p synopsizes the phase coherence matrix $[\langle\cos(\theta_i-\theta_j)\rangle]$ and the array coherence coefficient C_γ

$$C_\gamma \equiv C_\Sigma \, C_p \quad . \tag{A-21}$$

synopsizes the array coherence matrix $[\gamma_{ij}]$ in terms of Σ_A and C_p

A.3 (U) ARRAY SIGNAL GAIN

(U) The array gain, ag, is by definition the ratio of the signal $\langle S^2\rangle$ to noise $\langle N^2\rangle$ power ratio of the array beamformer output to the signal $\langle s^2\rangle$ to noise $\langle n^2\rangle$ power ratio of a single element, i.e.,

$$ag \equiv \frac{\langle S^2\rangle \langle N^2\rangle}{\langle s^2\rangle \langle n^2\rangle} \equiv \frac{asg}{\eta} \quad . \tag{A-22}$$

where

$$\eta \equiv \langle N^2\rangle \langle n^2\rangle \tag{A-22a}$$

and

$$asg \equiv \langle S^2\rangle \langle s^2\rangle \tag{A-23}$$

is the array signal gain, or, in decibel units,

$$ASG = 10 \log_{10} asg \, . \tag{A-24}$$

For a weighted (by W_j) array, the asg will be taken to be

$$asg \equiv \frac{\sum_{j=1}^{J} \sum_{\ell=1}^{J} W_j W_\ell \langle A_j A_\ell \cos(\theta_j-\theta_\ell)\rangle}{\left(\sum_{j=1}^{J} W_j \sum_{\ell=1}^{J} W_\ell\right) \frac{1}{J} \sum_{j=1}^{J} \langle A_j^2\rangle} \tag{A-25}$$

$$\xrightarrow[W_j W_\ell \to 1]{A_j A_\ell \to A_a} C_p \quad . \tag{2-25a}$$

From Eq. (A-25a) it is seen that C_p can be interpreted as the array signal gain for a phase-only beamformer: see Eqs. (A-3) and (A-20a). Note that the phase incoherence of $\langle\cos(\theta_j-\theta_\ell)\rangle$ and the amplitude nonhomogeneity reduce the ideal array signal gain of 0 dB to the actual array signal gain of Eq. (A-24). When the array amplitude response is ideal (i.e., $A_j = \bar{A}_a$ for all $j\in[1,J]$), the ideal array signal gain is still directly reduced by the phase incoherence. When the array has perfect phase coherence, the ideal array signal gain is still reduced by the array amplitude nonhomogeneity and amplitude fluctuations. As expected, when the array response is both phase coherent and homogeneous (i.e., $\langle A_j\rangle = \bar{A}_a$), the ideal array signal gain occurs if the amplitude fluctuations are negligible, i.e., $A_j = \bar{A}_a$. The advantage of Eq. (A-25) (i.e., incorporating both phase coherence and amplitude homogeneity into an array signal gain expression) over giving quantities at the output of just the array (such as phase coherence) is that it gives the performance degradation for a conventional linear beamformer at its output.

INITIAL DISTRIBUTION

DEPUTY UNDER SECRETARY OF DEFENSE R&E
(TACT. WARFARE PROGRAMS)
DIR. NAVAL WARFARE

ARPA RESEARCH CENTER
UNIT 1
T KOOIJ

ASSISTANT SECRETARY OF THE NAVY (RE&S)
DEP. ASST. SECRETARY (SYSTEMS)
G CANN

CHIEF OF NAVAL OPERATIONS
NOP-095
NOP-098
NOP-951 (2)
NOP-951F (2)
NOP-952 (2)

CHIEF OF NAVAL MATERIAL
NMAT-08T24 (GR SPALDING)

NAVAL ELECTRONIC SYSTEMS COMMAND
CODE 320 (J SINSKY)
PME-124-20 (R KNUDSEN)
PME-124-30
PME-124-60 (4)

NAVAL SEA SYSTEMS COMMAND
NSEA-06H1 (CC SMITH)

NAVAL AIR SYSTEMS COMMAND
NAIR-370

OFFICE OF NAVAL RESEARCH
ONR-102B

NAVAL RESEARCH LABORATORY
CODE 8103
CODE 8160 (BB ADAMS)

NAVAL INTELLIGENCE SUPPORT CENTER
CODE 222

NAVAL POSTGRADUATE SCHOOL
LIBRARY

NAVAL AIR DEVELOPMENT CENTER
CODE 303 (J HOWARD) (2)

NAVAL OCEANOGRAPHY COMMAND

OCEANOGRAPHER OF THE NAVY

NAVAL OCEAN RESEARCH AND DEVELOPMENT
ACTIVITY
CODE 110 (TECH. DIRECTOR) (2)
CODE 320 (2)
CODE 600 (DR RD GAUL)
CODE 200 (CDR T MC CLOSKEY)
CODE 340 (DR S MARSHALL)
CODE 360 (DR H EPPERT)

NAVAL OCEANOGRAPHIC OFFICE
CODE 3410 (J CARROLL)
CODE 3400 (WH GEDDES)

NAVAL OCEAN RESEARCH AND DEVELOPMENT
ACTIVITY LIAISON OFFICE

COMMANDER IN CHIEF
US NAVAL FORCES, EUROPE

COMMANDER IN CHIEF U.S.
ATLANTIC FLEET
PACIFIC FLEET
COMMANDER
CODE 352

COMMANDER THIRD FLEET
N-32
N-34

THE UNIVERSITY OF TEXAS
APPLIED RESEARCH LABORATORY
S MITCHELL (2)

WOODS HOLE OCEANOGRAPHIC INSTITUTE
E HAYES

BELL TELEPHONE LABORATORIES
WHIPPANY, NJ 07981
R LAUVER
PENNOTTI

WESTINGHOUSE ELECTRIC CORP.
PO BOX 20046
GELFORD CENTER
GREENSBORO, NC 27420
R SCUDDER (3)

PLANNING SYSTEMS, INC.
7900 WESTPARK DRIVE
MC LEAN, VA 22101
DR L SOLOMON

TRW, INC.
7600 COLSHIRE DR
MC LEAN, VA 22101
R MURAWSKI

MECHANICS RESEARCH, INC.
7929 WESTPARK DRIVE
MC LEAN, VA 22101

APPLIED HYDROACOUSTICS, INC.
656 QUINCE ORCHARD RD
GAITHERSBERG, MD 20760
F RYDER

COMPUTER SCIENCES CORP.
2251 SAN DIEGO AVENUE
SAN DIEGO, CA 92110

DEFENSE DOCUMENTATION CENTER (2)

DEPARTMENT OF THE NAVY
OFFICE OF NAVAL RESEARCH
875 NORTH RANDOLPH STREET
SUITE 1425
ARLINGTON VA 22203-1995

IN REPLY REFER TO:

5510/1
Ser 321OA/011/06
31 Jan 06

MEMORANDUM FOR DISTRIBUTION LIST

Subj: DECLASSIFICATION OF LONG RANGE ACOUSTIC PROPAGATION PROJECT (LRAPP) DOCUMENTS

Ref: (a) SECNAVINST 5510.36

Encl: (1) List of DECLASSIFIED LRAPP Documents

1. In accordance with reference (a), a declassification review has been conducted on a number of classified LRAPP documents.

2. The LRAPP documents listed in enclosure (1) have been downgraded to UNCLASSIFIED and have been approved for public release. These documents should be remarked as follows:

   Classification changed to UNCLASSIFIED by authority of the Chief of Naval Operations (N772) letter N772A/6U875630, 20 January 2006.

   DISTRIBUTION STATEMENT A: Approved for Public Release; Distribution is unlimited.

3. Questions may be directed to the undersigned on (703) 696-4619, DSN 426-4619.

BRIAN LINK
By direction

Subj: DECLASSIFICATION OF LONG RANGE ACOUSTIC PROPAGATION PROJECT (LRAPP) DOCUMENTS

DISTRIBUTION LIST:

NAVOCEANO (Code N121LC – Jaime Ratliff)
NRL Washington (Code 5596.3 – Mary Templeman)
PEO LMW Det San Diego (PMS 181)
DTIC-OCQ (Larry Downing)
ARL, U of Texas
Blue Sea Corporation (Dr.Roy Gaul)
ONR 32B (CAPT Paul Stewart)
ONR 321OA (Dr. Ellen Livingston)
APL, U of Washington
APL, Johns Hopkins University
ARL, Penn State University
MPL of Scripps Institution of Oceanography
WHOI
NAVSEA
NAVAIR
NUWC
SAIC

Declassified LRAPP Documents

Report Number	Personal Author	Title	Publication Source (Originator)	Pub. Date	Current Availability	Class.
NORDATN20	Bucca, P. J., et al.	CHURCH STROKE 1 ENVIRONMENTAL DATA REPORT	Naval Ocean R&D Activity	780201	NS; AU	C
NOSCTN380	Neubert, J. A.	BEARING STAKE COHERENCE DATA ANALYSIS PART 1: OAMS ARRAY (U)	Naval Ocean Systems Center	780206	NS; AU	C
ARLTR788	Mitchell, S. K., et al.	BEARING STAKE-VERTICAL ACODAC ACOUSTIC MEASUREMENTS DATA REPORT (U)	University of Texas, Applied Research Laboratories	780215	NS; AU; ND	C
N0003978C0117	Osborne, J. T.	PROJECT BEARING STAKE TRANSMISSSION LOSS AND OMNIDIRECTIONAL AMBIENT NOISE FROM BOTTOMED ARRAYS (U)	Western Electric Company	780505	NS; AU; ND	C
Unavailable	Unavailable	CHURCH STROKE II CRUISE V QUALITY ASSESSMENT OF PAR AND ACODAC TAPES (U)	University of Texas, Applied Research Laboratories	780517	AU	C
Unavailable	Unavailable	CHURCH STROKE II CRUISE V QUALITY ASSESSMENT OF PAR TAPES (U)	University of Texas, Applied Research Laboratories	780517	AU	C
NOSCTN452	Neubert, J. A.	BEARING STAKE COHERENCE DATA ANALYSIS: THE BOTTOM-MOUNTED ARRAY (U)	Naval Ocean Systems Center	780531	NS; AU; ND	C
ARLTM783	Unavailable	BEARING STAKE EXERCISE RECONSTRUCTION CHARTS (U)	University of Texas, Applied Research Laboratories	780601	NS; AU	C
Unavailable	Unavailable	BEARING STAKE TSVLA DATA (U)	US Nav Air Dev Center	780823	AU	C
NORDAR18	Fenner, D. F., et al.	BEARING STAKE EXERCISE: SOUND SPEED AND OTHER ENVIRONMENTAL VARIABILITY (U)	Naval Ocean R&D Activity	780901	ADC017390; NS; ND	C
Unavailable	Unavailable	BEARING STAKE EXERCISE (U)	Naval Ocean R&D Activity	780901	AU	C
Unavailable	Unavailable	MERCHANT SHIP SIGNATURES FROM THE CHURCH OPAL ACODAC (U)	University of Texas, Applied Research Laboratories	780926	AU	C
32ND NSUA V1	Dundore, D. M.	EFFECTS OF ACOUSTIC MUTLIPATH INTERFERENCE ON LARE APERTURE TOWED ARRAYS (U)	Naval Underwater Systems Center	781101	ND	C
32ND NSUA V1	Griffin, J. M.	DYNAMICS OF LAMBDA II AS MEASURED IN CURCH OPAL	Naval Underwater Systems Center	781101	ND	C
32ND NSUA V1	Kinney, W. A.	PERFORMANCE OF A TOWED ARRAY AT EXTREME RANGE	Naval Underwater Systems Center	781101	ND	C
32ND NSUA V1	Moseley, W. B.	COMBINED EFFECTS ON MULTIPATH INTERFERENCE, ARRAY DEFORMATIONS, AND SCATTERING ON LARGE APERTURE ARRAY PERFORMANCE	Naval Underwater Systems Center	781101	ND	C
NOSCTN624	Neubert, J. A.	BEARING STAKE ARRAY SIGNAL GAIN DATA ANALYSIS (U)	Naval Ocean Systems Center	781201	ADC018803; NS; AU; ND	C
NOSCTN383	Neubert, J. A.	BEARING STAKE COHERENCE AND ARRAY SIGNAL GAIN AREA ASSESSMENT REPORT (U)	Naval Ocean Systems Center	781201	NS; AU ADC018803	C
NOSCTN589	Fabula, A. G., et al.	BEARING STAKE COHERENCE DATA ANALYSIS: LATA	Naval Ocean Systems Center	781201	NS; AU; ND	C

ENCL (1)